Technische Universität München
Lehrstuhl für Echtzeitsysteme und Robotik

Computational Modelling and Information Processing within Neural Networks

Aurel Vasile Martiniuc

Vollständiger Abdruck der von der Fakultät der Informatik der Technischen Universität München zur Erlangung des akademischen Grades eines

Doktors der Naturwissenschaften (Dr. rer. nat.)

genehmigten Dissertation.

Vorsitzender:	Prof. Dr. Nassir Navab
Prüfer der Dissertation:	1. Prof. Dr. Alois Christian Knoll
	2. Prof. Dr. Hans-Joachim Bungartz

Die Dissertation wurde am 21.08.2014 bei der Technischen Universität München eingereicht und durch die Fakultät für Informatik am 10.01.2015 angenommen.

Publication list

The scientific work presented in this thesis is based on the following journal papers:

Chapter II: Aurel Vasile Martiniuc, Victor Bocos-Bintintan, Rouhollah Habibey, Asiyeh Golabchi, Alois Knoll, Axel Blau. Paired spiking robustly shapes spontaneous activity in neural networks *in vitro*. Frontiers in Neural Circuits (submitted).

Chapter III: Martiniuc A, Knoll A. Sharpening of directional selectivity from neural output of rabbit retina, 2010. Journal of Computational Neuroscience, DOI: 10.1007/s10827-0100266-z.
Erratum for printed publication: Martiniuc AV, Zeck G, Stürzl W, Knoll A. Sharpening of directional selectivity from neural output of rabbit retina. J. Comput. Neurosci. 30(2):409-26. (2011).

Chapter IV: A.V. Martiniuc and A. Knol. Interspike interval based filtering of directional selective retinal ganglion cells spike trains in rabbit retina. Journal of Computational Intelligence and Neuroscience, June 2012. doi:10.1155/2012/918030.

Chapter V:

[1] Aurel V. Martiniuc, Victor Bocos-Bintintan, Florian Röhrbein, Alois Knoll. Descriptive model for the prediction of motion direction from spike trains of ON-OFF directional selective retinal ganglion cells. Accepted to the Twenty-Third Annual Computational Neuroscience Meeting CNS*2014 (CNS2014), Quebec, Canada (*in press*).

[2] Aurel Vasile Martiniuc, Rouhollah Habibey, Asiyeh Golabchi, Victor Bocos-Bintintan, Alois Knoll, Axel Blau. Paired spiking is an ubiquitous response property in network activity. In Proceedings of the 9th International Meeting on Substrate-Integrated Microelectrode Arrays, A. Stett and G. Zeck (Eds.), NMI, p. 181-182 (2014).

Abstract

My main research interest described here is toward scientifically exploring the manner in which information is processed in the nervous system. The early visual system offers a prominent model to explore how information regarding the visual stimuli is encoded/decoded and transmitted from retina to cortex through the lateral geniculate nucleus (LGN). The retinogeniculate synapse holds a major advantage – to study fundamental aspects of information processing by neurons. Beside the similarity of the ON-OFF center surround arrangement of the receptive field for both retinal ganglion cells (RGCs) and LGN neurons, there is one main RGC that drives the response of its LGN neuron counterpart. This advantage of one-to-one synaptic connectivity is lost as advancing toward higher stages at the geniculo-cortical synapse. Here many LGN cells send convergent projections to one single cortical neuron.

However, in spite of this one-to-one connectivity, LGN neurons do not simply relay the input received from their RGCs counterparts; on the contrary, the incoming RGC spike trains are converted into new spike trains by the LGN cells in their editing process before transmitting the visual information further on toward the cortex. About half of the retinal spikes are lost in transmission at the retinogeniculate synapse.

How do LGN cells decide which retinal action potential (AP) deserves to be kept and which to be deleted so that the visual information to be preserved from an RGC to the LGN and transmitted further on? What is the mechanism responsible for this information processing? To answer these questions and other issues emerging from the particular manner in which the LGN edits retinal input, I focused on a prominent example of information processing at the retinogeniculate synapse: direction of stimulus motion.

Here I employ computational modeling, experimental extracellular recordings and applied mathematics for data analysis, in order to explore: (i) the sharpening in directional selectivity as a prominent example of information processing, (ii) the neural mechanisms

involved in establishing functional and effective connectivity and (iii) the degree of efficiency in information transmitting between neurons.

However, as the findings emerged from these scientific hypotheses are raising new questions, I further asked whether these neural mechanisms involved in information processing hold true for other types of neurons and/or other laboratory conditions. To this end, I explored spontaneous neural activity in cultures of dissociated hippocampal and cortical neurons using extracellular recordings from multi-electrode arrays (MEAs).

Paired spiking (PS) enhancement plays a key role in the concept of sparse coding efficiency. It acts as a temporal filter that deletes less informative spikes in the process of establishing functional and effective connectivity between neurons along their synaptic pathways and thus preserving information from one stage to the next.

Since PS activity is present not only under stimuli conditions (both *in vivo* and *in vitro*), but also under a spontaneous activity paradigm and in cultured neurons, presumably it represents a ubiquitous response property of neurons of different species and under different conditions (*in vivo* and *in vitro*, spontaneously and stimuli induced) involved in information processing within the nervous system.

Because this hypothesis holds true in cultured neurons, not only at local sites (single cell level) but also at network level, PS may be of help in understanding the manner in which neurons of different types perform synaptic plasticity (with implication in exploring learning and memory) and process information. Furthermore, PS activity may be valuable in shaping the network response control to obtain the desired output (i.e. by offering PS - like external stimuli) with possible applications in neurally-controlled artifacts (robotics, neuroprosthetics).

Zusammenfassung

Der Schwerpunkt der vorliegenden Arbeit lag auf der Untersuchung der Informationsprozessierung im Nervensystem. Das frühe visuelle System ist ein gut untersuchtes Modelsystem, an dem sich untersuchen lässt, wie Informationen über visuelle Reize von der Retina zum Kortex über den Metathalamus (LGN) übertragen sowie kodiert und dekodiert werden.

Die ‘retinogeniculate synapse’ erlaubt es, grundlegende Aspekte der neuronalen Informationsverarbeitung zu studieren. Ähnlich zum ON-OFF Arrangement des Wahrnehmungsfeldes sowohl der Retinalganglienzellen (RGCs) als auch der LGN Neuronen gibt es eine RGC, die die Antwort ihres LGN Neurons Gegenstücks antreibt. Diese synaptische eins-zu-eins-Verknüpfung geht an höheren Ebenen an der ‚geniculo-kortikalen‘ Synapse verloren. Dort projizieren mehrere LGN Zellen konvergent auf ein einziges kortikales Neuron.

Trotz der eins-zu-eins Verknüpfung leiten LGN Neurone nicht einfach die von den RGC Zellen erhaltene Eingabe weiter. Im Gegenteil, die LGN Zellen konvertieren die RGC Aktionspotenzialreihen in neue Reihen in einem Editierungsprozess bevor die visuelle Information an den Kortex weitergeleitet wird. Fast die Hälfte der retinalen Aktionspotenziale gehen dabei an der ‘retinogeniculate synapse’ verloren.

Wie entscheiden LGN Zellen, welches Aktionspotenzial behalten werden muss und welches gelöscht werden kann, ohne den visuellen Informationsfluss zu beeinträchtigen? Welcher Mechanismus liegt dieser Informationsprozessierung zugrunde?

Um diese und andere Fragen zu beantworten, die dem LGN Editierungsprozess des retinalen Eingangssignals entspringen, habe ich ein bekanntes Beispiel der Informationsverarbeitung an der „retinogeniculate synapse“ aufgegriffen: die Richtungserkennung eines sich bewegenden Stimulus.

Mittels Computermodellierung, extrazellulären Ableitungen und angewandter Mathematik für Datenanalyse wurden folgende Aspekte untersucht: (i) die Schärfung der Richtungsselektivität als bekanntes Beispiel der Informationsverarbeitung, (ii) die neuronalen Mechanismen der funktionalen und effektiven Verbindungsherstellung und (iii) der Effektivitätsgrad der Informationsweiterleitung zwischen Neuronen.

Da die Ergebnisse neue Fragen aufwarfen, wurde untersucht, ob diese neuronalen Informationsverarbeitungsmechanismen auch bei anderen Neuronentypen oder Laborbedingungen zu finden sind. Daher wurden die Untersuchungen auf extrazellulär abgeleitete spontane Aktivität in kortikalen und hippokampalen Neuronenkulturen ausgedehnt.

Dem 'paired spiking' (PS) spielt beim Konzept der Effizienzsteigerung durch Ausdünnung (sparse coding efficiency) eine Schlüsselrolle. Sparse coding übernimmt dabei die Rolle eines zeitlichen Filters, der weniger informative Aktionspotenziale bei der Etablierung funktioneller und effektiver Verbindungen zwischen den Neuronen entlang ihres synaptischen Pfades löscht, wobei die transportierte Information von der einen zur nächsten Stufe erhalten bleibt. Da PS nicht nur unter Stimulationsbedingungen auftritt (sowohl *in vivo* als auch *in vitro*), sondern auch in Spontanaktivität und in neuronalen *in vitro* Netzwerken zu finden ist, scheint es sich um einen weitverbreiteten Antworttyp neuronaler Informationsverarbeitung in Nervensystemen unterschiedlichen Spezies und unter unterschiedlichen Bedingungen (*in vitro, in vivo*, Spontan- oder stimulus-induzierte Aktivität) zu handeln.

Die Beobachtung, dass PS sowohl bei einzelnen Neuronen als auch auf Netzwerkebene gefunden wurde, könnte dabei helfen, synaptische Plastizität, Informationsverarbeitung und PS als einen stimulusartigen Kontrollmechanismus von Netzwerkaktivität besser zu verstehen, der sich in neuronal kontrollierten Artefakten (z.B. Robotik, Neuroprothesen) ausnutzen ließe.

Contents

I. Introduction

Overview

Focusing on investigating the manner in which information is processed within the nervous system by merging leading technologies in computational neuroscience, neurobiology, neuroengineering and neuroinformatics, this research work carries a high degree of complexity. The various modes of neurons to process information has gained substantial attention and become a priority for research groups worldwide. Research on this topic pursues many different goals − starting with multidisciplinary fundamental research and ending with evolutionary computing, with outstanding bio-inspired solutions already successfully applied in cutting edge technologies used in different and important fields nowadays (i.e. machine learning, artificial intelligence, medical image processing, and so forth). Despite the fact that computational neuroscience represents a relatively new science, huge international scientific efforts have brought it rapidly on an ascendant slope, with prominent results successfully assimilated worldwide.

In a highly multidisciplinary approach, the research efforts described here aim to gain new insights into topics such as spontaneous neural response in cultured neurons (spatiotemporal patterns of activity, functional and effective connectivity) and stimulated neural activity (with early visual system as a convenient model, elegantly envisaging the topic of direction selectivity (DS)) and thus to suggest models in bio-inspired information processing as well as in studying biological development and plasticity.

One of the steps is to characterize the neural activity at different temporal stages during development of neural networks. Investigating spontaneous electrophysiological activity of neuronal populations during development is one of the key issues for understanding the functional and effective neuronal connectivity formation and their implication in network

plasticity and adaptability. Moreover, spontaneous activity plays an important role in information processing and thus in influencing the stimulus induced activity, sometimes adding substantial noise (that has to be subtracted) or sometimes containing important information. A characteristic of spontaneous activity in developing neural networks is the occurrence of intermittent bursts, separated by periods of reduced activity. One of the scientific hypotheses tested in this research work is self-organization of cultured neurons under a spontaneous activity paradigm with the paired spiking activity (PS) concept playing a key role in revealing the manner in which neurons form functional and effective connectivity within the culture (and thus process information) and develop neural plasticity. Interspike interval (ISI) distribution, burst distribution and firing rate were also analyzed in detail for activity pattern analysis within the cultured neural networks at different stages of development. For this, we used the multielectrode array technique MEA (having the great advantage of allowing recordings and thus observation of activity at different sites in the network simultaneously) to extracellularly record the neural activity and thus realize a long term characterization of spontaneous activity in dissociated cultured cortical and hippocampal neurons.

Another important step was to investigate the stimuli induced neuronal activity. A prominent example of information processing within nervous system is represented by the early visual system. Of a large interest for me is to investigate the manner in which neurons at early stages of visual system edit information concerning direction of motion from time varying images.

Visual information is firstly encoded in trains of action potentials (APs) at the output of the retina by retinal ganglion cells (RGCs). Their axons project toward the higher brain areas via thalamus, the lateral geniculate nucleus (LGN). Here, excitatory and inhibitory synapses are already formed in both directions between the LGN and the primary visual cortex.

The estimation of motion direction from time varying retinal images is a fundamental task of visual systems. Neurons that selectively respond to directional visual motion are found in all species. In many of them already in the retina direction selective neurons signal their preferred direction of movement. Recent evidence suggests that direction selectivity is carried from the retina to higher brain areas. Here we used light stimuli and the extracellularly recorded neural response of direction selective neurons in order to understand how information regarding motion is carried on from one stage to another within the early visual system.

Using not only mechanistic but also descriptive approaches in this work and employing several recently introduced theoretical concepts in modern neuroscience (i.e. conditional firing probability (CFP), information rate (IR), transfer entropy (TE) and spike timing dependent plasticity (STDP), these research efforts will presumably not only improve the knowledge in biophysics of neural computation, but also suggest biologically inspired models which can be implemented in different related fields (for example image processing) by revealing fundamental aspects of how neurons encode and decode information at different synapses under different paradigms (i.e. spontaneous activity versus stimuli induced activity).

Stimuli induced activity - Direction selectivity

The first stages of the visual system are represented by the retina, the lateral geniculate nucleus (LGN) and the primary visual cortex. Visual information is firstly encoded in trains of APs at the output of the retina by one type of retinal cells called retinal ganglion cells (RGCs). Their axons are grouped together and leave the retina through the optic disc passing through the optic chiasm and ending (mostly) in the LGN (Hubel and Wiesel, 1961; Cleland et al, 1976; Kuffler, 1953). Excitatory and inhibitory synapses are then formed in both

directions between the LGN and the primary visual cortex (Hubel and Wiesel, 1962; Buehlmann *et al.*, 2010; Kara and Reid, 2003).

Information flow through the retina is following a direct path, from light receptors to bipolar cells and then to ganglion cells, and an indirect path, in which horizontal cells may be interposed between the receptors and bipolars, and amacrine cells between bipolars and retinal ganglion cells.

The direct path is highly specific or compact, in the sense that one receptor or only relatively few of them feed into a bipolar cell, and only one or relatively few bipolars feed into a ganglion cell. The indirect path is more complex, involving lateral connections. The main interest of my work is focused on RGCs. Ganglion cells receive the incoming signals and produce spike trains that contain precise temporal and spatial information about the patterns of light initially detected by the photoreceptors. There are numerous types of ganglion cells, each of which conveys information about a specific feature of an image detected by the photoreceptors. It has been established that the structure, function, and central projections of RGCs are highly correlated (Berry *et al.*, 1997).

The receptive field (RF) of a cell is defined as the area of visual space within which one can influence the activity of a neuron. The RF is very often used by neurophysiologists to study the function of visually responsive neurons, because it characterizes the transformation between the visual image and neuronal activity (Hubel and Wiesel, 1961). To describe how a neuron processes the visual image, one must characterize its RF in the joint space-time domain (Usrey et al, 1998). It is also well known that the LGN and RGCs have similar centersurround receptive fields.

The mammalian retina contains several different types of ganglion cells, most of which respond to one or more specific features of a visual image, such as contrast, color, or motion. Particular ganglion cell types (of some but not all mammalians) are motion

sensitive, meaning they respond to temporal changes in luminance within their receptive fields, corresponding both to images moving across the field of vision as well as to self-motion of the organism.

A subset of motion sensitive cells responds differentially to the directions of stimulus motion. These direction selective (DS) ganglion cells show interesting properties, most of which have been subject to extensive research efforts over the last 40 years. Firstly, Barlow and Levick in 1964 (Barlow *et al.*, 1963; Barlow and Levick; 1964) deduced that inhibitory inputs to a DS cell make ineffective excitation for movement in the cell's *null* direction, while excitatory inputs are strongly enhanced for movement in the preferred direction. Movement in intermediate directions produces intermediate levels of inhibition or excitation which are used to calculate the degree of directional tuning (Taylor and Vaney, 2002).

Research efforts conducted on rabbit retinas have revealed two different types of DS ganglion cells in the retina – ON OFF DS cells and ON DS cells. ON OFF DS cells show the response to the movement of a stimulus that is lighter or darker than the background field, while ON DS cells are excited only by objects that are lighter than the background. Several other discrepancies between these two cell types' responses construct a particular spike train signature for each of them (Zeck *et al.*, 2007).

ON OFF DS cells respond to high values of stimulus speeds. ON DS cells, in contrast, respond optimally to stimuli moving at slow speeds, have larger receptive fields and are less encountered than ON-OFF DSRGCs.

Four subtypes of ON OFF DS cells can be classified by the orientation of the preferred direction of the cell, which points to one end, either onto the horizontal or vertical ocular axis. Each of the four types responds preferentially to objects moving either to the left, right, top, or bottom. The retina is completely covered by the receptive fields of each subtype of ON-OFF DS cell (Devries and Baylor, 1997). ON DS cells comprise only three

distinct subtypes; the preferred directions of each ON DS cell points in one of three directions aligned with a different set of axes.

The ON-OFF and ON cell types send the directional information to different nuclei, the ONOFF DS cells to the dorsal LGN and the superior colliculus, whereas the ON DS cells represent the main input to the accessory optic system. The functional properties of cells in the accessory optic system are consistent with their input from ON-DS cells in many species including primates (Vaney *et al.*, 1981a; Vaney *et al.*, 1981b; Ackert *et al.*, 2006; Oyster *et al.*, 1968; Amthor *et al.*, 1989a; Amthor *et al.*, 1984; Jagadeesh *et al.*, 1997; Jensen *et al.*, 1983; Buhl and Peichl, 1986; Cleland *et al.*, 1971; Cleland *et al.*, 1976; Danjanovic *et al.*, 2009; Dann *et al.*, 1987; Grasse *et al.*, 1984; He and Masland, 1998; Hoffmann and Distler, 1989; Heberman *et al.*, 2009; Kim *et al.*, 2008).

Barlow *et al.*, 1965, characterized ON-OFF direction selective ganglion cells in the rabbit retina and proposed for the first time a model for direction selectivity, in which asymmetry of either excitation or inhibition is required. After many research efforts on this topic, there is not yet known exactly where and how direction selectivity in ON-OFF DSRGCs is achieved. Over the years it has been generally accepted that direction selectivity is mediated mainly by the suppression of excitation during movement in the null direction, but not in the preferred direction. Recent results show that excitation and inhibition are already direction selective, that is, excitation is larger during the preferred direction while inhibition is larger during the null direction. This implies that direction selectivity is already computed presynaptically to DSRGCs and an important role has been distributed to starburst amacrine cells (SbAC). SbACs are suggested to offer the spatial asymmetry needed for computation of motion direction by generating larger dendritic Ca^{2+} signals when motion is from their somata towards their dendritic tips rather than for motion in the opposite direction. However, evidences of direction selectivity computation at postsynaptic level were also

revealed, consisting mainly in postsynaptic interaction of the excitation with spatially offset inhibition. Presumably pre- and post-synaptic mechanisms, at multiple layers and sophisticated connectivity, both determine direction selectivity at DSRGCs (Stasheff and Masland, 2002, Amthor and Grzywacz, 1993, Fried *et al.*, 2002, Taylor and Vaney, 2002; Euler *et al.*, 2002; Koizumi *et al.*, 2004).

In a decisive work, Levick (Levick *et al.*, 1969) demonstrated that neurons postsynaptic to DSRGCs are signaling the direction of the visual stimulus motion more selectively than their counterparts. He found direction selective neurons in the LGN of rabbits to be more directional selective. Levick's model proposed a sharpening in directional selectivity at an LGN neuron based on convergent input of different DSRGCs, with similar receptive field, but with opposite preferred direction, upon the same LGN neuron. Blitz and Regehr (Blitz and Regehr, 2003 and 2005) have shown that most of the LGN cells are receiving inputs from one to three RGCs.

However, it is generally agreed that there is one single RGC that mainly drives one LGN neuron counterpart (Cleland *et al.* 1971, Kaplan *et al.* 1987, Usrey *et al.* 1998, Sinchich *et al.* 2007) so that one third of LGN neurons could receive also inhibitory inputs from the same RGC counterpart, but with 1 ms delay (so called locked inhibition) while two thirds could receive inhibitory inputs with different time delay from different RGCs – the so called nonlocked inhibition (Blitz and Regehr; 2005).

Recently, Casti *et al.* 2007, and Carandini *et al.* 2007, have shown that using simple models one could investigate the retinogeniculate synaptic mechanism. They are based on the idea that the most important factor influencing information transmission from RGCs to LGN neurons could be post-synaptic summation whereas presynaptic plasticity might not be a primordial mechanism in the editing of retinal spikes.

Paired spikes efficacy enhancement was already shown at the retinogeniculate synapse. Sequences of rapid firing activity have a better chance to induce postsynaptic spikes than

isolated input spikes (Carandini 2007, Usrey *et al.*, 1998; Bair, 1999). While single excitatory postsynaptic potentials (EPSPs) on their own do not reach threshold, rapid spiking activity in the DSRGC can trigger LGN spikes. The role of synaptic plasticity at the retinogeniculate synapse is not yet well understood since additionally inputs other than retinal afferents (cortical, reticular or brainstem) can complicate modeling of the LGN neuron discharge. In a simplified approach, taking into account only direct synaptic connections between DSRGCs and their postsynaptic counterparts, we showed further on in this work, that sharpening in direction selectivity at postsynaptic level is achieved based on intrinsic properties of ON-OFF DSRGCs combined with postsynaptic summation and spike threshold.

Receptive fields (RFs) become progressively more sophisticated along the synaptic hierarchies from retina to cortex. However, for the LGN cells the center surround RFs are similar to those of retinal afferents (Hubel & Wiesel, 1962; Kuffler, 1953; Reid *et al.*, 2004). With this advantage in mind, together with the fact that the receptive field center of LGN cells receives its main input from only one retinal ganglion cell (RGC) (Cleland *et al.*, 1971; Sincich *et al.*, 2007; Usrey *et al.*, 1999), the retinogeniculate synapse is of major interest for studying the role of interspike interval (ISI) based mechanisms for spike filtering and visual information processing (Casti *et al.*, 2007, Rathbun *et al.*, 2007; Carandini *et al.*, 2007; Sincich *et al.*, 2009; Rathbun *et al.*, 2010). Already at the next stage within the early visual system, neurons in layer 4 of the primary visual cortex receive many more convergent inputs from LGN counterparts (Reid and Usrey, 2004) and thus they rely more on the interaction between different inputs than on the ISIs of individual inputs as part of the mechanism to reach the spike threshold (Usrey *et al.*, 2000).

Retinal spikes with preceding short ISIs have greater chances to induce APs at their postsynaptic target than “isolated” spikes. The efficacy to evoke APs at the postsynaptic target in the LGN decreases considerably with an increase of retinal ISIs. For retinal ISIs

longer than about 30 ms there is no detectable influence of ISIs on the production of postsynaptic spikes (Usrey *et al.*, 1998; Sincich *et al.*, 2007). Furthermore, recent studies suggest that this temporal filter acting upon retinal spiking activity is correlated with a visual stimulus. Therefore visual information regarding optimal stimulus features is preserved and transmitted further on at the postsynaptic target (Rathbun *et al.*, 2007, Uglesich *et al.*, 2009, Sincich *et al.*, 2009; Rathbun *et al.*, 2010).

To investigate the manner in which RGCs of different types process information in response to light stimuli I have used data sets recorded from retinal ganglion cells of the adult isolated rabbit retina. The data acquisition using a 60 channel multi-electrode array (Multichannelsystems, Reutlingen, Germany) and off-line analysis has been already described in (Zeck and Masland 2007).

Direction selectivity was tested using a square wave spatial grating moved in $N = 8$ equally separated directions $\varphi_i = i \cdot (2\pi/N)$, $i = 0,1,\ldots,N-1$. For each direction the grating (spatial frequency 1 cycles/mm) was presented for 7 seconds at a temporal frequency of 1 Hz followed by a stimulus-free interval of the same length. The total stimulus length ranged from 600 to 1200 seconds. The spatial extent of the moving grating was ~ 7 μm^2 on the retina. Thus, multiple cells were stimulated and recorded simultaneously.

Individual tuning curves were obtained considering the firing rate of each cell for each of the eight equidistant directions.

To quantify the directional tuning of a neuron, we used the direction selectivity index (*DSi*) as described by Taylor and Vaney (2002),

$$DSi = \frac{\left\| \sum_i \vec{v}_i \right\|}{\sum_i r_i}, \qquad \vec{v}_i = r_i \begin{pmatrix} \cos\varphi_i \\ \sin\varphi_i \end{pmatrix}.$$

$\vec{v}_i$ is a vector pointing in the direction of the stimulus with the length equal to the number of spikes recorded during presentation of the stimulus (r_i). The *DSi* explains the directional tuning based on the firing rates for different particular movement directions of the visual stimulus. The minimum value of 0 characterizes a non-directional neuron, whereas the maximum value of 1 characterizes a neuron that responds to a single direction of movement. The higher the *DSi*, the higher is the direction selectivity. For ON-OFF DSRGCs usually the DSi is around 0.5 while for ON DSRGCs the DSi was found to be around 0.3 (Zeck *et al.*, 2007; He and Masland, 1998).

I then looked into more details and investigated intrinsic properties of RGCs like rapid boats of firing activity. In the literature, burst-like neural activity was described as (at least) two spikes occurring after a prolonged period of silence, i.e. inter spike interval (ISI) larger than 50 ms, followed by an ISI shorter than 5 ms (Godwin *et al.* 1996b; Guido *et al.* 1995; Lu *et al.* 1992). Burst rate r^{burst} was defined as the number of burst-like firing events per time. The index of selectivity for bursting activity was then calculated similarly to that for the firing rate:

$$DSi^{burst} = \frac{\left\| \sum_i \vec{v}_i^{burst} \right\|}{\sum_i r_i^{burst}} \quad , \quad \vec{v}_i^{burst} = r_i^{burst} \begin{pmatrix} \cos \varphi_i \\ \sin \varphi_i \end{pmatrix}$$

To check the sharpening in direction selectivity, we modeled the postsynaptic neuron representing the LGN cell which receives recorded input from retinal ganglion cells. To do so I used an 'Integrate and Fire' model with afterhyperpolarization effect and varied the conductance values within a biophysically reasonable range as described in the literature (Casti et al, 2008):

$$C_m \frac{dV}{dt} = -(V - V_{\text{rest}})g_m - (V - E_a)\sum_f g_a(t - t_f) - (V - E_e)\sum_s g_e(t - t_s)$$

The time-dependent conductances are modeled using a model described by (Rall 1967; Jack *et al.* 1975):

$$g_X(t) = \begin{cases} g_{\max,X} \dfrac{t}{\tau_X} e^{1-\frac{t}{\tau_X}}, & t \geq 0 \\ 0, & t < 0 \end{cases}, \quad X \in \{a, e, i\}$$

While the relay cells in the LGN do not simply pass the incoming retinal input further on toward the striate cortex we defined a transfer ratio which let us know the percentage of successful retinal spikes in generating APs at s postsynaptic simulated neuron:

$$TFR = \frac{\#\text{SPN spikes}}{\#\text{DSRGC spikes}}$$

To compare the direction selectivity of the output of the simulated postsynaptic neuron (SPN) with that of the driving neuron, we define the index of sharpening *iS* as:

$$iS = \frac{DSi(SPN)}{DSi(DSRGC)}.$$

iS > 1 means that the SPN shows higher directional selectivity than the presynaptic neuron. For spike transfer ratios below 0.07, or above 0.7, we set *iS* to zero.

Further on, in order to investigate which properties of spike trains effect sharpening, we also generated "artificial spike trains". These spike trains have the same average spike rates for different stimulus directions - and thus the same *DSi* - as spike trains recorded from DSRGCs. The firing probability was equally distributed over time according to a Poisson

process except for defined refractory periods after each spike event. Spike trains with a refractory period of 2 ms, 5 ms and 20 ms were generated.

In the next investigation I asked how time spiking is shaping the neural activity already presynaptic to LGN cells? I used the data generated by extracellularly stimulation of RGCs with a white noise stimulus. The experimental set-up consisted in a sixty channel multielectrode array MEA with a 30 µm spatial resolution (Multichannelsystems, Reutlingen, Germany) for electrophysiological recordings.

The receptive field was mapped using a white noise stimulus (temporal flat power spectrum in the 1–30 Hz range) which comprised a 16×16 array of squares (pixels) with a frame rate of 50 Hz. The luminance of each square was independently modulated by an msequence (Reid *et al.*, 1997). The size of each square was 75 µm and the size of the receptive field of each cell was calculated by reverse-correlating the stimulus and spike response, and considering checkers whose intensity at the temporal maximum of the mean effective stimulus exceeded by a factor of 3 the SD of the squares in the background (DeVries & Baylor, 1997). The stimulus duration was T= 30 s and the stimulus was repeated n = 30 times.

A spike-triggered average (STA) was calculated after the spikes were sorted into different categories according to ISI values $0 < ISI \leq 10$ ms; $10 < ISI \leq 20$ ms; $20 < ISI \leq 50$ ms; $50 < ISI \leq 100$ ms. In the last category, the STA was calculated for all spikes in the spike trains.

We calculated the STA as the average over all the stimuli which shortly preceded a spike (Paninski, 2003; Schwartz *et al.*, 2006).

$$STA(\tau) = \frac{1}{\langle Nsp \rangle} \langle \sum_{i=1}^{Nsp} S(ti - \tau) \rangle ,$$

, where *Nsp* is the number of spikes, *ti* is the time of occurrence $\langle Nsp \rangle_{i=1}$ of spike i, *s(t)* is the stimulus at time t, and the angle brackets represent averaging over trials.

We represent the spike train *ρ(t)* as a sum of infinitesimally narrow, idealized spikes in the form of Dirac *δ* functions:

$$\rho(t) = \sum_{i=1}^{Nsp} \delta(t - ti)$$

Thus, STA(τ) can be expressed as an integral of the stimulus times of the neural response function:

$$STA(\tau) = \frac{1}{\langle Nsp \rangle} \int_0^T r(t)s(t-\tau)dt \,,$$

, where *T* is the total duration of a trial and *r(t)* is the firing $\langle Nsp \rangle_0$ rate at time t. The correlation function of the firing rate r at time t and stimulus s at time (t+τ) is denoted by:

$$Corr(\tau)_{rs} = \frac{1}{T} \int_0^T r(t)s(t+\tau)dt \,.$$

Finally, the STA(τ) as the correlation between stimulus and neural response was calculated by:

$$STA(\tau) = \frac{T}{\langle Nsp \rangle} Corr(-\tau)_{rs} = \frac{1}{\langle r \rangle} Corr(-\tau)_{rs} \,, \text{MCorr} = \max\left(|\text{STA}\ (\tau)|\right)$$

The maximum of an STA (τ), given by MCorr (Martiniuc and Knoll, 2012), was indicating the maximum correlation between a stimulus and a neuronal response, for each of the ISI categories, and has the dimension of light intensity.

To compare the direction selectivity for different ISI values with the direction selectivity for the entire recorded activity we defined the following index as ISI directional index (SI):

$$SI = \frac{DSi(ISI)}{DSi(DSRGC)}.$$

DSi (DSRGC) represents the index of selectivity calculated for all recorded activity as and *DSi(ISI)* represents the directional tuning calculated for the separated retinal spikes according with different ISI values, as mentioned above. This index is quantified similarly to the DSi as described by Taylor and Vane (2002) taking into account that for each stimulus movement direction we took the total number of ISIs (of a certain value) into account instead of the total number of spikes.

To calculate the post stimulus time histograms (PSTH) we aligned the spike sequences with the onset of stimuli that repeated n times. For periodic stimuli (grating bars), we moved the response sequence back to time zero after each time period T, and counted n as the total number of periods of data. We then divided the stimulus period T into N bins of size Δ and counted the number of spikes ki from all n sequences that fall in the bin i. The optimal bin size Δ results from minimizing: $(2k-\sigma)/\Delta^2$, where k is the mean of ki and σ is the variance of ki (Shimazaki and Shinomoto, 2007).

We then averaged the calculated PSTH for the n stimuli repetitions (n = 30 for white noise stimulus and n = 7 for grating drifting bars stimulus) and obtained the time-varying average firing rates <r(t)>.

In order to evaluate the information about the stimulus carried by single spikes we used the above calculated time varying average firing rates <r(t)> and computed the estimates of entropy (H) as follows (Strong *et al.*, 1998; Brenner *et al.*, 2000; Sincich *et al.*, 2009; Casti *et al.*, 2009; Rathbun *et al.*, 2010):

$$H = \frac{1}{T}\int dt \frac{r(t)}{< r(t) >} \log_2 \frac{r(t)}{< r(t) >}$$

We calculated H for n = 20 cells for a white noise stimulus and n = 12 cells for a drifting grating bar stimulus and for each of the ISI categories mentioned at the beginning. Additionally, for the second stimulus we calculated H for each of the eight equidistant directions of stimulus movement.

Thus, we could estimate the entropy tuning for each cell, and evaluate the amount of information carried at each direction of stimulus movement similarly with the equation we used to estimate the direction selectivity index (*DSi*) as described by Taylor and Vaney (2002):

$$DSiH = \frac{\left\| \sum_i \vec{v}_i H \right\|}{\sum_i H_i} \quad , \vec{v}_i H = H_i \begin{pmatrix} \cos\varphi_i \\ \sin\varphi_i \end{pmatrix}$$

H_i represents the entropy for each of the stimulus direction of movement.

To take into account the problem of the size limitation of data and to correct the resulting bias, the information rates were estimated by extrapolating the entropy H_c from segments of the total data in an increasing order for different bin sizes ($\nabla\tau$) and fit by (Strong *et al.*, 1998):

$$H(T, \nabla\tau) = H_c(\nabla\tau) + \frac{H1(T, \nabla\tau)}{size} + \frac{H2(T, \nabla\tau)}{size^2}$$

The linear dependence gave a good fit for all cells included in our analysis. This measure of information rates does not make any deduction about the number of relevant stimulus features. It informs about the amount of information (bits/spikes) contained in single spikes.

Spontaneous activity – Cultures of dissociated neurons

Both *in vivo* and *in vitro,* synchronously correlated activity, known as bursting activity, is one of the mechanisms which shape interconnectivity and process information, either at single cell level

or at multiple sites being dynamically linked in space and time (van Pelt *et al.,* 2004; Wagenaar *et al.,* 2005; Wagenaar *et al.,* 2006; Sun *et al.,* 2010; Rolston *et al.,* 2007; Mazzoni *et al.,* 2007; McCabe *et al.,* 2006).

Bursting not only occurs in brain slices with partially intact interconnectivity (Blankenship and Feller 2010; Rolston *et al.,* 2007), but can be also found in neural cultures derived from dissociated brain tissue where it becomes predominant as cultures mature (Wagenaar *et al.,* 2005; Wagenaar *et al.,* 2006). Bursting activity varies not only with culture age (Nadasdy 2000; van Pelt *et al.,* 2004), but also with other factors, i.e. culture density (Wagenaar *et al.,* 2006).

However, different spatio-temporally recurring patterns occur in both stimulus-induced (Ferrández *et al*., 2013) and spontaneous activity. They are usually dynamic over time (i.e. the spatial location of active sites may change), thereby having different, yet characteristic spatio-temporal shapes (Shahaf and Marom, 2001; van Pelt *et al.,* 2005; Sun *et al.,* 2010; DeMarse *et al*., 2001; Pasquale *et al.,* 2008; Pasquale *et al.,* 2010; Ruaro *et al.,* 2005; Nadasdy 2000; Nomura *et al.,* 2009).

Without any external stimulus, cultured neurons show significant changes in their spontaneous neural activity at different stages toward maturity. Moreover, network activity fluctuations at later stages may be a consequence of repetitive internal stimuli that revive prior network activity and alter network connectivity to compensate for the lack of external stimuli. Such self-organized events based on spontaneous neural activity were previously reported at different culture ages (Rolston *et al.,* 2007; Pasquale *et al.,* 2010; Sun *et al.,* 2010).

Both, *in vivo* and *vitro*, stimuli may trigger bursting (Krahe 2004; Akerberg 2011) and PS activity. The early visual system is a prominent example. There, PS activity in retinal ganglion cells is driving suprathreshold responses at postsynaptic targets in the lateral geniculate nucleus (Usrey *et al.,* 1998; Sincich *et al.,* 2007; Weyand, 2007). PS enhancement contributes to preserving the information of a visual stimulus from one processing stage to the next (Rathbun *et al.,* 2010; Sincich *et al.,* 2009; Uglesich *et al.,* 2009). It has been shown that the second spike in

a pair evoked a postsynaptic potential with maximum efficacy for interspike intervals (ISIs) in the range of 2 - 5 ms. Efficacy rapidly decreased to zero for ISIs larger than 40 ms (Usrey *et al.,* 1998; Sincich *et al.,* 2007).

However, little is known on the evolution and role of PS activity in neural cultures derived from dissociated brain tissue, on its relationship to bursting activity and on its participation in the organization of functional and effective network connectivity. To answer these questions, I defined activity consisting of two spikes being separated by an interval of up to 5 ms followed by an inter-paired-spike interval (IPSI) larger than 40 ms as PS activity. I then analyzed 58 streams of continuously extracellularly recorded spontaneous neural activity in random networks for PS occurrence and for the spatio-temporal evolution of PS activity patterns over several weeks. In this context, I wondered whether any PS-induced effect was locally confined or led to changes on network level. I finally investigated PS activity robustness and independence in driving spontaneous neural activity concerning functional and effective connectivity and synaptic plasticity.

The data for this analysis was provided by a recently developed cell culture perfusion system that allowed us to continuously track both network activity and morphology on the lab bench at ambient CO_2 levels under rather well controlled environmental conditions (i.e. pH, temperature and osmolality).

Following standard tissue dissociation protocols (Banker and Goslin, 1998), hippocampal and cortical neurons were harvested from dissociated brain tissue extracted from embryonic rats at E18. They were plated at a density of ~60,000 neurons/mm^2 on autoclaved and pretreated microelectrode arrays (hippocampal on 8 × 8 30/200iR TiN and cortical on 6 × 10 30/500iR TiN, , Multi Channel Systems, Germany). Cultures were kept in timed perfusion culture at 35.5 - 36.5°C during spike-train acquisition.

Extracellular signals were recorded and processed by a commercial 60-channel, 10 Hz - 3 kHz bandpass filter-amplifier data acquisition system (25 kHz sampling rate per channel) for upright microscopes with heating platform (MEA60, Multi Channel Systems, Germany). The recording environment was shielded by a grounded metal cap. To reduce data file size, only upward (positive) and downward (negative) spike cutouts from 57 (cortical) and 58 (hippocampal) out of 60 recording electrodes were stored in 5 min packets. They consisted of 5 ms pre-spike and 5 ms post-spike fragments after first threshold crossing at ± 5.5 SD with respect to peak-to-peak noise. Only timestamps from downward threshold-crossings were extracted using Neuroexplorer (Nex Technologies). After removing simultaneous timestamps that occurred on all channels due to electrical or handling artefacts, subsequent 5 min datasets comprised of 58 timestamp streams were bundled in 12 hours timestamp packets for further analysis in Matlab (MathWorks). In the following, these half day packets will be called trials of duration $T_{Trial} \leq 12$ h. On some days, trials encompassed less than 12 h due to temporary interruptions for system reconfiguration, maintenance work or power failure. Our recording sessions consisted of 65 trials (32.5 DIVs) for the hippocampal culture and 106 trials (53 DIVs) for the cortical culture.

The MEA socket in its base plate featured a resistive heating element and a Pt-100 temperature sensor. An external T-control unit (Multi Channel Systems HC-1) kept the temperature of the socket surface at ≤36.5 °C. The amplifier was mounted onto a fixed, custom-made stage of an inverted microscope (Zeiss Axiovert 200). To avoid the need for lifting the cap during MEA insertion, a custom-made spacer between the base-plate with embedded heating plate and the amplifier stage created a gap for the free passage of the cap tubing. For the same reason, the lower right corner of each MEA had been diagonally cut off with a diamond pen.

Time-lapse pictures were taken by a remote-controlled (Breeze Systems PSRemote) digital consumer camera (Canon G2/G9) attached to the camera port of the microscope. Initially, cultures were constantly illuminated by the built-in halogen lamp of the microscope.

One notable advantage of this outside-incubator lab bench experimental set-up is that it did not require any other cell culture infrastructure such as incubators and sterile hoods which limit experimental possibilities. Usually, most cell culture studies, depending on experimental screening tools at ambient conditions, rely on taking exemplary, quasi-static data snapshots over limited temporal periods, mainly to prevent drifts in pH and osmolality. Instead we used a perfusion concept tailored to microelectrode array (MEA)-based long-term electrophysiology and time-lapse morphology studies of network dynamics in neural cultures (Blau *et al.*, 2009).

Based on the previously described findings by Ursey (Usrey *et al.,* 1998) and Sincich (Sincich *et al.,* 2007), we investigated the occurrence and effect of paired spiking on neural activity in network cultures. Equally, we scanned all the NSTs using the above mentioned algorithm and quantified the PS activity at network level for each trial. In this case, the two spikes separated by an interval of up to 5 ms and followed by an IPSI larger than 40 ms did not necessarily have to be recorded from the same electrode.

In order to evaluate the information about the stimulus (PS) carried by individual spikes following a PS within the time window of T_{PS} = 2 s, we used the above calculated time varying firing rates r(t) and computed the entropy estimates (H) as follows (Strong *et al.*, 1998; Brenner *et al.*, 2000; Sincich *et al.*, 2009):

$$H = \frac{1}{T_{PS}} \int_0^{T_{PS}} \frac{r(t)}{< r >} \log_2 \frac{r(t)}{< r >} dt$$

where T_{PS} = 2 s represents the duration of a stimulus set and <r> the average firing rate; the bin size was Δt = 5 ms.

For each particular trial, we obtained the average estimate for information content per spike by averaging the estimated entropy by the number of stimulus repetitions n:

$$\langle H \rangle = \frac{1}{n} \sum_{i=1}^{n} H_i$$

To account for limited dataset size and to correct the resulting bias, the information content per spike was estimated as a function of bin size Δt. We performed a linear fit to these data to extract the intercept corresponding to the limit when Δt approaches zero. We used the shuffle verification method to check for robustness of information content per spike.

To investigate whether PS activity plays a role in shaping the dynamic interconnectivity map at different developmental stages, we adopted a variant of a cross-correlation algorithm initially introduced as conditional firing probability (CFP; le Feber *et al.,* 2007). This method was widely used in the investigation of activity relationships between different electrodes to reveal the formation and strength evolution of functional connectivity within *in vitro* networks (Zullo L *et al.,* 2012; Chiappalone *et al.,* 2007; Garofalo *et al.,* 2009). Here, we used CFP to reveal any PS-related cross-correlations between different sites within the network. Above mentioned concepts (i.e. information content per spike and CFP) quantify statistical dependences in observed variables (i.e. recorded spike trains) describing functional connectivity maps and does not allow us to investigate the direction of information flow (i.e.

the causality) between the recorded units. By definition (Wienner, 1956), an effective connectivity between two neurons exists when knowledge about the past of one neuron predicts the future activity of its counterpart better than the prediction based on the past activity of the receiver (neuron) alone. This effective connectivity is quantified by the information – theoretic measure called transfer entropy (TE), first time introduced by Schreiber (Schreiber, 2000). TE is an asymmetric measure of interactions between two coupled neurons that allow us to determine the direction of information flow between recorded units. In our work TE is positive, and thus the information is directed from the recorded unit A to the recorded unit B (i.e. there is an

effective connectivity from the unit A to the unit B) when the information about the spiking activity recorded at the unit A improves prediction of the spiking activity in the future of the unit B better than can be predicted only by the past spiking activity recorded at the unit B alone. Thus, to identify and assess effective connectivity within our recorded spiking activity of the cultured neurons, we used a recently introduced toolbox for TE calculation (Ito *et al.*, 2011) derived from original definition given by Schreiber (Schreiber, 2000) as follows:

$$TE_{A\to B} = \sum p(B_{t+1}, B_t^k, A_t^l) \log_2 \frac{p(B_{t+1}|B_t^k, A_t^l)}{p(B_{t+1}|B_t^k)}$$

The complete description of the TE toolbox algorithm is thoroughly done in Ito *et al.*, 2011. Briefly, for our work A_t depicts whether at time t we recorded a spike at unit A (and thus the value is one) or we have no spike at the same unit (and thus the value is zero). Similarly B_t and B_{t+1} describe the status of unit B at the moments t and t+1. Conditional probabilities of observing the particular status of units A and B described in parentheses are marked by vertical bars while the sum is over all possible combinations B_{t+1}, B_t^k and A_t^l, where parameters k and l express the number of time bins in the past that allow us to take into account the time delay and the length of the message when calculating TE. For biophysical reasonability we chose k = 1:30 ms and l =1:250 ms.

Paper 1

Paired spiking robustly shapes spontaneous activity in neural networks *in vitro*

Aurel Vasile Martiniuc[1]*, Victor Bocos-Bintintan[2], Rouhollah Habibey[3], Asiyeh Golabchi[3], Alois Knoll[1], Axel Blau[3] [1]

Computer Science Department VI, Technical University Munich, Garching, Germany.

[2]Faculty of Environmental Science & Engineering, Babeş-Bolyai University, Cluj-Napoca, Romania. [3] Department of Neuroscience and Brain Technologies, Italian Institute of Technology, Genoa, Italy.

*__Correspondence:__Mr. Aurel Vasile Martiniuc, Computer Science Department, Robotics and Embedded Systems, Boltzmannstraße 3, Garching 85748, Germany, martiniv@in.tum.de

Submitted to *Frontiers in Neural Circuits*

Summary of the paper

In this paper I explored the active implication of paired spiking activity in shaping the neural activity recorded from dissociated cultures of neurons from cortex and hippocampus. The work is original from many points of view. One major noticeable aspect is that up to my knowledge there are no scientific works dedicated to paired spiking activity in cultured neurons. In this paper I show that PS not only that exists under spontaneous activity paradigm in such neuronal cultures but also it establish spatio-temporal patterns that starts from early days in vitro (DIVs) and lasts until the end of recordings. Their shapes, however are getting more and more complex as the culture matures by attracting new neighbours neurons and increasing the number of repetitions and the inter pair spike intervals (IPSIs). Additionally, PS activity is robustly involved in establishing functional and effective connectivity within the neural network at different stages of development. Paired spiking activity (PS) was reported in vivo and in intact brain architecture, for different cell types and now in cultures of dissotiated tissue under spontaneous (non-stimulated) paradigm. Presumably it acts as an internal surrogate stimulus that robustly drives the neural ativity during different developmental stages reviving the activity in lack of any stimulus. If that holds true, exploring PS may open new doors in scientific efforts concerning closed-loop paradigm in controlling the neural output as response to a stimulus protocol with possible applications in robotics and/or neuroprosthetics.

My contribution to this paper is as follows: I participated in defining the scientific project, analyzing the recorded neural data, writing the paper, editting the paper and I am the corresponding author.

II. Paired spiking robustly shapes spontaneous activity in neural networks *in vitro*

Abstract

In vivo, neurons establish functional connections and preserve information along their synaptic pathways from one information processing stage to the next in a very efficient manner. Paired spiking (PS) enhancement plays a key role by acting as a temporal filter that deletes less informative spikes. We analyzed the spontaneous neural activity evolution in a hippocampal and a cortical network over several weeks exploring whether the same PS coding mechanism appears in neuronal cultures as well. We show that self-organized neural *in vitro* networks not only develop characteristic bursting activity, but feature robust *in vivo* like PS activity. PS activity formed spatiotemporal patterns that started at early days *in vitro* (DIVs) and lasted until the end of the recording sessions. Initially random-like and sparse PS patterns became robust after three weeks *in vitro* (WIVs). They were characterized by a high number of occurrences and short inter-paired spike intervals (IPSIs). Spatially, the degree of complexity increased by recruiting new neighboring sites in PS as a culture matured. Moreover, PS activity participated in establishing functional connectivity between different sites within the developing network. Employing transfer entropy (TE) as an information transfer measure, we show that PS activity is robustly involved in establishing effective connectivities. Spiking activity at both individual sites and network level robustly followed each PS within a short time interval. PS may thus be considered a spiking predictor. These findings suggest that PS activity is preserved in spontaneously active *in vitro* networks as part of a robust coding mechanism as encountered *in vivo*. We suggest that, presumably in lack of any external sensory stimuli, PS may act as an internal surrogate stimulus to drive neural activity at different developmental stages.

Keywords: cultured neurons, paired spiking activity, uninterrupted recording, bursting activity, neural information content per spike

1. Introduction

Both *in vivo* and *in vitro,* synchronous correlated activity known as bursting is one of the information processing mechanisms that shape network interconnectivity, both at single cell and network level (van Pelt *et al.,* 2004; Wagenaar *et al.,* 2005; McCabe *et al.,* 2006; Wagenaar *et al.,* 2006; Rolston *et al.,* 2007; Mazzoni *et al.,* 2007; Sun *et al.,* 2010). Bursting not only occurs in brain slices with partially intact interconnectivity (Blankenship and Feller 2010; Rolston *et al.,* 2007), but is also found in neural cultures derived from dissociated brain tissue where it becomes predominant as cultures mature (Wagenaar *et al.,* 2005; Wagenaar *et al.,* 2006). Bursting activity varies with culture age (Nadasdy 2000; van Pelt *et al.,* 2004), and other factors, i.e. culture density (Wagenaar *et al.,* 2006).

Different spatio-temporally recurring patterns occur in both stimulus-induced (Ferrández*et al*., 2013) and spontaneous activity. They are usually dynamic over time (i.e. the spatial location of active sites may change), thereby having different, yet characteristic spatio-temporal shapes (Shahaf and Marom, 2001; van Pelt *et al.,* 2005; Sun *et al.,* 2010; DeMarse *et al*., 2001; Pasquale *et al.,* 2008; Pasquale *et al.,* 2010; Ruaro *et al.,* 2005; Nadasdy 2000; Nomura *et al.,* 2009).

Without any external stimulus, cultured neurons show significant changes in their spontaneous neural activity at different stages toward maturity. Moreover, network activity fluctuations at later stages may be a consequence of repetitive internal stimuli that revive prior network activity and are thought to alter network connectivity to compensate for the lack of external stimuli. Such self-organized events based on spontaneous neural activity were previously reported at different culture ages (Rolston *et al.,* 2007; Pasquale *et al.,* 2010; Sun *et al.,* 2010).

Both, *in vivo and vitro*, stimuli may trigger bursting (Krahe 2004; Akerberg 2011) and PS activity. The early visual system is a prominent example. PS activity in retinal ganglion cells is driving suprathreshold responses at postsynaptic targets in the lateral geniculate nucleus (Usrey *et al.,* 1998; Sincich *et al.,* 2007; Weyand, 2007). PS enhancement contributes to preserving the

information of a visual stimulus from one processing stage to the next (Rathbun *et al.,* 2010; Sincich *et al.,* 2009; Uglesich *et al.,* 2009). It has been shown that the second spike in a pair evoked a postsynaptic potential with maximum efficacy for inter-spike intervals (ISIs) in the range of 2 - 5 ms. Efficacy rapidly decreased to zero for ISIs larger than 40 ms (Usrey *et al.,* 1998; Sincich *et al.,* 2007).

However, little is known on the evolution and role of PS activity in neural cultures derived from dissociated brain tissue, on its relationship to bursting activity and on its participation in the organization of functional and effective network connectivity. To address these questions, we defined activity consisting of two spikes being separated by an interval of up to 5 ms followed by an inter-paired-spike interval (IPSI) larger than 40 ms as PS activity (Methods 2.3). We then analyzed 58 streams of continuously extracellularly recorded spontaneous neural activity in random networks for PS occurrence and for the spatio-temporal evolution of PS activity patterns over several weeks. In this context, we wondered whether any PS-induced effect was locally confined or led to changes on network level. We finally investigated the robustness of PS activity and its independence in driving spontaneous neural activity, thereby affecting functional and effective connectivity.

2. Materials and methods

2.1 Continuous 59-channel MEA electrophysiology and spike train assembly

The data for this analysis was provided by a recently developed cell culture perfusion system that allowed us to continuously track both network activity and morphology on the lab bench at ambient CO_2 levels under rather well controlled environmental conditions (i.e. pH, temperature and osmolality). Technological and procedural details will appear in a dedicated article (Saalfrank *et al.*, submitted). With this setup, the activity evolution in a hippocampal and a cortical network on MEAs was continuously recorded over 30 and 53 days *in vitro* (DIV),

respectively. These datasets were analyzed for PS activity. To reduce data file size, only upward (positive) and downward (negative) spike cutouts from 57 (cortical) and 58 (hippocampal) out of 59 recording electrodes were stored in 5 min packets. They consisted of 5 ms pre-spike and 5 ms post-spike fragments after first threshold crossing at ± 5.5 SD with respect to peak-to-peak noise (Suppl. Fig. 1(A)). Only timestamps from downward thresholdcrossings were extracted using Neuroexplorer (Nex Technologies). After removing simultaneous timestamps that occurred on all channels due to electrical or handling artefacts, subsequent 5 min datasets comprised of ≤ 58 timestamp streams were bundled in 12 hour timestamp packets for further analysis in Matlab (MathWorks). In the following, these halfday packets will be called trials of duration $T_{Trial} \leq 12$ h. On some days, trials encompassed less than 12 h due to temporary interruptions for system reconfiguration, maintenance work or power failure. Our recording sessions consisted of 65 trials (32.5 DIVs) for the hippocampal culture and 106 trials (53 DIVs) for the cortical culture.

2.2 Local and network firing and burst rates

Firstly, we quantified the local firing rates (LFRs) at individual sites as the number of recorded spikes divided by T_{Trial} for each local spike train (LST) (Suppl. Fig. 1(B)). At network level, we pooled all spikes from all 57 and 58 sites, respectively, for each trial into a single network spike train (NST) by sorting them in a time-ascending order. The NST represented the MEA-wide activity for each trial. The network firing rate (NFR) was then quantified as the total number of spikes in an NST divided by T_{Trial} (Suppl. Fig. 1(C)) To further investigate activity dynamics, we used the burst rate (BR), a well-known parameter for characterizing synchronous network activity. We scanned all LSTs at the 57 (cortical) and 58 (hippocampal) individual sites for each trial and defined bursting activity as events with more than 10 subsequent spikes being individually separated by an ISI of less than 100 ms, followed by an interburst interval (IBI) larger than 200 ms (Wagenaar *et al.,* 2005) (Suppl. Fig. 1(C)). The local burst rate (LBR) at individual sites was calculated by dividing the number of bursts by T_{Trial}. Equally, the network

burst rate (NBR) was obtained by scanning the NST for bursts using above mentioned criterion and dividing the number of bursts by

T_{Trial}.

2.3 Paired spiking activity

Based on the previously described findings by Ursey (Usrey *et al.,* 1998) and Sincich (Sincich *et al.,* 2007), we investigated the occurrence and effect of paired spiking on neural activity in network cultures. As sketched in Suppl. Fig. 1(D), we defined PSs at individual sites as the neural activity consisting of two spikes recorded from the same electrode separated by an interval of up to 5 ms, followed by an IPSI larger than 40 ms (in order to assure that a second spike in a PS does not influence a first spike in a second PS for two consecutive PSs). Equally, we scanned all the NSTs using the above mentioned algorithm to quantify the PS activity at network level for each trial. In this case, the two spikes separated by an interval of up to 5 ms and followed by an IPSI larger than 40 ms did not necessarily have to be recorded from the same electrode.

To describe the PS activity dynamics for each trial, we calculated the number of active sites with PSs (NAS_{PS}) as being the number of sites with at least two PS repetitions during T_{Trial}. Equally, we calculated the NAS_B for bursts as the number of sites with more than one burst per trial.

To check if PS activity forms robust spatiotemporal patterns, we firstly calculated the IPSI as being the difference between two consecutive PSs at both network level and individual sites. From the IPSI histograms for each trial we extracted the highest number of IPSI repetitions and the most frequently encountered IPSI value ($IPSI_{mfo}$) at individual sites.

Moreover, to confirm that PS activity was neither governed strictly by firing rates (and thus represented an intrinsic neural response property) nor, at network level, by chance as a procedural result of projecting spiking activity from individual sites onto a single NST timeline, we generated Poisson-like network spike trains for comparison. In these, the firing probability

was distributed according to a homogenous Poisson process without refractory period. If PS activity were strictly governed by firing rate, Poisson-like spike trains with the same firing rate as the recorded NSTs would give a similar PS distribution. Additionally, we shuffled the NSTs 100 times for each trial and quantified PS activity to check the degree of randomness of NST PS activity. NST spike times were randomly rearranged with the randperm (Matlab, MathWorks) function. 100 repetitions were chosen to warrant statistical significance at acceptable computational costs.

To generate above mentioned Poisson-like spike trains, we used Matlab user-written routines.The Poisson distribution P represents the probability that a homogenous Poisson process generates n spikes in a period of trial duration T_{Trial}:

$$P(n) = \frac{(rT_{Trial})^n}{n!}\exp(-rT_{Trial}) \qquad (1\text{-a})$$

where r is the spike count rate defined as the total number of spikes divided by T_{Trial} for each LST and NST.

Timestamps were generated by the following interspike interval formula:

$$t_{i+1} - t_i = -(1/r)\ln(rand) \qquad (1\text{-b})$$

where rand is a random number uniformly distributed over the open interval (0 : 1); t_i represent the spike timestamps for i = 1, 2,..., n spikes (Martiniuc and Knoll, 2012).

2.4 Post-stimulus time histogram and time-varying firing rates at network level

To investigate the hypothesis that PS activity might replace external stimuli sources, we considered each PS a stimulus-resembling event for the network. Thus, for this particular investigation at network level, we considered PS onset (first spike) as the beginning of a stimulus (t = 0 s) with a duration of T_{PS} = 2 seconds, which is close to the shortest IPSI duration found for each trial.

To calculate the post-stimulus time histograms (PSTHs), the timestamps of PS-elicited spikes during a T_{PS} were aligned relative to t = 0 s for each period T_{PS}. n reflects the number

of PS stimuli at network level in a trial. n_{min} was found to be 200. We divided the stimulus period T_{PS} into N bins of duration Δt = 5 ms and counted the number of spikes k_i from all n sequences that fall into bin i. After averaging for the n stimulus repetitions and dividing by bin duration Δt, we obtained the time-varying firing rates r(t) with respect to stimulus (PS) onset.

2.5 Information content per spike

In order to evaluate the information about the stimulus (PS) carried by individual spikes following a PS within T_{PS}, we used the above calculated time varying firing rates r(t) and computed the entropy estimates (H) as follows (Strong *et al.*, 1998; Brenner *et al.*, 2000; Sincich *et al.*, 2009):

$$H = \frac{1}{T_{PS}} \int_0^{T_{PS}} \frac{r(t)}{< r >} \log_2 \frac{r(t)}{< r >} dt \qquad (2)$$

where T_{PS} = 2 s represents the above mentioned duration of a stimulus and <r> the average firing rate; also in this case, the bin size was Δt = 5 ms.

For each particular trial, we obtained the average estimate for the information content per spike by averaging the estimated entropy by the number of stimulus repetitions n:

$$\langle H \rangle = \frac{1}{n} \sum_{i=1}^{n} H_i \qquad (3)$$

To account for limited dataset size and to correct the resulting bias, the information content per spike was estimated as a function of bin size Δt. We performed a linear fit to these data to extract the intercept corresponding to the limit when Δt approaches zero. We used the shuffle verification method to check for the robustness of information content per spike. Briefly, we randomly rearranged each NST as described in section 0 and computed estimates of the information content per spike as mentioned above (Eq. 2). For each of the

shuffled NSTs, we repeated this procedure100 times and obtained a standard deviation of estimated information content that was smaller than one standard deviation of the fitting intercept obtained from above mentioned linear fit.

This measure of information content does not make any assumption about the stimulus features; it only reveals the information content carried by individual spikes.

2.6 Conditional firing probability

The highly variable spontaneous spiking activity of cultured neurons features robust patterns (i.e. bursting activity), which might participate in the establishment of functional connections between different sites within the culture. To investigate whether PS activity plays a role in shaping the dynamic interconnectivity map at different developmental stages, we adopted a variant of a cross-correlation algorithm initially introduced as conditional firing probability (CFP; le Feber *et al.,* 2007). This method was widely used in the investigation of activity relationships between different electrodes to reveal the formation and strength evolution of functional connectivity within *in vitro* networks (Zullo L *et al.,* 2012; Chiappalone *et al.,* 2007; Garofalo *et al.,* 2009). Here, we used CFP to reveal any PS-related cross-correlations between different sites within the network. That is, at each electrode i (i = 1 : 57 or 58, respectively) considered as the reference, we selected the second spike in each PS as a reference with new relative time $t_i = 0$. We then calculated the CFP as the probability of spike occurrences at any of the other 56 or57 recording electrodes j (j = 1: 56 or57, respectively) within the time interval T_{CFP} [$t_i : t_i$ + 500 ms] divided by the total number of second reference spikes of a PS at reference electrode i over the entire trial duration of T_{Trial} = 12 h. The spikes found at electrode j during T_{CFP} were aligned relative to each t_i and binned with a bin size of Δt = 1 ms. If any of the resulting 57*57or 58*58 CFP(i,j) distribution curves showed a clear peak, we considered electrode j being correlated to the PS activity on reference electrode i.

The peak amplitude was a measure of correlation strength. Its timestamp reflected the PSrelated synchronization delay between the two neurons.

Additionally, two boundary conditions were chosen as restrictive validity criteria: a CFP(i,j) was rejected if the width at 80% of the peak value was shorter than 5 ms (five bin sizes; to avoid false correlations caused by outliers) and for synchronization delays larger than 250 ms (to avoid curves that decreased to zero beyond the 500 ms window).

2.7 Transfer entropy

Above mentioned concepts (i.e. information content per spike and CFP) quantify statistical dependences of observed variables (i.e. recorded spike trains), thereby describing functional connectivity maps which do not allow us to investigate the direction of information flow (i.e.

the causality) between the recorded units. By definition (Wienner, 1956), an effective connectivity between two neurons exists when knowledge about the past of one neuron predicts the future activity of its counterpart better than the prediction based on the past activity of the receiver (neuron) alone. This effective connectivity is quantified by an information–theoretic measure called transfer entropy (TE) that was introduced by Schreiber (Schreiber, 2000). TE is an asymmetric measure of interactions between two coupled neurons which reveals effective connectivities and indicates the direction of information flow between recorded units. It permits to predict the spiking activity of a post-synaptic neuron by taking past spiking activity of its pre-synaptic partner into account. In our work, TE is positive and thus the information is directed from a sender unit A to a receiver unit B (i.e. there is an effective connectivity from unit A to unit B) only when the information about the spiking activity recorded at unit A improves the prediction of the spiking activity in the future of unit B better than any prediction derived from past spiking activity recorded at the unit B alone. Thus, to identify and assess effective connectivity within the neural

network from recorded spiking activity, we used a recently introduced toolbox for calculating the TE (Ito *et al.*, 2011) derived from the original definition given by Schreiber (Schreiber, 2000) as follows:

$$TE_{A\to B} = \sum p(B_{t+1}, B_t^k, A_t^l) \log_2 \frac{p(B_{t+1}|B_t^k, A_t^l)}{p(B_{t+1}|B_t^k)} \qquad (4)$$

A complete description of the TE toolbox algorithm can be found in Ito *et al.*, 2011. Briefly, p describes a probability, A_t depicts whether at time t a spike at unit A was recorded (and thus $A_t = 1$) or not ($A_t = 0$). Similarly, B_t and B_{t+1} describe the status of unit B at times t and t+1. Conditional probabilities of observing the particular status of units A and B are marked by vertical bars while the sum is over all possible combinations B_{t+1}, B_t^k and A_t^l, where parameters k and l express the number of time bins in the past that allow us to take the time delay and the message length into account when calculating TE. For biophysical reasonability, we chose k = 1:30 ms and l =1:250 ms.

In this general framework, we exclusively considered PS activity at unit A (the sender) while unit B (the receiver) encompassed the entire recorded spiking activity. In this way, we could estimate whether PS activity at unit A was involved in information transfer toward unit B.

Furthermore, we exemplarily chose the eight closest recording units as depicted in Figure 6(A) to check if PS was involved in information transfer and thus in establishing effective connectivity between these eight closest neighbors within the network. Thus, each of the closest eight units was scanned for PS activity and considered as the sender with respect to the entire spiking activity of the remaining seven closest neighbors. This resulted in a TE map, which depicts the PS information transfer dynamics of each of the selected senders (eight units A) toward the selected receivers (seven units B). For computational reasons, we split each trial duration T into 30 minutes subsets of recorded data.

We applied the same algorithm at network level to investigate the effect of information transfer from the above mentioned eight units A toward the rest of the network. In this case, we calculated the PS-related TE for each of the eight selected channels with respect to the entire NST as the only receiver unit B.

Further on, we calculated the differences between the resulting TEs:

$$\Delta TE = TE_{A\to B} - TE_{B\to A} \quad (5)$$

When ΔTE is positive, the information transfer is directed from A to B; in the opposite case, the information flows from B to A.

3. Results

3.1 Evolution of firing and burst rates through different developmental stages

Taking advantage of the uninterrupted extracellular recording technology for cultured neurons based on 59-channel microelectrode arrays (MEA), we analyzed the day to day evolution of spontaneous neural activity at both individual sites and network level. We extracellularly recorded activity from two different networks cultured under similar conditions. Quasicontinuous datasets from 7 DIV (first extracellularly recorded spikes emerged from the 5 μV noise floor and crossed the -5.5 SD of the peak-to-peak noise spike detection threshold) to 39 DIV for the hippocampal culture and from 24 DIV to 77 DIV for the cortical culture were analyzed.

For the hippocampal culture, the evolution of spiking activity at network level could be clearly divided into three periods (Figure 1(A) – blue bars) as follows: 7 DIV to 14 DIV as the first period (C1-1), 15 DIV to 26 DIV as the second period (C1-2) and 27 DIV to 39 DIV as the last period (C1-3). An obvious finding was a significantly increasing network firing rate (NFR – Methods 2.2) ($p < 0.05$, t-test) from one period to the next, starting with a

mean firing rate of 1.2 spikes/s in the first period to 12.7 spikes/s in the last as indicated by the yellow mean values in Figure 1(A). This increasing spontaneous spiking activity in maturing cultures is in accordance with previously reported results (van Pelt *et al.,* 2005). Significant changes have also been found at individual sites where the number of active sites during the same developmental periods increased as the culture grew toward maturity. In contrast, we found fluctuating neural activity periods containing or terminating with high network firing rates (Figure 1A) – red bars) for the more mature cortical culture. We could distinguish six time periods marked by an increasing period followed by a decreasing trend. The individual periods lasted from 24 DIV to 37 DIV (C2-1) with a mean of 15±8 spikes/s, from 38 DIV to 45 DIV (C2-2) with a mean of 25±11 spikes/s, from 46 DIV to 50 DIV (C2-3)with a mean of 8.5±7 spikes/s, from 51 DIV to 65 DIV (C2-4)with a mean of 7±3.4 spikes/s, from 66 DIV to 71 DIV (C2-5)with a mean of 6±2 spikes/s and from 72 DIV to 77 DIV with a mean of 5.5±1.8 spikes/s for the last period (C2-6).

Firing rates are usually used to reveal characteristic communication mechanisms that are different for spontaneous and induced activity, respectively. In contrast, bursting activity plays a role in filtering spontaneous neural activity (van Pelt *et al.,* 2004; Wagenaar *et al.,* 2005). In our recordings, spiking activity tended to induce bursts of synchronized activity at different developmental stages.

Similarly to the network firing rate (NFR Figure 1(A) –blue trace), the hippocampal culture showed a significantly ($p < 0.05$) increasing trend in bursting activity at network level (see Methods 2.2, Figure 1(B) –blue bars) over the three periods. A mean of 0.018 bursts/s during the first period increased to a mean of 0.22 bursts/s for the last period (Figure 1(B) – yellow dots). This developmental trend has already been reported in other network studies (van Pelt *et al.,* 2004). However, while the number of active bursting sites (NAS_B) increased from the first period to the second, it returned close to the value of the first period at the end of the recording. It dropped sharply during a power blackout (temperature dropped and

stayed at room temperature for several hours), from which it recovered slowly to its previous value (see Figure 1(D) and corresponding yellow circles depicting means). In the second period, these extremely high NAS_B are explained by massive neural avalanches that take place within the network and recruit neurons at most sites (ca. 82% of the 58 recording electrodes) for a short time Figure 1(C) exemplarily shows such a network avalanche that arose at 18 DIV.

In the more mature cortical culture, we found less bursting activity at network level than in the hippocampal culture at earlier developmental stages, but with a high NAS_B. That is, a larger number of neurons contributed to the network bursting, but with a lower number of bursts/s, which did not lead to a comparable increase in the NBR. In addition, the NBR, NAS_B and NFR of the cortical culture oscillated within each of the six periods, as indicated in Figure 1(A), (B) and (D)– red bars).

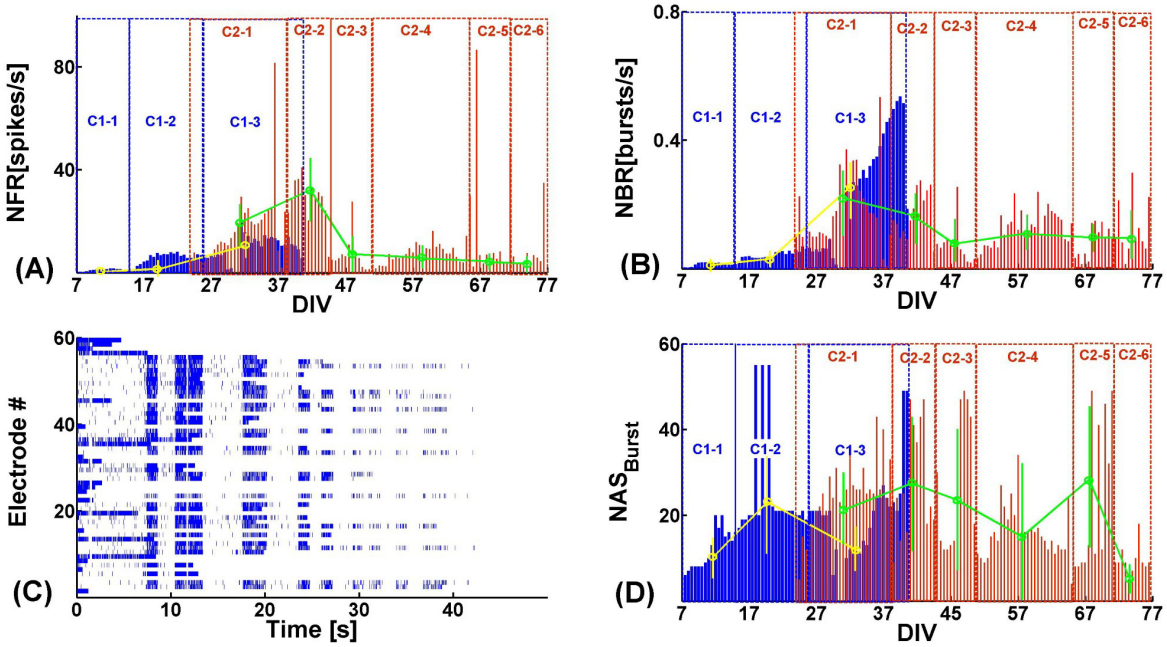

Figure 1 Evolution of network firing rate (NFR) (**A**) and network burst rate (**B**) over time for the first hippocampal (blue) and second cortical (red) culture. Three (hippocampal, blue rectangular delimiters, C1-1 to C1-3) and six (cortical, red rectangular delimiters, C2-1 to C2-6) recording periods were distinguished by significant changes in their NFRs. For each period, the mean NFRs and their SDs are displayed as circles with

error bars. (**C**) Example of a network avalanche at 18 DIV.(**D**) Number of active sites (NAS_B) with respect to bursting activity in the hippocampal (blue) and cortical (red) culture.

3.2 Evolution of paired spiking activity at individual sites and at network level

Activity patterns consisting of PSs separated by ISIs of up to 5 ms were rarely encountered in the young hippocampal culture. Instead, random isolated spiking rather than synchronized rapid firing dominated neural activity as reported before (van Pelt *et al.*, 2005). While spike pairing was very low at early DIVs, it consistently increased after 3-4 weeks *in vitro* (WIV). This trend was robust not only at individual sites (Figure 2(C) –blue bars), but also at network level (Figure 2(D) –blue bars). The mean of PS occurrences at individual sites significantly ($p < 0.05$) increased about thirtyfold from 193 for the first period to 5741 for the last period (Figure 2(C) - yellow circles indicating mean highest number of PS at individual sites). At network level, the mean number of PSs in the first period was 486 and increased tenfold to 4911 in the last period (Figure 2(D) –yellow circles). In contrast, PS activity in the more mature cortical culture did not grow monotonically, but fluctuated rather synchronously with both the firing and burst rates at network level Figure 2(C), (D) –red bars, and Figure 1(A), (B)).

Interestingly, the IPSI (see Methods 2.3), a parameter which quantifies the temporal gap between two consecutive PS, exemplarily suggests that PS activity becomes robust as the culture ages. For the hippocampal culture, the duration of the most frequently occurring (mfo) $IPSIs_{mfo}$ at both individual sites ($\leq$ 90 s, index 'L') and network level ($\leq$ 48 s, index 'N') was very long and fluctuated highly with a low number of repetitions in the first three WIVs Figure 3(A) (individual sites), (B) (network level)–blue bars). The non-uniform temporal distribution of PS activity during this developmental period denotes that PS was not yet robust.

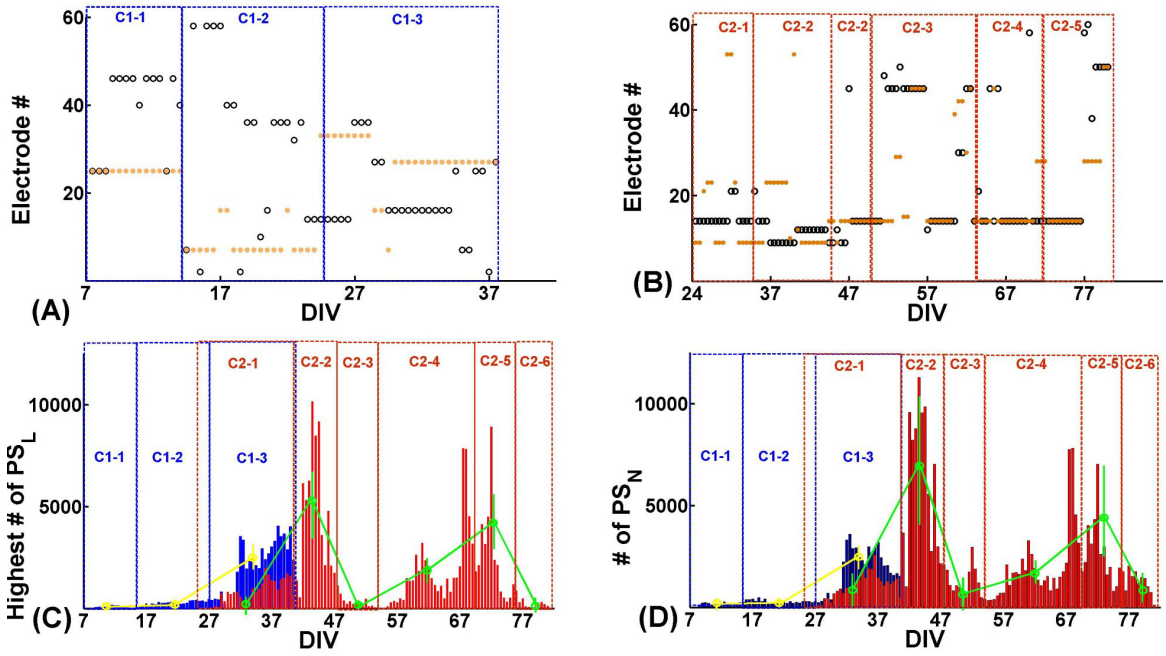

Figure 2 Highest PS activity (black circles) and highest bursting activity (orange circles) in the hippocampal (**A**) and cortical (**B**) culture may not necessarily be recorded from the same electrode in subsequent trials. (**C**) Number of occurrences of the most frequently, locally occurring PS_L in the hippocampal (C1, blue bars) and cortical culture (C2, red bars) at the individual recording sites denoted on the y-axes in (A) and (B). (**D**) Total number of PS_N occurrences at network level for the hippocampal (C1, blue bars) and the cortical culture (C2, red bars). Circles and error bars in (C) and (D) display mean PS values and their SDs (yellow: hippocampal; green: cortical).

Remarkably, PS_N activity at network level shows higher than average values exactly at those DIVs with strong activity avalanches (as exemplified Figure 1(C) at 18 DIV). This suggests that such extremely high neuronal activity at individual sites (as revealed by the NAS_{PS} in Figure 4(A) –blue bars) accounts for the elevated PS_N activity at network level, while firing rates kept a uniformly increasing trend at those DIVs (Figure 1(A)). After three WIVs, PS activity dramatically increased (Figure 2(C)(individual sites), (D) (network level)–blue bars) while the duration of the most frequently occurring $IPSIs_{mfo}$ decreased and robustly settled at 2-3 s until the end of the recording session (Figure 3(A) (individual sites), (B) (network level)– blue bars). Interestingly, the duration of the $IPSIs_{mfo}$ at network level (Figure 3(B))

stabilized earlier than at individual sites (Figure 3(A)). Over the same period, the number of the $IPSIs_{mfo}$ increased consistently both at individual sites and network level (Figure 3(C) and (D) –blue bars). These three trends (increasing overall number of PS, decreasing duration of $IPSI_{mfo}$, increasing number of the most frequently occurring $IPSI_{mfo}$) suggest that PS activity develops homogeneously and consistently throughout the network to result in robust PS activity patterns with an increasing number of occurrences with rather constant ISIs and IPSIs, especially after three WIVs.

For the more mature cortical culture, we observed the same inverse correlation between duration and number of the $IPSIs_{mfo}$ (see Figure 3(A) and (D) –red bars), however, oscillating over time. There were recurring periods with large IPSI values and low numbers of IPSI repetitions followed by periods with lower IPSI values but high repetition frequencies.

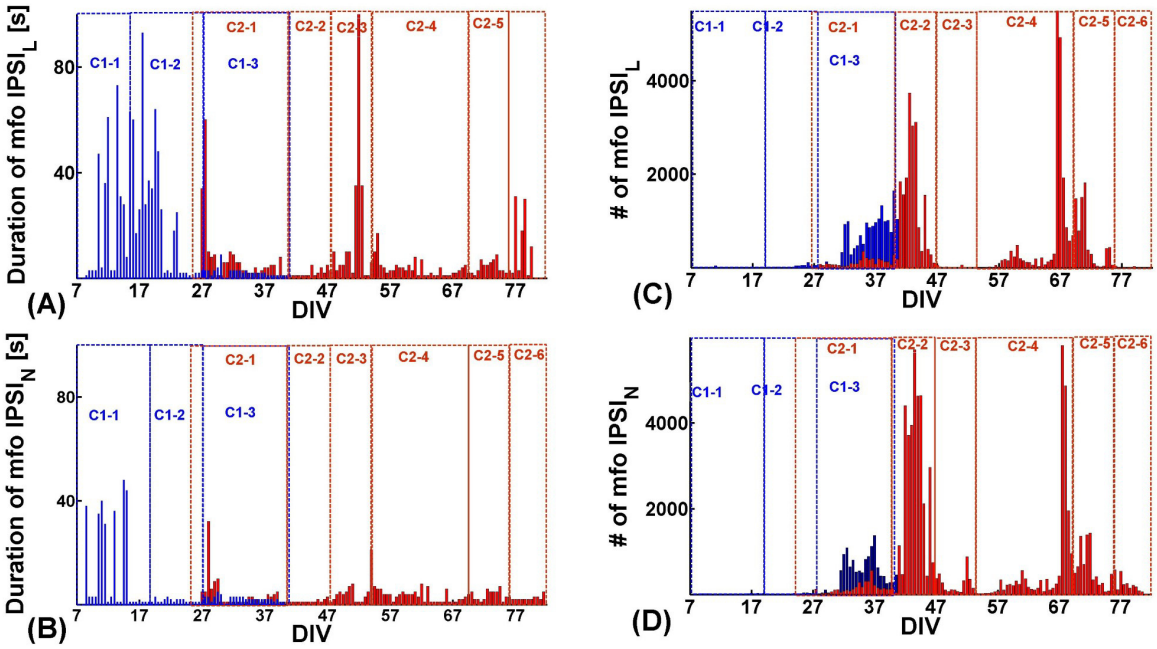

Figure 3 Duration of the most frequently occurring (mfo) $IPSI_{mfo}$ at individual sites (**A**) and at network level (**B**) for the hippocampal culture (C1, blue bars) and the cortical culture (C2, red bars) and its evolution from one period to the next (C1-1 to C1-3 and C2-1 to C2-6, respectively). Number of the $IPSI_{mfo}$ at individual sites (**C**) and at network level (**D**) (with the same color and period coding as in (**A**) and (**B**)).

3.3 PS activity versus burst activity

In order to check if PS activity is one of the driving forces for the self-organization of functional network connectivity, we investigated the relationship between bursting and PS activity. For the hippocampal culture, on average only 11% of bursts contained PS at early DIVs. Their number slightly increased to 16% in the last recording period. Except for four trials (6.25% of total trials), PS activity could be found in less than 40% of the bursts (see Figure 4(B) –blue bars). The same trend was observed for the cortical culture where, except for seven trials (3.18% of total trials), the percentage of bursts that contained PS remained below 50% (see Figure 4(B) –red bars).

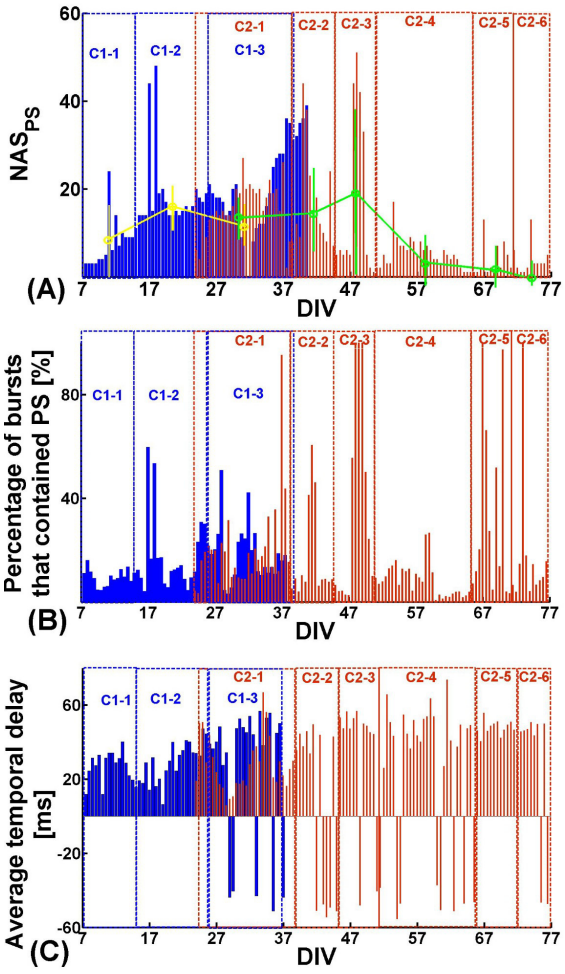

Figure 4 (**A**) NAS for PS activity for the hippocampal (blue) and the cortical (red) culture. (**B**) Percentage of bursts that contained PS at individual site level. (**C**) Average temporal delay in ms with which a burst followed a PS at individual sites.

For both the hippocampal and cortical network, PS and bursting activity were present at most sites (Figure 5(A)). However, in most cases, highest PS activity was recorded from different electrodes than those that recorded the highest bursting activity, as pointed out by the black circles (PS) and orange circles (burst) in Figure 2(A) (hippocampal) and (B) (cortical). For the hippocampal culture, highest PS and bursting activity were spatially collocated in only six trials (9.3% of total trials). In contrast, the electrodes with highest PS and bursting activity coincided in 42 trials (38.18 % of total trials) for the cortical culture. 41 of them occurred after 44 DIV. In both cases, the network location with dominant PS and bursting activity could change over the days. Over the course of the entire recording, highest PS activity was detected on 12 different electrodes (21%) for the hippocampal culture and on 11 electrodes (19%) for the cortical culture. Highest bursting activity could be associated with just five electrodes (8.3%) in the hippocampal culture (Figure 2(A)) while it occurred on 12 electrodes (20%) in the cortical culture (Figure 2(B)).

Importantly, in almost 92% of the recording trials PS activity preceded bursting activity (Figure 4(C)–blue bars) in the younger hippocampal culture and in 84% of the recording trials for the more mature cortical culture (Figure 4(C) –red bars). Additionally, the average temporal delay between a PS and a burst mostly remained below 50 ms. This suggests that PS presumably initiated bursting activity. Interestingly, this PS-burst coupling occurred on the same electrode of the cortical culture in 34 instances, suggesting robustness of PS-dominant sites. This electrode also recorded highest PS activity in almost 50% of the trials.

We further investigated the stability of the spatio-temporal distribution of PS patterns. The middle insets in Figure 5(i1 – i6) exemplarily show color-coded PS spiking activity maps at individual sites in the hippocampal culture for six trials at different developmental stages. Robust spatial patterns of PS activity were found over the entire recording period; two examples are highlighted by blue circles.

A total of 12 sites with stable PS patterns could be identified in more than 50% of the 60 trials. Among these sites, eight lasted longer than 73% of the total recording period. They formed robust, long-lasting patterns that presumably recruited new neighboring sites in different trials. Furthermore, seven of these sites also formed robust burst patterns as marked by yellow circles in Figure 5(A).

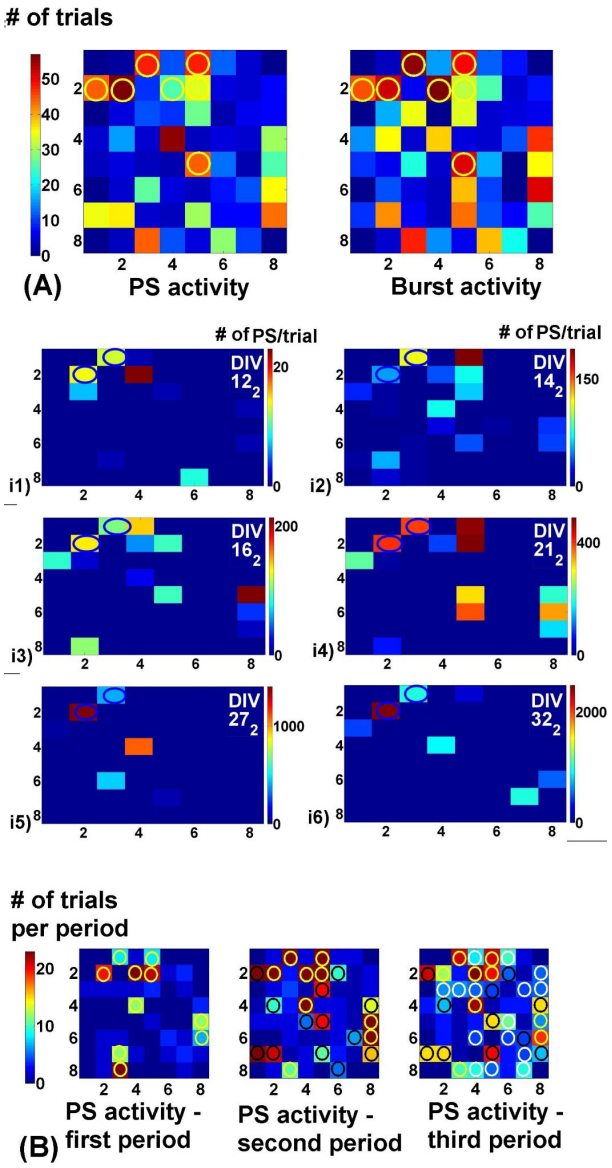

Figure 5(**A**) Spatial PS and burst pattern distribution with respect to the 8 x 8 electrode matrix for the hippocampal culture. Yellow circles mark the seven electrodes from which both PS and bursting activity could be recorded according to the criterion described in Methods 2.2 and 2.3. One trial represents half a DIV (Methods 2.1). Marked electrodes recorded activity in the majority of the trials, though not necessarily

consecutively. (**B**) Evolution of PS pattern complexity in the hippocampal culture from one period to the next: the NAS with PS patterns increased during development. In most cases, new PS emerged on electrodes adjacent to those with previous PS activity.

Figure 5(B) exemplarily shows PS activity patterns that had formed during the first period (yellow circles) and lasted until the end of the recording session, patterns that had newly formed during the second period and lasted until the end (black circles) and new neighboring sites that emerged only during the third recording period (white circles). Thus, 10 sites formed patterns that lasted for more than four trials during the first period, 22 sites for the second period and 34 sites for the last period. That is, for each new period, up to 12 neighboring sites were recruited in generating PS activity, thereby increasing the degree of PS pattern complexity as the network entered later developmental stages.

For the second, more mature cortical culture, 54 sites (93%) participated in PS activity that lasted for at least two trials, while in more than 50% of the trials the number of sites decreased to four. This suggests that at later developmental stages the role of dominant sites gains importance.

3.4 Information content per spike and CFP analysis

Next we asked to what degree spontaneous *in vitro* PS activity preserves its role encountered *in vivo* and thus participates in the formation of functional connectivity and in information processing within the cultured neural network at different developmental stages. With this motivation in mind, we considered PS activity as an internal stimulus and thus calculated the PS-related CFP (see Methods 2.6) and PS-related information content (see Methods 2.5) in the hippocampal network both at individual sites and at network level.

Because 12 sites presented robust, long-lasting PS activity for more than 50% of the total trials (Figure 5(A)), we exemplarily calculated the PS-related correlation between eight

closest neighbors out of these 12 sites as indicated in Figure 6(A) (red ellipses). We used CFP to construct the inter-connectivity maps for both the interconnectivity strength (Figure 6(B)) and the temporal delay (Figure 6(C)). For each trial and site i (i = 1:8), we quantified the PSrelated CFP (i,j) for all possible pairs (j = 1:7). Interestingly, we found no connectivity during the first11 DIV, coinciding with the period in which PS activity was not robust yet (i.e. with large IPSIs and few repetitions).

In contrast, from 17 DIV onward the number of connections significantly increased ($p < 0.01$) and remained high until 27 DIV. This corresponds to the second period, where PS activity gained robustness. The highest number of connections was found in this period (Figure 6(D)), which decreased thereafter. Moreover, the temporal delay of the correlations between formed pairs increased until 18 DIV with a mean of up to 45.2 ms (±20 ms) and consistently decreased thereafter with a mean of 16.2 ms (±10 ms) (Figure 6(E) and (F)). Connectivity strength stayed rather constant over several DIVs with almost identical means of around 0.07 (±0.03) for all three recording periods (Figure 6(E)).

Next we looked at the PS-related information content per spike (Eq. 2, Methods 2.5) for each selected channel pair (i,j) of the eight interconnected sites. The resulting information content map is presented in Figure 8(A). Information content per spike was highest during the second period, thereby correlating with the highest numbers of connections between these eight most active channels (Figure 8(B) compared with Figure 6(B) and (D)). This trend is also reflected by the mean values (Figure 8(B)). The initial increase in information content per spike from 0.8±0.2 bits/spike during the first period to 2.2±0.3 bits/spike in the second period is followed by a decrease to 1.2±0.6 bits/spike during the last period. While this statistical measure associates the information content per spike with PS, it does not make any statement on how the content is actually carried by the PS and on whether the PS is the only information carrying mechanism.

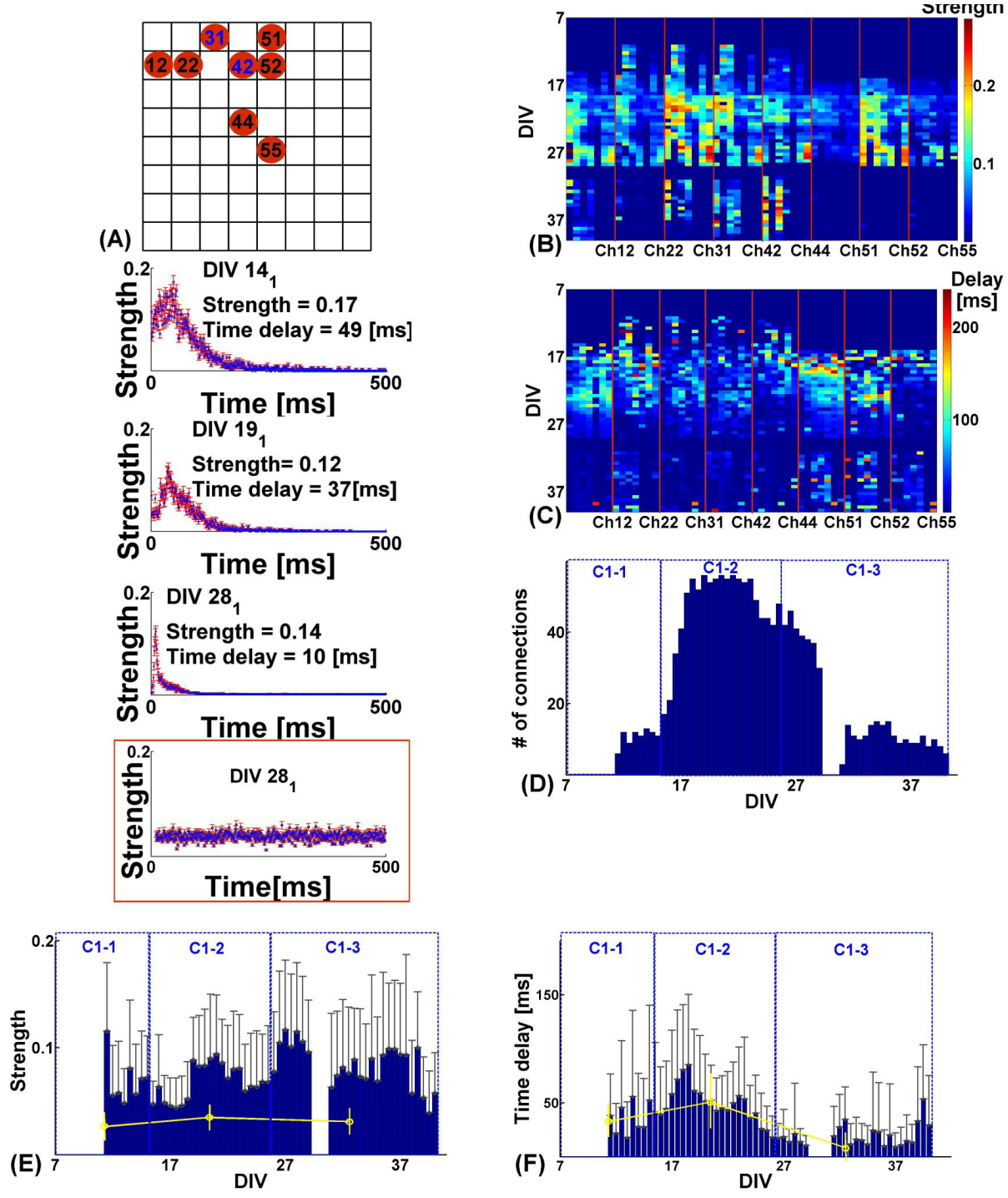

Figure 6 (**A**) Spatial arrangement of the eight closest, most PS-active sites in the hippocampal culture with respect to the 8x8 MEA matrix layout. The first number in a pair refers to the column, the second to the row. The insets under (A) exemplarily show PS-related CFP curves of reference channel 31 vs. channel 42 at three different DIVs (14, 19 and 28). The flat CFP curve framed by a red box illustrates the lack of PS-related connectivity for artificial spike trains that mimic channels 31 and 42. Connectivity evolution over time

expressed in strength (**B**) and temporal response delay (**C**) between the exemplarily selected eight most active PS sites. Each pixel column represents one of the seven recording sites connected to the respective reference channel indicated on the x-axis and pointed out in (A). Sorting order is column, then row. The red vertical bars delimit the eight reference channel permutations. (**D**) Evolution of the number of connections between the selected channels. (**E**) Evolution of the average connectivity strength for the selected channels and their means for each period (yellow circles). (**F**) Evolution of the average connectivity time delays for the selected channels and their means for each period (yellow circles).

The three observations, i) the decreasing trend in temporal delay between PS-induced correlated activity, ii) it's almost constant interconnectivity strength at later developmental stages and iii) the formation of robust spatiotemporal PS activity patterns as the culture matured may indicate that PS activity participates in the development and stabilization of functional connections at individual sites. To check for the robustness of the PS-related connectivity map, we constructed artificial Poisson-like spike trains according to Eq. 1 (Methods 2.3) for these eight electrodes (marked in Figure 6(A) by red circles) for all trials. We then investigated whether the artificial spike trains that mimic the recorded spike trains (i.e. artificial spike trains have the same firing rates as the recorded ones) develop similar connectivity maps as the real spike trains. Robustly, we found no PS-related connectivity between the constructed spike trains for any of the trials in the artificial spike trains. Insets of Figure 6(A) exemplarily show the connectivity between PS activity of channel 31 and spiking activity at channel 42 for three different DIVs. As mentioned before, while for the recorded spike trains the strength of the connectivity remained fairly constant, the time delay decreased during the last period (28 DIV). In contrast, the red box inset exemplarily shows no connectivity between the two artificial spike trains that mimic the same two electrode recordings over the same period.

Next we investigated whether the PS-related connectivity trend at individual sites is also found at network level for the different developmental stages. Firstly, we checked the

robustness of each NST by asking whether PS activity at network level is a “by chance” result of mapping all spikes from individual sites onto a single timeline. We therefore shuffled all of the NSTs repeatedly for 100 times and quantified PS activity for each individual case. We found the PS activity for each trial to be almost zero (Figure 7(C) – blue bars represent PS in recorded NSTs; inset with red bars represent PS in shuffled NSTs). To mimic the recorded NSTs, we further constructed artificial Poisson-like spike trains with similar firing rates as the NSTs (Eq.1, Methods 2.1). Also in this case, such artificial NSTs showed statistically significant ($p<0.001$) different PS activity as if it was strictly governed by firing rates (Figure 7(C) – green bars). These Poisson-like spike trains lack a spike history (i.e. without refractory period). Thus, very large NST firing rates and an exponential ISI distribution (Eq. 1b) favor short ISIs (i.e. up to five ms), which leads to an unrealistically high number of PS occurrences.

Next, we checked for PS-correlated activity at network level by calculating the CFP (Methods 2.6) for every NST, this time with respect to developmental evolution of network-wide, PSinduced activity instead of local connectivity. As before, the second spike in a spike pair (that matched the PS criterion of $\leq$5 ms) of an NST served as the reference for calculating the CFP with respect to the following 500 ms of NST activity. This auto-correlation-like analysis provided information on the strength and time delay of PS-related spiking activity for individual NSTs. If repeated for all NSTs, the evolution of PS-correlated activity can be plotted for all trials (Figure 7(A) and (B)). Remarkably, we found that PS-related spiking activity startedat11 DIV for all of the trials. Its time delay increased until 18 DIV and significantly decreased during the last recording period, which is strikingly similar to the previously observed trend at individual sites as reported above.

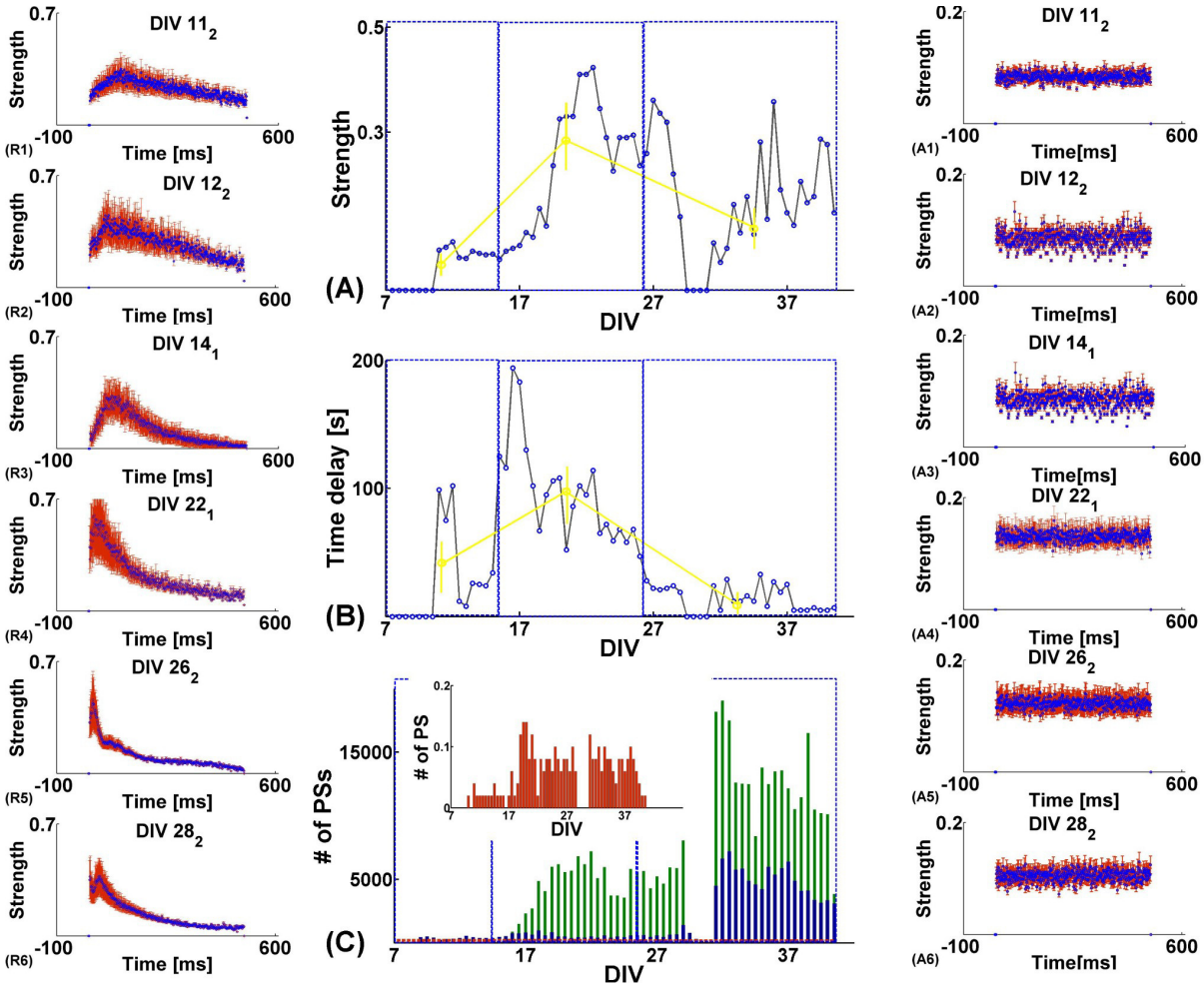

Figure 7 (**A**) Evolution of PS-related CFP strength for all hippocampal NSTs. (**B**) Evolution of PS related CFP time delay for all NSTs. (**C**) The number of PS for artificial spike trains at network level (green bars) and the number of PS at network level for recorded NSTs (blue bars). The inset shows a zoom ontothe number of PSs for shuffled NSTs (red trace). The insets **R1 – R6**(left side column) display examples of PS-related CFPs at network level for different DIVs (11, 12, 14, 22, and 28). The insets **A1 – A6**(right side column) display examples of PSrelated CFPs at network level for artificial spike trains for the same DIVs(11, 12, 14, 22, and 28).

The mean time delay (Figure 7(B) – yellow circles) increased during the second recording period to 74.5±30 ms and decreased in the third period to 12.4±10 ms while the mean correlation strength (Figure 7(A) – yellow circles) increased during the second period to 0.28±0.09 and decreased to 0.14±0.09 in the last recording period.

Furthermore, despite significantly larger PS activity found in artificial spike trains that were supposed to mimic NSTs, we found no correlated spiking activity in any of the trials (insets A1 – A6 to the right side of Figure 7). In contrast, insets R1 – R6 on the left side of Figure 7 exemplarily show the CFP of PS-related spiking activity for six of the NSTs indicating a decreasing time delay of the PS-correlated spiking activity.

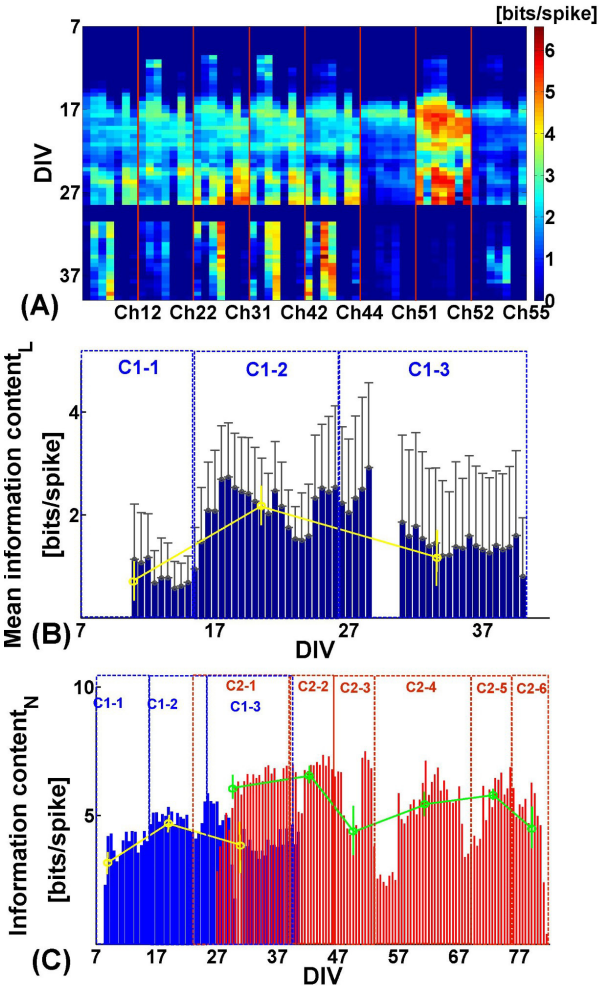

Figure 8(**A**) Matrix of PS-related information content expressed in bits/spike between the exemplarily selected eight most active PS sites in the hippocampal culture (Figure 6). Each pixel column represents one of the seven recording sites being connected to the respective reference channel indicated on the x-axis. Sorting order is column, then row. The red vertical bars delimit the eight reference channel permutations. (**B**) Evolution of the PS-related mean information content in bits per spike (blue bars) for the selected channels and its respective average for a given period (yellow circles). (**C**) Evolution of information content for PS-related activity in both

cultures at network level for each period. Blue bars represent the hippocampal culture with mean and standard deviations in yellow; red bars represent the cortical culture with mean and standard deviation in green.

Finally, after noticing that PS activity is involved in developing functional connections at individual sites and that spiking activity at network level is correlated with each second spike in a PS (with a decreasing time delay) for all NSTs, we checked whether PS activity may also be involved in information processing at network level.

We calculated the PS-related information content per spike at network level for each NST considering PS activity as an internal stimulus (Eq. 2, Methods 2.5). Indeed, we found that in both cultures PS activity is involved in information processing at network level as well (Figure 8(C)). Moreover, in the hippocampal culture, the trend found at local sites was preserved at network level. For the first period, we found a mean of 3.4 bits/spike (SD= 1.3 bits/spike), which increased during the second period to 4.9 bits/spike (SD = 0.4 bits/spike) and decreased in the last period to 3.6 bits/spike (SD = 1.2 bits/spike). For the cortical culture, the information content increased and decreased for different periods from 4.4 bits/spike (SD = 1.8 bits/spike) up to a value of 6.5 bits/spike (SD = 0.8 bits/spike).

3.5 PS activity participates in controlling the direction of information flow within the coupled neuronal units

Up to know we have seen that PS activity is involved establishing functional connectivity and carries information both at local side and at network level. We then asked whether PS is also controlling the direction of information flow within the cultured network. A TE analysis (Methods 2.7) may reveal how presynaptic PS activity predicts activity at its postsynaptic target or even at network level.

We exemplarily choose the eight most closest recorded units mentioned above (as depicted in Figure 6) and calculated ΔTE (Eq. 5) for PS activity for each of the channels with respect to the entire spiking activity of the remaining seven channels for different time lags and message lengths (Ito *et al.*, 2011). We found that PS activity is robustly involved in information transfer between cultured neurons. Figure 9(A) shows the constructed ΔTE map, which indicates a very low effective connectivity between selected recording units at an early developmental stage (i.e. the first 17 DIVs) with a mean $\Delta TE = 0.2 \cdot 10^{-2}$ bits/s and $SD = 0.18 \cdot 10^{-2}$ bits/s. Additionally, for some channels, PS activity did not established any effective connectivity during this period. Only three out of eight selected channels showed effective connectivities with their postsynaptic partners. Those disappeared and reappeared in different recording periods indicating that PS activity was not robust yet and consequently could not reliably predict or cause spiking activity at their targets. This situation changed dramatically from 17 DIV onward. ΔTE significantly increased ($p<0.001$) up to 29 DIV indicating that PS activity established robust and effective connectivities. Only on channel 51 PS activity established less effective connectivities during this developmental stage. For this developmental period we found a mean $\Delta TE = 1.13 \cdot 10^{-2}$ bits/s with a $SD = 0.14 \cdot 10^{-2}$ bits/s. From 30 DIV onward until the end of the recording period, ΔTE decreased with a mean of $0.4 \cdot 10^{-2}$ bits/s and a $SD = 0.13 \cdot 10^{-2}$ bits/s while only four (50%) channels with PS activity had established effective connectivity with large ΔTEs. Remarkably, PS activity could predict 98.58% of the spiking activity at their targets. Only in 1.42% of the cases ΔTE took on negative values (Figure 9(A), dark blue pixels), which shows that PS activity at individual sites could be predicted reversely from the spiking activity of their postsynaptic partners. Further on we asked if the local effect is preserved at network level. In this case, the PS activity at the eight selected channels represented now the senders and the NSTs were considered the receivers. As Figure 9(B) shows, the trend that was observed at local sites was also found at network level. Again, until 17 DIV, spiking activity of NSTs

could be poorly predicted by PS activity only (mean $\Delta TE = 0.4 \cdot 10^{-2}$ bits/s with SD = $0.3 \cdot 10^{-2}$ bits/s). Only two channels (i.e. 31 and 42) could be identified in causing spiking activity in the NSTs. From 17 DIV to 29 DIV, the mean ΔTE significantly increased to $1.5 \cdot 10^{-2}$ bits/s with a SD = $0.2 \cdot 10^{-2}$ bits/s suggesting that PS activity at local sites increasingly drove network activity. However, from 30 DIV onward, PS activity increased only slightly (mean $\Delta TE = 1.7 \cdot 10^{-2}$ bits/s with a SD = $0.3 \cdot 10^{-2}$ bits/s), mostly due to the same trend as observed at local sites. That is, the same four channels (50% out of the eight selected channels) presented larger ΔTE values and thus strengthened their influence on the spiking activity of each NST. Moreover, at network level, ΔTE never took on negative values, suggesting that PS activity at selected local sites always predicted NST activity and not vice versa.

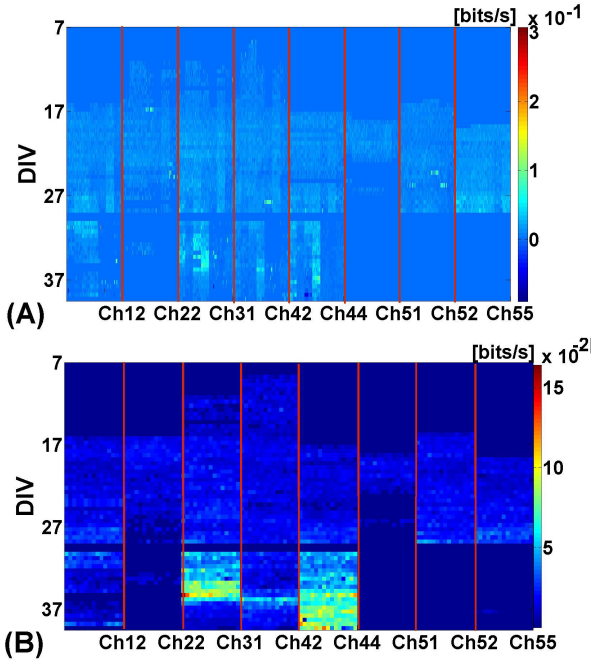

Figure 9(**A**) Matrix of PS-related ΔTE (Methods 2.7) for eight recording sites. Vertical red bars delimit the sender channel that connects with the remaining seven receiver channels. Individual pixels represent the PSrelated ΔTE averaged over a 30 minutes period and over the seven receiver channels. Each pixel row covers one DIV. (**B**) Matrix of PS-related ΔTE for eight senders (delimited by red bars) and the entire network as the receiver. Each pixel represents the ΔTE averaged over a 30 minutes period, each row covers one DIV.

4. Discussion

Neurons from dissociated brain tissue are capable of self-organizing their interconnectivity in cell culture. They become active even in the absence of any external sensory stimuli (Feller *et al.,* 1999). Besides random spiking and concerted bursting, neural networks use various modalities and activity patterns to both transfer information and form as well as maintain functional connections (Sun *et al.,* 2010). Such spontaneous, often synchronized neural activity increases in firing rate and in the number of active sites from one developmental stage to the next as observed *in vivo* (Nadasdy 2000; Chiu *et al.,* 2001; Weliky *et al.,* 1999) as well as *in vitro* (van Pelt *et al.,* 2004, Wagenaar *et al.,* 2006; Rolston *et al.,* 2007; Pasquale *et al.,* 2010). Our un interrupted long-term recording study over several weeks confirmed this trend in two different neural *in vitro* networks, in a young hippocampal culture and for the first two periods in a more mature cortical culture. At later developmental stages, the activity and number of active sites slightly decreased. In addition, bursting frequency at network level did not increase anymore. Instead, it distributed spatially by involving more active sites. In contrast to previously reported snapshot activity recordings, our almost continuous recordings revealed large activity variations at particular DIVs. We therefore asked what networkinherent coding mechanisms shape and drive network activity.

Interestingly, we found that predominantly robust PS activity rather than bursts drove neural activity in the investigated cultures. PS not only developed stable spatiotemporal patterns, but also participated in shaping the interconnectivity map. Previous reports on its role *in vivo* and *in vitro* suggest that PS activity may act as a temporal filter and be part of a mechanism involved in information processing at different hierarchical information processing stages (Krahe 2004; Akerberg 2011; Rathbun *et al.,* 2010; Sincich *et al.,* 2009; Uglesich *et al.,* 2009).

In this study, the following main findings in support of these statements emerged from the analysis of the continuously recorded datasets:

1. The network firing rate, network burst rate and number of active sites increased as a hippocampal culture grew toward maturity and slightly decreased when the respective cultures started to decay.
2. At later developmental stages, spontaneous neural activity in a cortical culture oscillated periodically over several days. While activity could be very high at some DIVs, on average it evolved rather constantly.
3. PS activity became robust after three WIVs when IPSIs settled down to 2-3 s and the number of PS occurrences significantly increased at both individual sites and at network level. This may signal the passing of a critical maturation stage in spontaneously active *in vitro* networks.
4. In both cultures, highest PS activity could change its spatial location from one DIV to the next, which in most cases did not coincide with the location of the highest bursting activity. Furthermore, highest PS activity involved a larger number of neurons than the highest bursting activity, which stayed spatially confined to a few dominant electrodes throughout the entire recording period.
5. Although PS activity was found both outside and inside of bursting activity, it is an independent type of neural response, typically spatially separated from bursting activity. For the majority of the trials, the percentage of bursts which contained PS activity remained below 50%.
6. In most trials, PS activity preceded bursting activity at the same recording site with a lead of several tens of milliseconds. This suggests that PS may act as an internal surrogate stimulus, which triggers synchronized neural activity and avalanches (i.e. exemplified at 18 DIV, Figure 1(C)).

7. Its relation to other types of activity furthermore suggests that PSs act as network-intrinsic stimulus sources also at network level. From 11 DIV onward, network spiking activity was strongly correlated to the second spike of a PS with decreasing temporal delay as cultures matured.
8. Besides temporal patterns consisting of short IPSIs and frequent occurrence, PS activity formed increasingly complex spatial patterns during development by recruiting neighboring sites. Some of them fluctuated temporally; others lasted until the end of the recording session. A similar, yet activity type-unspecific increase in pattern complexity has been reported before (Rolston *et al.,* 2007; Sun *et al.,* 2010).

These findings combined with the above mentioned results suggest that PS activity evolves in distinct spatiotemporal patterns within a non-stimulated, spontaneously active network. PS presumably initiates synchronized bursting activity that may be responsible for forming particular functional connections both *in vivo* and *in vitro* (Rolston *et al.,* 2007; Sun *et al.,* 2010; Chiappalone *et al.,* 2012; Blankenship *et al.,* 2010; Mazzoni *et al.,* 2007; Pimashkin *et al.,* 2011).

9. CFP and information content per spike have been proven to reveal the statistical dependency between coupled neurons (Maccione *et al.*, 2012; le Feber *et al.*, 2007). Our CFP analysis revealed that PS activity is likely involved in the establishment and shaping of functional connections between different individual sites within the network. While we found few or no PS-related correlations between different sites at early stages when PS activity was not yet robust, the number of connections increased as the culture matured. They were characterized by rather constant average strengths and decreasing time delays for subsequent developmental stages. Interestingly, the PS-related information content per spike at individual sites was highest for the same period that the number of connections was found to be highest.

These findings suggest a consolidation of PS-correlated activity at individual sites over time.

10. As the elevated PS-related information content per spike indicated, PS activity was involved in information transmission at individual sites and at network level. This finding is in concordance with previous studies on the role of different spiking patterns in spontaneous neural activity (Wagenaar *et al.,* 2006; Pasquale *et al.,* 2010; Sun *et al.,* 2010; Rolston *et al.,* 2007; Nadasdy 2000). It suggests that the network presumably uses only a fraction of the total number of spikes to transmit most of the information. As mentioned earlier, this concept of sparse coding was also found in the early visual system. It improves the overall coding efficiency by a mechanism that deletes the less informative spikes from one stage to the next (*i.e.* from the retina to the lateral geniculate nucleus (LGN)) while preserving relevant information with a lower number of spikes (Sincich *et al.,* 2009; Uglesich *et al.,* 2009).
11. The transfer entropy (Schreiber, 2000), an asymmetric information theoretic measure recently introduced to neuroscience, allows to estimate the direction of information flow within a network of locally coupled neurons (Ito *et al.*, 2011 – for spiking cortical network; Gourevitch and Eggermont, 2006 – for auditory cortical neurons; Garofalo *et al.*, 2009) or even between different brain areas (Battaglia *et al.*, 2012 – inter-areal brain circuits; Buehlmann and Deco, 2010; Lindner *et al.*, 2011 – directed interactions from the retina to the tectum; Lungarella and Sporns, 2006 – sensorimotor networks). Here we used TE to independently confirm that PS activity, besides forming spatio-temporal patterns and being involved in the formation of functional connectivity within the cultured neurons, also predicts the directionality of a connection at both local sites and network level Figure 9(A). TE analysis also strongly supported the trends revealed by information content per spike and CFP analysis. Presumably, PS activity was expansively involved in driving

neuronal communication between 17 DIV and 29 DIV to arrive at a relative stability after 29 DIV where the PS neurons played a key role in driving neural activity in the already mature network.

The construction of NSTs by simply collecting the entire spiking activity and arranging the time stamps in an ascending temporal order may seem problematic at first glance. This way of constructing NSTs does not seem to have any biological relevance. However, using artificial spike trains and shuffling methods, we could show that PS in NSTs does not occur by chance. While artificial spike trains have similar firing rates as the recorded trains, no correlated activity between neurons (other than by chance) is expected due to the lack of connectivity between individual neurons. The absence of PS-related connectivity for artificial spike trains suggests that PS activity is not a random and strictly firing rate-dependent neural phenomenon. Instead, it seems to be an intrinsic mechanism of cultured neurons in support of shaping neural interconnectivity. The local effect of PS activity seems to be preserved in NSTs as well. TE Figure 9(B) revealed a similar trend in the prediction of spiking activity at network level by PS. CFP analysis revealed a strong correlation between spiking activity at network level and each second spike in a PS. A similarity between CFP and information content per spike shapes strengthened the hypothesis that PS is involved in carrying information at network level as well. In summary, PS seems to play a key role in shaping the local and network-wide input-output relationship in cultured neural networks.

The two main hypotheses stated in this study have to be tested further in future experimental work. Firstly, in lack of any external stimulus, does PS indeed act as an internal surrogate stimulus that is capable of shaping neural activity by driving the input – output relationship of the spiking activity at network level? If this assumption turned out to be true, controlled PSlike electrical stimulation (similar to Zullo *et al.*, 2012) instead of single pulses or tetanic stimuli could more reliably drive a predictable neural output, *i.e.* in a closed-loop stimulation paradigm (Rolston *et al.,* 2010; Ruaro *et al.,* 2005; Novellino *et al.,* 2007). PS-

like stimulation may find possible application in neurally-controlled artefacts (robotics, neuroprosthetics). Secondly, because PS activity cannot only be found downstream of a stimulus both *in vitro* and in intact brain architectures (Usrey *et al.*, 1998; Sincich*et al.*, 2009), but also in spontaneously firing neural *in vitro* networks, it may represent an ubiquitous information processing response property of neurons of different species and organization. However, little is known on how PS depends on the neural cell type. A prominent example is the early visual system, where the PS contribution to information processing varies for different retinal ganglion cell types and the number of synaptic connections they are engaged in (Martiniuc *et al.*, in preparation). A combined electrophysiology and imaging *in vitro* study on how PS depends on cell type and cell morphology will shed more light on this question.

Acknowledgements

We thank Francesca Succol and Marina Nanni for their expert advice and assistance in the cell culture preparation. IIT intramural funds in support of this research are highly appreciated.

References

Akerberg, O.A. and Chacron, M.J. (2011).In vivo conditions influence the coding of stimulus features by bursts of action potentials. *J.Comput.Neurosci.*31(2), 369-83.

Banker, G. and Goslin, K.(1998).*Culturing Nerve Cells*. Cambridge: The MIT Press.

Battaglia, D., Witt, A., Wolf, F. and Geisel, T. (2012). Dynamic effective connectivity of inter-areal brain circuits.*PLoSComputBiol***8:** 3. doi:10.1371/journal.pcbi.1002438.

Bienenstock,E.L.,Cooper,L.N.,and Munro, P.W. (1982). Theory for the development of neuron selectivity: orientation specificity and binocular interaction in visual cortex. *J Neurosci.*2, 32–48.

Blankenship A. G. and Feller M. B. (2010).Mechanisms underlying spontaneous patterned activity in developing neural circuits.*Nat. Rev. Neurosci.*11, 18–29.

Blau, A., Neumann, T., Ziegler, C., and Benfenati, F.(2009).Replica-molded poly(dimethylsiloxane) culture vessel lids attenuate osmotic drift in long-term cell culturing. *JBiosci*.34(1), 59-69.

Brenner, N., Strong, S. P., Koberle, R., Bialek, W. and de Ruyter van Steveninck, R.R. (2000). Synergy in a neural code.*Neural Comput*12, 1531–1552.

Brewer, G. J.,Boehler, M. D., Ide, A. N. and Wheeler, B. C.(2009).Chronic electrical stimulation of cultured hippocampal networks increases spontaneous spike rates. *J Neurosci Methods*184, 104-109.

Buehlmann, A. and Deco, G. (2010).Optimal information transfer in the cortexthrough synchronization.*PLoSComputBiol* 6(9):e1000934,doi: 10.1371/journal.pcbi.1000934.

Chiappalone, M., Vato, A., Berdondini, L., Koudelka-Hep, M, and Martinoia, S. (2007). Network dynamics and synchronous activity in cultured cortical neurons.*International Journal of Neural Systems*17, 87–103.

Chiu, C. Y. andWeliky, M. (2001).Spontaneous activity in developing ferret visual cortex in vivo.*J Neurosci,* 21(22), 8906-8914.

DeMarse, T.B., Wagenaar, D.A., Blau, A. and Potter, S.M. (2001) The neurally controlled animat: Biological brains acting with simulated bodies. *Autonomous Robots* 11, 305–310.

Feller, M. B. (1999). Spontaneous correlated activity in developing neural circuits. *Neuron*22, 653–656.

Ferrández, J.M., Lorente, V., de la Paz, F.and Fernández, E. (2012). Training biological neural cultures: Towards Hebbian Learning. *Neurocomputing* 114, 3-8.

Garofalo, M., Nieus, T., Massobrio, P. andMartinoia, S. (2009). Evaluation of the performance of information theory-based methods and cross-correlation to estimate the functional connectivity in cortical networks.*PLoS ONE* 4(8):e6482.doi:

10.1371/journal.pone.0006482.

Graham, D. J., and Field, D. J. (2007).Statistical regularities of art images and natural scenes: spectra, sparseness and nonlinearities.*Spatial Vision*21, 149-164.

Gourevitch, B., Eggermont, J. J. (2007). Evaluating information transfer betweenauditory cortical neurons.*J Neurophysiol*97, 2533–2543.

Krahe, R. and Gabbiani, F.(2004).Burst firing in sensory systems. Nat Rev Neurosci, 5(1), 13-23.

le Feber, J., Rutten, W. L. C., Stegenga, J., Wolters, P. S. and Ramakers, G. J. A.(2007). Conditional firing probabilities in cultured neuronal networks: a stable underlying structure in widely varying spontaneous activity patterns. *Journal of Neural Engineering*4, 54–67.

Lindner, M., Vicente, R., Priesemann, V.and Wibral, M. (2011). TRENTOOL: a Matlab open source toolbox to analyze information flow in time series data with transfer entropy. *BMC Neurosci.*12,119.

Lungarella, M. and Sporns, O. (2006).Mapping information flow in sensori motor networks.*PLoSComputBiol*2(10):e144.doi: 10.1371/journal.pcbi.0020144.

Maccione, A.,Garofalo, M ., Nieus, T., Tedesco, M.,Berdondini, L. and Martinoia,S. (2012). Multiscale functional connectivity estimation on low density neuronal cultures recorded by high density CMOS Micro Electrode Arrays.*Journal of Neuroscience Methods* 207(2). doi:10.1016/j.jneumeth.2012.04.002.

Martiniuc, A. V. and Knoll, A. (2012). Interspike Interval Based Filtering of Directional Selective Retinal Ganglion Cells Spike Trains. *Comput. Intell Neurosci.* doi:10.1155/2012/918030.

Martiniuc, A. V., Zeck, G., Stürzl, W. and Knoll, A. (2011). Sharpening of directional selectivity from neural output of rabbit retina.*J. Comput. Neurosci.*30(2), 409-26.

Mazzoni, A., Broccard, F. D., Garcia-Perez, E., Bonifazi, P., Ruaro, M. E. and Torre, V.(2007).On the dynamics of the spontaneous activity in neuronal networks.*PLoS ONE* 2(5),e439.doi: 10.1371/journal.pone.0000439.

McCabe, A. K., Chisholm, S. L., Picken-Bahrey, H. L. and Moody, W. J. (2006).The selfregulating nature of spontaneous synchronized activity in developing mouse cortical neurones. *J. Physiol*.577, 155–167.

Nadasdy, Z. (2000).Spike sequences and their consequences. *J. Physiol.*94, 505-524.

Nomura, M., Ito, D., Tamate, H.,Gohara, K. and Aoyagi, T. (2009).Estimation of Functional Connectivity that Causes Burst-like Population Activities.*Forma* 24 (1), 11-16.

Novellino, A., D'Angelo, P., Cozzi, L., Chiappalone, M., Sanguineti, V. and Martinoia S. (2007).Connecting neurons to a mobile robot: an in vitro bidirectional neural interface.*Comput.IntellNeurosci.***12725**, doi: 10.1155/2007/12725.

Olhausen, B.A. and Field, D.J. (2004).Sparse coding of sensory inputs. *Curr Opin Neurobiol* 14, 481– 487.

Pasquale, V., Massobrio, P., Bologna, L. L., Chiappalone, M. and Martinoia, S. (2008). Selforganization and neuronal avalanches in networks of dissociated cortical neurons. *Neuroscience*153, 1354–1369.

Pasquale, V., Martinoia, S. and Chiappalone, M. (2010).A self-adapting approach for the detection of bursts and network bursts in neuronal cultures. *Journal of Computational Neuroscience* 29(1-2), 213-229.

Pimashkin, A., Kastalskiy, I., Simonov, A., Koryagina, E., Mukhina, I. and Kazantsev, V. (2011).Spiking signatures of spontaneous activity bursts in hippocampal cultures. *Front. Comput.Neurosci.***5**:46.doi: 10.3389/fncom.2011.00046.

Rathbun, D. L, Warland, D.K., andUsrey, W.M.(2010).Spike timing and information transmission at retinogeniculate synapse. *The Journal of Neuroscience*30(41), 13558-13566.

Rolston, J.D., Wagenaar, D.A. and Potter, S.M.(2007).Precisely timed spatiotemporal

patterns of neural activity in dissociated cortical cultures.*Neuroscience* 148, 294–303.

Rolston, J., Gross, R. and Potter, S. (2010). Closed-loop, open-source electrophysiology. *Front. Neurosci.***4**:31. doi: 10.3389/fnins.2010.00031.

Ruaro, M.E., Bonifazi, P. and Torre, V. (*2005*).Toward the neurocomputer: Image Processing amd pattern recognition with neuronal cultures. *IEEE Trans. Biomed. Engineering* 52(3), 371-383.

Schreiber, T. (2000). Measuring information transfer. *Phys Rev Lett*85, 461–464.

Shahaf, G. and Marom, S. (2001). Learning in Networks of Cortical Neurons. *The Journal of Neuroscience*21 (22), 8782–8788.

Sincich, L. C., Adams, D. L., Economides, J. R.and Horton, J.C. (2007). Transmission of spike trains at retinogeniculate synapse. *The Journal of Neuroscience*27(10), 2683–2692.

Sincich, L. C., Horton, J. C. andSharpee, T. O. (2009). Preserving Information in Neural Transmission.*The Journal of Neuroscience*29(19), 6207– 6216.

Sjöström, P.J., Turrigiano, G.G., and Nelson, S.B. (2003).Neocortical LTD via coincident activation of presynaptic NMDA and cannabinoid receptors. *Neuron*39, 641–654.

Strong, S.P., Koberle, R., de Ruyter, van Steveninck, R. R. and Bialek, W.(1998). Entropy and information in neural spike trains. *Phys Rev Lett*80, 197–200.

Sun, J. J., Kilb, W. and Luhmann, H. J. (2010). Self-organization of repetitive spike patterns in developing neuronal networks *in vitro*. *Eur. J. Neurosci.* 32(8), 1289-99.

Uglesich, R., Casti, A., Hayot, F. and Kaplan, E.(2009). Stimulus size dependence of information transfer from retina to thalamus. *Front SystNeurosci.***3**: 10.doi: 10.3389/neuro. 06.010.2009.

Usrey, W. M., Reppas, J. B. and Reid, R. C. (1998). Paired-spike interactions and synaptic efficacy of retinal inputs to the thalamus. *Nature*395(6700), 384-387.

van Pelt, J., Corner, M.A., Wolters, P.S., Rutten, W.L. and Ramakers, G.J.(2004). Long term stability and developmental changes in spontaneous network burst firing patterns

in dissociated rat cerebral cortex cell cultures on multi-electrode arrays. *Neurosci. Lett.*361, 86–89.

van Pelt, J., Vajda, I., Wolters, P.S., Corner, M.A. and Ramakers, G.J.(2005). Dynamics and plasticity in developing neuronal networks in vitro. *Prog.Brain Res.*147, 173–188.

Vicente R, Wibral M, Lindner M, and Pipa G. (2011). Transfer entropy—a model-free measure of effective connectivity for the neurosciences. *J ComputNeurosci***30**: 45–67. doi : 10.1007/s 10827 – 010 – 0262-3.

Wagenaar, D. A., Madhavan, R., Pine, J. and Potter, S. M. (2005). Controlling bursting in cortical cultures with closed-loop multi-electrode stimulation. *J Neurosci*25, 680-8.

Wagenaar, D. A., Pine, J. and Potter, S. M. (2006). Searching for plasticity indissociated cortical cultures on multi electrode arrays. *J. Neg.Res. Biomed***5**:16.doi:10.1186/1477-5751-5-16.

Wagenaar D A, Nadasdy Z, Potter S M. Persistent dynamic attractors in activity patterns of cultured neuronal networks. (2006). *Phys Rev E Stat Nonlin Soft Matter Phys.*73(5 Pt 1): 051907.

Weyand, T. G.(2007). Retinogeniculate Transmission in Wakefulness. *Journal of Neurophysiology*98, 769–785.

Wibral, M., Pampu, N., Priesemann, V., Siebenhuehner, F., Seiwert, H., Lindner, M., Lizier, J. T. and Vicente, R. (2013). Measuring information-transfer delays. *PLoS ONE* **8**(2) :e55809. doi: 10.1371/journal.pone.0055809.

Wiener, N. (1956). "The theory of prediction," in: *Modern Mathematics for Engineers*, ed. E. F. Beckenbach (New York:McGraw-Hill), 165-190.

Weliky, M., Katz, L. C. (1999). Correlational structure of spontaneous neuronal activity in the developing lateral geniculate nucleus in vivo. *Science* 285(5427), 599-604.

Zullo, L., Chiappalone, M., Martinoia, S. and Benfenati, F. (2012). A "spike-based" grammar underlies directional modification in network connectivity: effect on bursting activity and implications for bio-hybrids systems**.** *PLoS ONE***7**(11):e49299.doi: 10.1371/journal.pone.0049299.

Supplementary information

Paired spiking activity robustly shapes spontaneous activity in neural networks *in vitro*

Aurel Vasile Martiniuc[1*], Victor Bocos-Bintintan[1], Rouhollah Habibey[3], Asiyeh Golabchi[3], Alois Knoll[1], Axel Blau[3]

1 Computer Science Department VI, Technical University Munich, Garching, Germany

[1] Faculty of Environmental Science & Engineering, Babeş-Bolyai University, Cluj-Napoca, Romania

3 Department of Neuroscience and Brain Technologies, Italian Institute of Technology, Genoa, Italy

[*]Corresponding author email*:* martiniv@in.tum.de

Pictorial definition of spike train and burst parameters

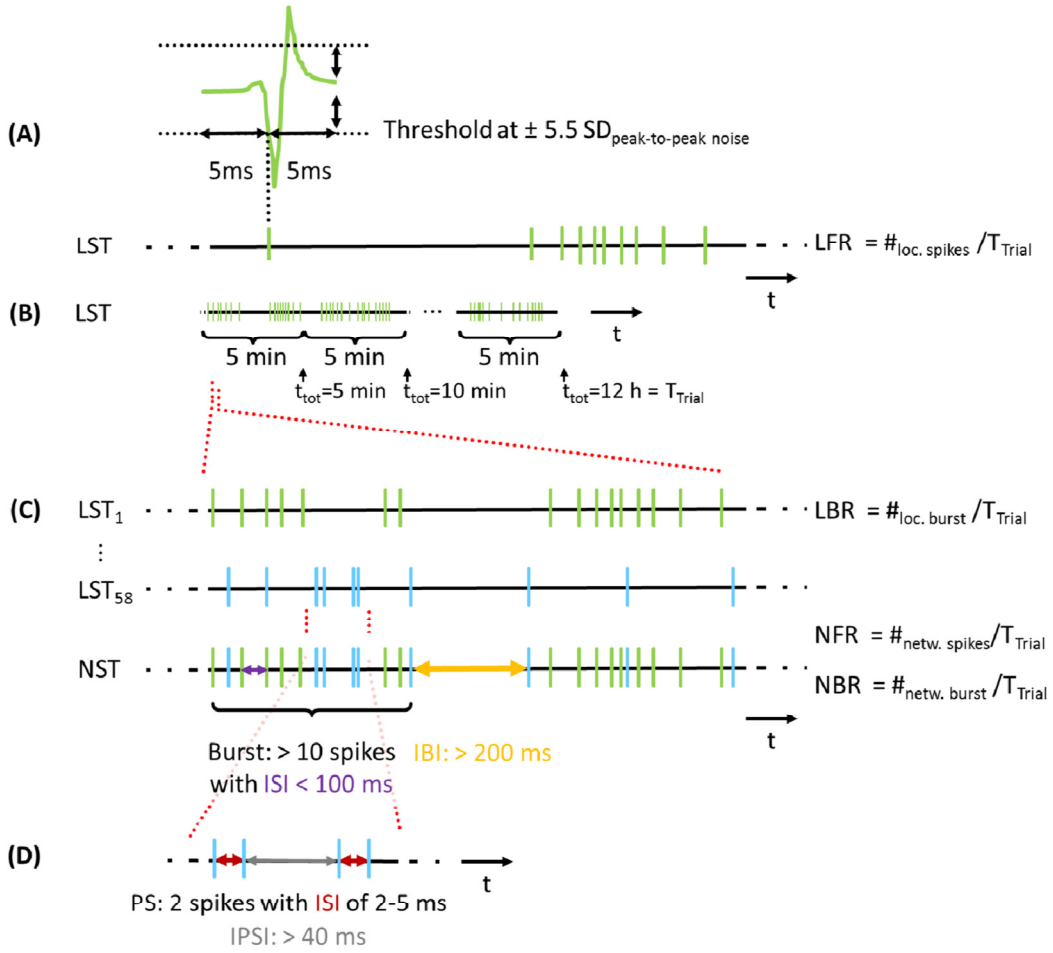

Suppl. Fig. 1 Graphical depiction of spike train and burst parameters. **(A)** Spike cutout: only upward (positive) and downward (negative) spike cutouts from 57 (cortical) and 58 (hippocampal) out of 59 recording electrodes were stored in 5 min packets. They consisted of 5 ms pre-spike and 5 ms post-spike fragments after first threshold crossing at ± 5.5 SD with respect to peak-to-peak noise. Only timestamps from downward threshold-crossings were extracted using Neuroexplorer (Nex Technologies). After removing simultaneous timestamps that occurred on all channels due to electrical or handling artefacts, subsequent 5 min datasets comprised of ≤ 58 timestamp streams were bundled in 12 hour timestamp packets for further

analysis in Matlab (MathWorks). These half-day packets were called trials of duration T_{Trial} ≤ 12 h.

(B) We quantified the local firing rates (LFRs) at individual sites as the number of recorded spikes divided by T_{Trial} for each local spike train (LST).

(C) At network level, we pooled all spikes from all 57 and 58 sites, respectively, for each trial into a single network spike train (NST) by sorting them in a time-ascending order. The NST represented the MEA-wide activity for each trial. The network firing rate (NFR) was then quantified as the total number of spikes in an NST divided by T_{Trial}. To further investigate activity dynamics, we used the burst rate (BR) for characterizing synchronous network activity. We scanned all LSTs at the 57 (cortical) and 58 (hippocampal) individual sites for each trial and defined bursting activity as events with more than 10 subsequent spikes individually separated by an ISI of less than 100 ms, followed by an interburst interval (IBI) larger than 200 ms (Wagenaar *et al.,* 2005). The local burst rate (LBR) at individual sites was calculated by dividing the number of bursts by T_{Trial}. Equally, the network burst rate (NBR) was obtained by scanning the NST for bursts using above mentioned criterion and dividing the number of bursts by T_{Trial}.

(D) Definition of a paired spike. Two subsequent spikes with inter-spike intervals (ISIs) between 2 and 5 ms were considered paired spikes (PS). Only PS with inter-paired-spike intervals (IPSIs) over 40 ms were counted.

MEA layout

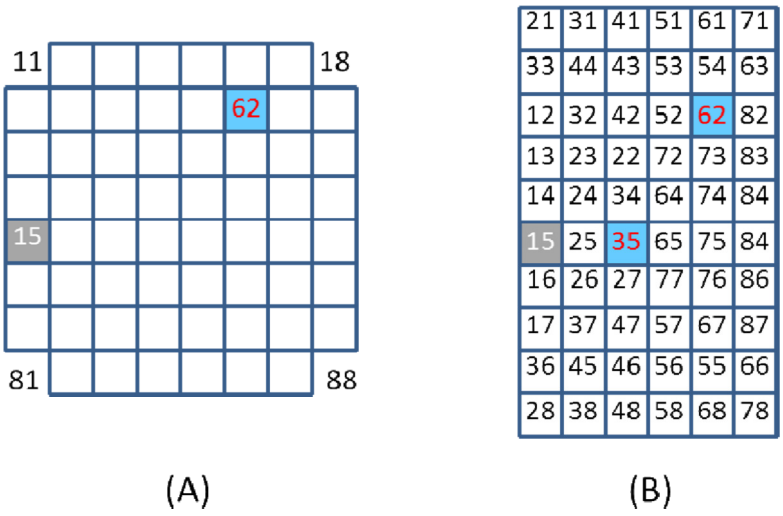

Suppl. Fig. 2 MEA electrode layout and channel association for the 8 x 8 MEA with the hippocampal culture **(A)** and for the 6 x 10 MEA with the cortical **(B)** culture. Grey squares indicate the relative position of the grounded counter electrode 15 (column, row). Blue squares with red numbers indicate switched-off channels.

References

Wagenaar, D. A., Madhavan, R., Pine, J. and Potter, S. M. (2005).Controlling bursting in cortical cultures with closed-loop multi-electrode stimulation.*J Neurosci*25, 680-8.

Paper 2

Sharpening of Directional Selectivity from Neural Output of Rabbit Retina

Aurel Vasile Martiniuc[1] and Alois Knoll[1]

[1]Computer Science Department VI, Technical University Munich, Garching, Germany.

Journal of Computational Neuroscience, August 2010. DOI: 10.1007/s10827-010-0266-z.

Summary of the paper

In this paper we scientifically investigate the sharpening in direction selectivity from retinal recorded output toward simulated postsynaptic target in the lateral geniculate nucleus. To do so we adopt a simple integrate-and-fire neuron model, inspired by recent work of Casti *et al.* (2008), to investigate how directional selectivity changes in cells postsynaptic to directional selective retinal ganglion cells (DSRGC).

Our model analysis shows that directional selectivity in the postsynaptic cells increases over a wide biophysical parameter range. We compared the neural recorded response of DSRGCs with artificial poisson-like spike trains that mimic the recorded cells and demonstrated that the sharpening in direction selectivity is not strictly governed by firing rate. Instead intrinsic properties of a particular cell type (i.e. ON-OFF DSRGC) consisting in boats of rapid firing activity at preffered direction combined with excitatory post synaptic summation and the static non-linearity of spike threshold at postsynaptic target might be responsible for sharpening in direction selectivity, while direct excitatory feedforward (one to one connection) suffice.

My contribution to this paper is as follows:

I participated in defining the scientific project, I analyzed the recorded neural data, I participated in writing the paper, I participated in editing the paper, I was the corresponding author and I did the major and minor revisions according to peer reviewing process by scientific committee within the editorial board of the journal.

III. Sharpening of Directional Selectivity from Neural Output of Rabbit Retina

Abstract

The estimation of motion direction from time varying retinal images is a fundamental task of visual systems. Neurons that selectively respond to directional visual motion are found in almost all species. In many of them already in the retina direction selective neurons signal their preferred direction of movement. Scientific evidences suggest that direction selectivity is carried from the retina to higher brain areas. Here we adopt a simple integrate-and-fire neuron model, inspired by recent work of Casti *et al.* (2008), to investigate how directional selectivity changes in cells postsynaptic to directional selective retinal ganglion cells (DSRGC). Our model analysis shows that directional selectivity in the postsynaptic cells increases over a wide parameter range. The degree of directional selectivity positively correlates with the probability of burst-like firing of presynaptic DSRGCs. Postsynaptic potentials summation and spike threshold act together as a temporal filter upon the input spike train. Prior to the intricacy of neural circuitry between retina and higher brain areas, we suggest that sharpening is a straightforward result of the intrinsic spiking pattern of the DSRGCs combined with the summation of excitatory postsynaptic potentials and the spike threshold in postsynaptic neurons.

Keywords: retina; ganglion cells; direction selectivity; integrate and fire model

Abbreviations:

DSRGC: direction selective retinal ganglion cell

LGN : lateral geniculate nucleus

SPN: simulated postsynaptic neuron

EPSP: excitatory postsynaptic potential

IPSP: inhibitory postsynaptic potential

DSi: Directional Selectivity index

AHP: After-Hyperpolarization

TFR: (spike) transfer ratio iS: Index of sharpening

AOS: Accessory Optic System

1. Introduction

As early as in the mammalian retina the motion perception is signaled toward higher brain areas by so-called direction selective ganglion cells (DSRGCs). These cells signal stimulus motion in a preferred direction and are silent to movement in the opposite, null direction.

DSRGCs have been extensively characterized in the rabbit retina (Barlow *et al.* 1964; Barlow and Levick 1965; Vaney *et al.* 1981b) but occur in many other species as well: mouse (Weng *et al.* 2005; Kim *et al.* 2008; Huberman *et al.* 2009), cat (Stanford and Sherman 1984), rat (Dann and Buhl 1987), turtle (Jensen and Devoe 1983), ground squirrel (Michael 1966) and teleost fish (Damjanovic *et al.* 2009).

Retinal direction selective cells can be separated in ON-OFF cells - if they respond at the beginning and the end of an incremental or decremental light stimulus - and in ON cells – if they respond at the beginning of an incremental light stimulus only. In the mouse retina a new OFF direction selective cell type has been recently discovered (Kim *et al.* 2008). The ON-OFF and ON cell types send the directional information to different nuclei: the ON-OFF

DS cells project to the dorsal lateral geniculate nucleus and the superior colliculus (Cleland *et al.* 1976, Vaney *et al.* 1981a). The ON DS cells represent the main input to the Accessory Optic System (AOS, Buhl and Peichl 1986). The functional properties of cells in the accessory optic system are consistent with their input from ON-DS cells in many species including primates: cat (Grasse *et al.* 1984), rat (van der Togt *et al.* 1993), and primates (Mustari and Fuchs 1989; Hoffmann and Distler 1989). A study performed in the rabbit's dorsal geniculate nucleus (Levick *et al.* 1969) reports a higher directional selectivity for LGN neurons compared to retinal ON-OFF DSRGCs. It remained unclear, however, how the sharpening of directional selectivity may be achieved. Directional selective cells in higher brain areas are rarely recorded in contrast to the abundant putative presynaptic DSRGCs (however, in cat DSRGCs are rarely encountered too, Cleland and Levick 1974).

In this study we took advantage of simultaneously recorded DSRGCs (both ON-OFF and ON DS) and asked under what conditions neurons postsynaptic to the DSRGC provide a more accurate directional tuning than the presynaptic cells. We investigated in our simulations, monosynaptic connections where the recorded spike train of a single DSRGC provides the presynaptic input to a postsynaptic model neuron. We also tested how polysynaptic inputs arrangements, from multiple DSRGCs, act upon the directional tuning at postsynaptic target.

Recently, Casti (Casti *et al.* 2008) demonstrated that using a simple approach, consisting in recorded retinal spikes, a variant of leaky integrate-and-fire model (firstly introduced by Woergoetter and Koch 1991) and excluding the diverse array of ion channels involved at retinogeniculate synapse and any feedback inputs, there is no need for any special synaptic mechanism beyond simple summation of EPSPs, necessary to accurately simulate the LGN discharge. Carandini, used a similar approach (he used a voltage based model instead a conductance based one) to indicate that "thalamic integration of spikes from the dominant retinal input depends primarily on postsynaptic summation and on basic

mechanism of spike generation" (Carandini *et al.* 2007). Therefore, we adopted a simple integrate-andfire model that has been validated recently for the retinogeniculate pathway of the cat and proposed for a general use (Casti et al 2008) in the same simple manner as described above (without taking into account neither synaptic plasticity nor feedback inputs), and asked how directional tuning is modified at postsynaptic level to DSRGCs. We also tried to give an explanation for the sharpening in DS observed under these conditions, based on intrinsic property of one type of DSRGC. We have explored all the parameters involved, under the physiological plausible range. Apparently, at presynaptic stage, the key role is played by burst-like activity in the ON-OFF DSRGCs while at postsynaptic stage the most important parameters are the height of the spike threshold relative to the PSP amplitude and the postsynaptic cell's time constant.

The simulated postsynaptic neuron (SPN) receives excitatory input and, in some simulations, also inhibitory input from its retinal presynaptic partners. We show that sharpening of directional tuning occurs over a wide range of biophysically reasonable parameters for ON-OFF direction selective cells but less so for ON direction selective cells. To explain the discrepancy we characterized the spike train properties of the two cell types.

We found that burst-like activity, which is more accentuated in one cell type (ON-OFF DSRGC), is one of the key factors responsible for the broad parameter range that lead to directional sharpening. Burst-like activity commonly found in ON-OFF DSRGCs apparently carries the information regarding the direction of stimulus motion. Additionally, the main effect responsible for the enhancement of direction-selectivity is presumably the spike threshold for the integrate-and-fire model, i.e. the SPN has a selective reduction in gain for input spike trains with long intervals, and an increase in gain for short intervals. Similar previous research efforts have also indicated that spike threshold at postsynaptic level substantially contributes to sharpening of direction selectivity in cat primary visual

cortex (Jagadeesh *et al.* 1997, Carandini *et al.* 2000, Volgushev *et al.* 2000, Priebe and Ferster 2005).

Furthermore, we investigate a hypothetical case of model neurons that receive direction selective input from multiple DSRGCs. The parameter range describing the strength of presynaptic excitatory input is shifted toward lower values, in order to achieve sharpening in directional tuning at the SPN. Past a specific strength of presynaptic excitatory conductance, if two strong excitatory inputs from two cells tuned to the same direction arrive simultaneously at the same postsynaptic neuron, almost every EPSP will give rise to an action potential (AP) at the postsynaptic neuron and no sharpening in direction selectivity can be achieved under our simulation conditions. We also found that a SPN receiving convergent excitatory input from two DSRGCs with the same preferred direction will signal better the direction of the stimulus motion than if the two DSRGCs would hold opposite preferred directions.

2. Methods

2.1 Experimental Data

We used data recorded from retinal ganglion cells of the adult isolated rabbit retina. The data acquisition using a 60 channel multi-electrode array (Multichannelsystems, Reutlingen, Germany) and off-line analysis has been described in (Zeck and Masland 2007).

Direction selectivity was tested using a square wave spatial grating moved in $N = 8$ equally separated directions $\varphi_i = i \cdot (2\pi/N)$, $i = 0,1,\ldots,N-1$.. For each direction the grating (spatial frequency 1 cycles/mm) was presented for 7 seconds at a temporal frequency of 1 Hz followed by a stimulus free interval of the same length. The total stimulus length ranged from 600 to 1200 seconds. The spatial extent of the moving grating was ~ 7 μm^2 on the retina. Thus, multiple cells were stimulated and recorded simultaneously.

Individual tuning curves were obtained considering the firing rate of each cell for each of the eight equidistant directions. Data from 10 ON-OFF DSRGCs and from 3 ON DSRGCs were used in this study.

2.2 Direction Selectivity Index

To quantify the directional tuning of a neuron, we used the direction selectivity index (*DSi*) as described by Taylor and Vaney (2002),

$$DSi = \frac{\left\| \sum_i \vec{v}_i \right\|}{\sum_i r_i} \quad , \qquad \vec{v}_i = r_i \begin{pmatrix} \cos\varphi_i \\ \sin\varphi_i \end{pmatrix}. \tag{1}$$

$\vec{v}_i$ is a vector pointing in the direction of the stimulus with the length equal to the number of spikes recorded during presentation of the stimulus (r_i). The *DSi* explains the directional

tuning based on the firing rates for different particular movement directions of the visual stimulus. The minimum value of 0 characterizes a non-directional neuron whereas the maximum value of 1 characterizes a neuron that responds for a single direction of movement. The higher the *DSi*, the higher direction selectivity is.

2.3 Measure of burst-like activity

In order to have a better understanding of the mechanism that presumably underlies the sharpening in direction selectivity of neurons postsynaptic to DSRGCs, we evaluated the burst-like firing of DSRGCs and postsynaptic model neurons. Burst-like firing events were defined as (at least two) spikes occurring after a prolonged period of silence, i.e. inter spike interval (ISI) larger than 50 ms, followed by an ISI shorter than 5 ms (Godwin *et al.* 1996b; Guido *et al.* 1995; Lu *et al.* 1992). Burst rate r^{burst} was defined as the number of burst-like firing events per time. Thus, we scanned the spike train of each cell (10 ON-OFF DSRGC and 3 ON DSRGC) for each stimulus direction (8 different directions) and each stimulus repetition (7 stimulus repetitions at each direction). The burst rate was then quantified as total number of calculated bursts divided by total duration of stimulus presentation for each cell.

To further investigate the role of presynaptic property (i.e. burst-like activity) we calculated the index of directional selectivity from burst rates (DSi^{burst}) in the same manner as from firing rates in response to stimulus presented at 8 different directions of movement.

$$DSi^{burst} = \frac{\left\| \sum_i \vec{v}_i^{burst} \right\|}{\sum_i r_i^{burst}}, \qquad \vec{v}_i^{burst} = r_i^{burst} \begin{pmatrix} \cos \varphi_i \\ \sin \varphi_i \end{pmatrix}. \tag{2}$$

Once that we identified the bursts in presynaptic spike trains, we asked how many APs in the postsynaptic spike trains are at origin a spike within a presynaptic burst-like event. Thus, we were able to separate in the postsynaptic spike trains those APs originating in burstlike firing in the DSRGCs from the other postsynaptic APs and to see the contribution of burst-like activity in the presynaptic neurons over the edited postsynaptic spike trains.

Further, we quantified the influence of the presynaptic burst-like activity in editing the corresponding SPN spike trains.

In this sense, for all pre- and postsynaptic pairs, we counted every postsynaptic AP with timing higher than 0 ms and lower than 5 ms (Kara et al 2003; Usrey 2002; Bair 1999) comparing with timing of each spike within a burst of its presynaptic counterpart. Those spikes in SPN trains were accounted as originating in a burst of presynaptic spikes. We defined burst efficacy (B^e) as the number of spikes at the SPN, at the preferred stimulus direction, evoked by burst-like activity of the DSRGC divided by the total number of spikes at the SPN, at preferred direction.

$$B^e = \frac{\#\text{SPN spikes due to bursts (at preferred direction)}}{\#\text{SPN spikes (at preferred direction)}} \qquad (3)$$

, where "#" stands for "number of".

To quantify the directional tuning of the activity in the SPN due to burst-like activity in the presynaptic cell, after we identified the number of APs in the SPN trains having at origin a presynaptic burst, we calculated the index of directional selectivity at SPN due to presynaptic burst-like activity ($DSi\ SPN^{burst}$) in the same manner as from firing rates in Eq. (1).

2.4 Modeling postsynaptic neurons

For modeling neurons postsynaptic to DSRGCs, we used a conductance-based "integrate and fire" (I&F) neuron model that had originally been introduced by Wörgötter and Koch (1991). A variant of this model was used by Casti *et al.* (2008) to describe the response of LGN neurons to input from retinal ganglion cells (RGCs). The membrane potential $V\,t(\,)$ of the I&F neuron is governed by:

$$C_m \frac{dV}{dt} = -(V - V_{\text{rest}})g_m - (V - E_a)\sum_f g_a(t - t_f) - (V - E_e)\sum_s g_e(t - t_s). \qquad (4)$$

An action potential is generated whenever the membrane reaches the threshold V_{thresh} (Fig.1). The first term on the right side of Eq. (4) describes the leakage current while the second term describes the effect of afterhyperpolarization (AHP) following each action potential. The input of the neuron is provided through excitatory channels (third term on right side) resulting in EPSPs. In a single case, we also considered "locked inhibition", i.e. inhibition that follows excitation with a fixed delay Δt_{ie} (see section 3.1, Fig. 3b), and an additional inhibitory current $-(V - E_i)\sum_s g_i(t - t_s - \Delta t_{ie})$ was added.

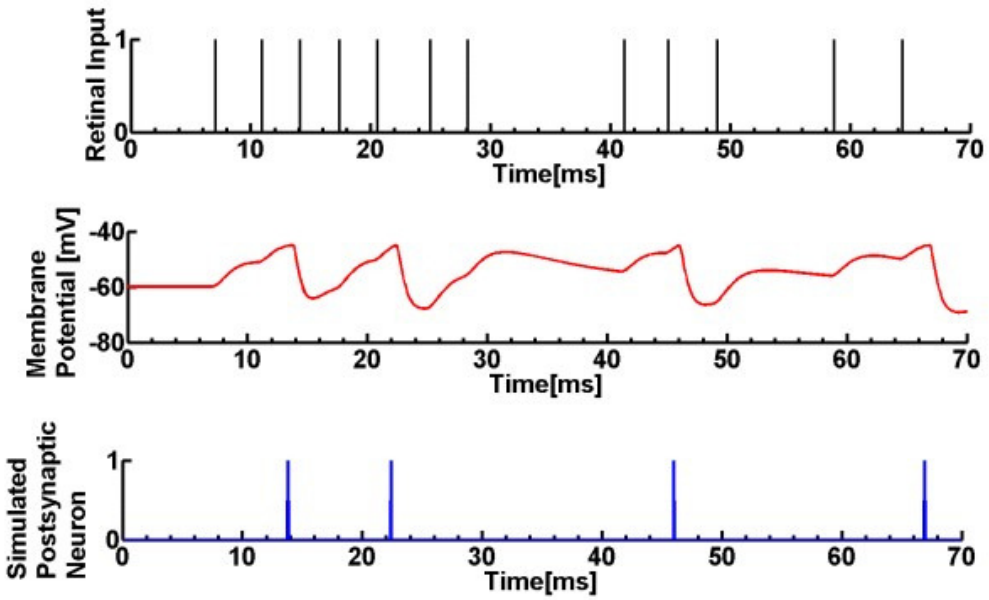

Fig. 1. Simulation of a neuron postsynaptic to direction selective retinal ganglion cell (Transfer ratio for the presented data segment is 0.3). Upper plot shows spike sequence of a retinal direction selective ganglion cell that provides (excitatory) input to a simulated postsynaptic neuron. Middle plot describes time course of the membrane potential V_m of a SPN computed by integration of Eq. (4). Lower plot represents spike sequence of the SPN. Resulting firing events of the SPN (firing threshold is V_{thresh} = -45mV).

The time-dependent conductances are modeled using "alpha-functions" (Rall 1967; Jack *et al.* 1975).

$$g_X(t) = \begin{cases} g_{\max,X} \dfrac{t}{\tau_X} e^{1-\frac{t}{\tau_X}}, & t \geq 0 \\ 0, & t < 0 \end{cases}, \qquad X \in \{a, e, i\}. \tag{5}$$

We also introduce the membrane time constant given by:

$$\tau_m = g_m^{-1} C_m \tag{6}.$$

Table 1 explains each model parameter and summarizes the values used for the different model parameters. In the majority of plots, we varied the maximum excitatory conductance (while other parameters were kept constant). We set all parameters that were kept constant, to

values found by Casti *et al.* (2008) to best describe the behavior of LGN neurons. The differential equation (4) was integrated using a first order Euler method with a time step of 0.1 ms.

Table 1: Parameter values used in this study (for parameter that can have different values, its typical value is highlighted in bold face). The membrane conductance can be calculated from Eq. (4), $g_m = \tau_m^{-1} C_m$.

Parameter	**Value(s)**
Membrane time constant τ_m	5 / 8 / **10** / 12 / 15 / 20 ms
Membrane capacitance C_m	1 nF
(Membrane conductance g_m	0.2 / 0.125 / **0.1** / 0.07 / 0.05 µS)
Resting potential V_{rest}	-60 mV
Threshold potential V_{thresh}	-45 mV
Excitatory reversal potential E_e	20 mV
Inhibitory reversal potential E_i	-90 mV
Afterhypolarisation reversal potential E_a	-95 mV
Maximum excitatory conductance $g_{max,e}$	0.02 / 0.03 / 0.04/0.05 / 0.06/0.07 / 0.1 / 0.15 µS
Maximum inhibitory conductance $g_{max,i}$	**0** / 0.02 / 0.03 / 0.04 / 0.06 / 0.1 / 0.15 µS
Maximum afterhypolarisation conductance $g_{max,a}$	0.59 µS
Excitatory time constant τ_e	1 ms
Excitatory time constant τ_i	1 ms
Afterhypolarisation time constant τ_a	0.5 ms
Time delay for locked inhibition Δt_{ie}	1 ms

2.5 Spike Transfer Ratio

Similar to Casti *et al.* (2008), we define the spike transfer ratio,

$$TFR = \frac{\#\text{SPN spikes}}{\#\text{DSRGC spikes}}, \qquad (7)$$

where "#" stands for "number of". According to Casti *et al.*, the biological plausible *TFR* values of LGN-cells for input from (non-direction selective) RGCs is between 0.07 and 0.7 (with median 0.34, see table 2 in Casti *et al.* 2008). Consequently, in our study, we imposed the constraint that *TFR* values of SPN spike train have to be in the above mentioned limits in order to be biologically plausible.

In our simulations, the *TFR* usually depends on stimulus direction φ_i and thus *DSi* and *iS* are often calculated from simulation runs with different *TFR*. For this reason, we use the maximum *TFR* value over all stimulus directions as the relevant parameter.

$$TFR = \max_i TFR(\varphi_i) . \qquad (8)$$

2.6 Index of Sharpening

To compare the direction selectivity of the output of the simulated postsynaptic neuron (SPN) with that of the driving neuron, we define the index of sharpening as:

$$iS = \frac{DSi(SPN)}{DSi(DSRGC)} . \qquad (9)$$

$iS > 1$ means that the SPN shows higher directional selectivity than the presynaptic neuron. For spike transfer ratios below 0.07, or above 0.7, we set iS to zero.

2.7 Artificial spike trains

In order to investigate which properties of spike trains effect sharpening, we also generated "artificial spike trains". These spike trains have the same average spike rates for different stimulus directions - and thus the same *DSi* - as spike trains recorded from DSRGCs. The firing probability was equally distributed over time according to a Poisson process except for defined refractory periods after each spike event. Spike trains with refractory period of 2 ms, 5 ms and 20 ms were generated.

3. Results

3.1. Sharpening of direction selectivity from ON-OFF direction selective cells

We first characterized the directional tuning of a simulated postsynaptic neuron (SPN) that receives input from a single direction selective retinal ganglion cell (DSRGCs). The spike trains of the DSRGCs have been recorded with a multi-electrode array. The SPN model adopted here incorporates several biophysical parameters that shape the spike transfer ratio: the passive membrane properties of the simulated postsynaptic neuron (SPN), (i.e. the membrane time constant), the synaptic conductance that determines the strength of PSPs and the spike threshold.

In a first simulation we varied the strength of synaptic excitatory conductance (parameter $g_{max,e}$). All other parameters were kept fixed (Table1). Similar, biological plausible values have been reported by Wörgötter and Koch (2001) and Casti *et al.* (2008).

Fig. 2a shows an example of the directional tuning of an ON-OFF DSRGC and its SPN counterpart for different $g_{max,e}$ values. This retinal cell had a preferred direction of 90 degrees,

and its DSi was 0.49. With excitatory synaptic input only, the SPN counterpart, is more directional selective than its retinal partner. The degree of sharpening – expressed as an index of sharpening (iS) – corresponds to the ratio of post- and presynaptic direction selective indexes, Eq. (9). We calculated iS values higher than 1 for a parameter range between $g_{max,e}$ = 0.06 µS (iS=1.4) up to $g_{max,e}$ =0.1(iS=1.2).

The degree of sharpening for ten ON-OFF direction selective neurons is shown in Fig. 2b. For all simulated cells we obtain sharpening of directional selectivity up to a value of $g_{max,e}$ that leads to a transfer ratio of 0.7 ($g_{max,e}$ =0.1 µS).

Weak synaptic inputs (i.e. $g_{max,e}$ < 0.04 µS) did not lead to sharpening in direction selectivity, because most of the spikes were not transmitted any more across the synapse (transfer ratio, Eqs. (7) and (8) below 0.07). As the strength of excitatory synaptic input grew, for four (out of ten) cells iS exceeded 1 already at $g_{max,e}$ =0.04 µS (Fig 2b). Excitatory synaptic inputs with $g_{max,e}$ ≥0.05 µS always led to iS>1. The mean value of iS =1.30 (std=0.20, n=10) at $g_{max,e}$ =0.05 µS, slightly decreased to iS=1.11 (std=0.06, n=10) at $g_{max,e}$ =0.1 µS. For a strong synapse ($g_{max,e}$ =0.12 µS) the transfer ratio (TFR) exceeds the maximum value of 0.7. At this value almost every EPSP is capable of evoking an action potential at the SPN. Thus the DSi of the SPN approaches the DSi of presynaptic cell resulting in iS≈1. This is shown by blue dashed lines in Fig. 2b which point out that iS stays close to 1 if TFR was ignored. Mean iS (at $g_{max,e}$ =0.12 µS without taking into consideration TFR) = 0.97(std= 0.02, n=10).

The degree of sharpening depends also on the tuning of the presynaptic cell. For an excitatory synapse of $g_{max,e}$ = 0.06 µS, the iS decreases for increasing direction selectivity indices of the retinal driver as indicated in Fig 2c. For ON-OFF DSRGCs with low DSi, sharpening at the postsynaptic neuron is stronger than that observed for high presynaptic DSi. Fig. 2d illustrates the finding that less sharpening is obtained if the retinal ganglion cell itself is highly tuned. In conclusion, sharpening in directional selectivity was achieved for all tested ON-OFF DSRGCs and was more prominent for presynaptic inputs with a lower DSi.

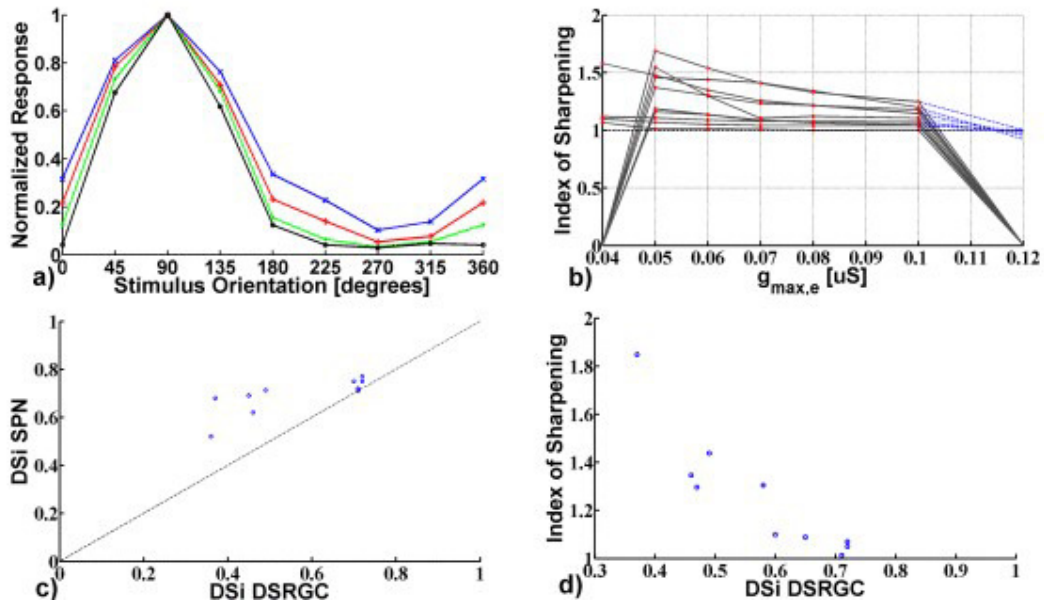

Fig.2 The directional tuning of model neurons increases if ON-OFF direction selective cells provide monosynaptic input. Index of Sharpening iS = DSi(SPN)/DSi(DSRGC), Eq. (9). Red dots indicate the values for which transfer ratio was between the considered limits of 0.07-0.7

a) Normalized (mean) responses (averaged over 7 trials) of an ON-OFF (blue curve) and of SPNs receiving excitatory input from the DSRGC for different synaptic conductances $g_{max,e}$. While the DSRGC has direction selectivity index DSi = 0.49, the simulated neurons have higher DSi values and thus iS > 1: For $g_{max,e}$ = 0.1 µS (red curve) we have DSi=0.59 resulting in iS = 1.2. For $g_{max,e}$ = 0.08 µS (green curve), we have DSi = 0.66 and iS = 1.34, for $g_{max,e}$ = 0.06 µS (black curve) DSi = 0.72 and iS = 1.4

b) Index of sharpening (iS) computed for 10 ON-OFF DSRGCs and their simulated postsynaptic counterparts for different maximum excitatory conductance $g_{max,e}$ (gray curves). On the average, we find sharpening (iS > 1) for $g_{max,e} \geq 0.04$ µS up to 0.1 µS. For $g_{max,e} \geq 0.12$ µS no significant sharpening is observed (DSi(SPN) ≈ DSi(DSRGC), iS ≈ 1) because each input spike triggers an output spike in the simulated postsynaptic neuron for high synaptic conductances, see blue dashed lines. For DSRGCs with high DSi, maximum iS=DSi(SPN)/DSi(DSRGC) is usually lower than for DSRGCs with low DSi.

c) Direction selectivity index for postsynaptic model neuron is higher than direction selectivity index of ON-OFF DSRGCs (for all cells). For this figure $g_{max,e}$ = 0.06 µS.

d) The degree of sharpening depends on presynaptic direction selectivity. The higher the DSi of presynaptic cell the lower the iS at SPN.

In a next set of simulations, we investigate how robust sharpening is, with respect to variations (of postsynaptic parameter) of the EPSPs' time constant (Fig 3a) and the introduction of an additional inhibitory conductance (Fig 3b).

We varied the EPSP's time constant and analyzed the additional effect that this parameter has on the iS. As EPSP time constant increases we found that sharpening is achieved at low $g_{max,e}$ values (Fig.3a, red contour indicates the areas where sharpening at postsynaptic target was achieved). For a constant strength of excitatory conductance we always find that sharpening is reduced as time constant of EPSP is increasing. This finding is simply explained by the fact that if the EPSP is prolonged the temporal summation of EPSPs will give rise to a large number of spikes at SPN and thus to a lower iS. By contrary, at low τ_e values, sharpening is achieved for strong excitatory synaptic input only.

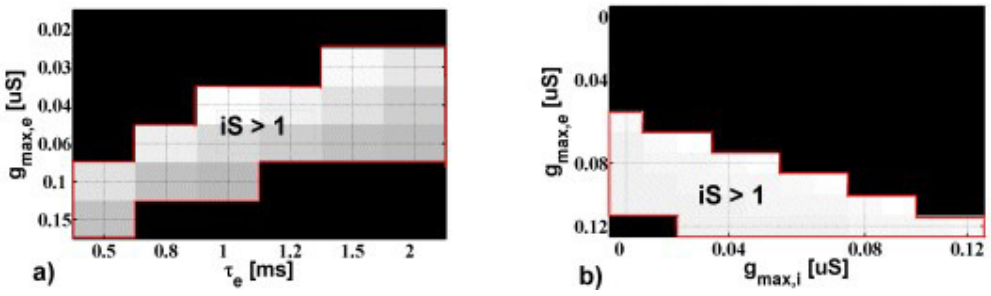

Fig. 3 Index of sharpening for a postsynaptic model neuron that receives input from a ON-OFF DSRGC in dependence on maximum excitatory conductance $g_{max,e}$ and EPSP time constant τ_e **a)** or maximum inhibitory conductance $g_{max,i}$ **b)**. The red contour line highlights areas where TFR is within the range [0.07, 0.7] and index of sharpening is higher than 1.

A stimulus that is larger than the center of the receptive field could provoke additional inputs from neighboring retinal cells directly or by mean of local interneurons (Alitto and Usrey 2005, Carandini *et al.* 2007). To investigate the effect of such a situation we added, in addition to excitatory input, inhibitory synaptic input convergent on the same postsynaptic model neuron.

For the inhibitory conductance we used a fixed time delay of 1 ms with respect to the excitatory inputs. Both, excitatory and inhibitory synaptic inputs are sent by the same DSRGC. Time locked excitation and inhibition has been found in the retinogeniculate pathway (Regher *et al.* 2005). Variation of these parameters under the transfer ratio restriction (i.e. $0.07 \leq TFR \leq 0.7$) demonstrates that over a wide range of model parameters the postsynaptic neuron has a higher index of direction selectivity than its presynaptic main driver.

As expected, if $g_{max,i}$ increased (strong inhibition) $g_{max,e}$ must also increase in order to achieve sharpening at SPN. Thus, if $g_{max,e}$ takes low values ($g_{max,e}$ <0.05 μS, Fig.3b) no sharpening at the postsynaptic level can be obtained.

Altogether, the scenarios presented so far suggest that direct monosynaptic excitatory input is sufficient to achieve sharpening at postsynaptic neuron for a wide range of biologically plausible synaptic strengths. Additional parameters, describing postsynaptic neuron properties or involving polysynaptic mechanism, do not radically change the sharpening in direction selectivity at the SPN.

3.2. Sharpening of direction selectivity from ON direction selective cells

In addition to the ON-OFF direction selective neurons, we investigated a second type of direction selective cells – the ON DS cells. These cells have broader directional tuning and thus smaller DS indices than ON-OFF DS cells.

In contrast to the extensive sharpening of small DS indices from ON-OFF cells (Fig 2c) we find little sharpening for the three ON DS cells investigated (Fig.4a). The simulations were performed analogous to the ON-OFF DS cells with the constraint on the transfer ratio. For one of the cells we found sharpening at SPN only for a single $g_{max,e}$ value (Fig. 4a, $g_{max,e}$ = 0.1 μS, iS = 1.1) while the other two cells presented iS higher than 1 for a restricted range of $g_{max,e}$ values

($g_{max,e} \geq 0.07$ µS and $g_{max,e} \leq 0.1$ µS for one cell and $g_{max,e} \geq 0.06$ µS and $g_{max,e} \leq 0.1$ µS for the other cell). The degree of sharpening is less pronounced than in the case of ONOFF DSRGCs and in mean it starts exceed 1 only at $g_{max,e}$ =0.07 µS when iS = 1.11. Beyond $g_{max,e}$ = 0.1 µS no sharpening is achieved due to the fact that such strong synaptic input is generating almost at each EPSP an AP at SPN so that iS tends to be almost 1 (as indicated by the blue curve in Fig 4a if TFR were ignored). Thus, for ON DS RGCs we found less sharpening when comparing with ON-OFF DSRGCs in the same simulation conditions.

3.3. Sharpening of directional selectivity from artificial spike trains mimicking direction selective neurons.

Apparently, the presynaptic degree of directional tuning does not provide evidence how the sharpening works. We therefore considered artificial spike trains that mimicked the firing rate and thus directional tuning of ON-OFF as well as ON DS cells. The spike trains followed a Poisson distribution. We calculated the postsynaptic sharpening for a total of ten artificial spike trains. Each spike train mimicked the directional tuning of the ten recorded ON-OFF DS. Additionally, we built artificial spike trains with similar index of selectivity as one ON DS cell having DSi=0.34. For each of the firing rates we consider three refractory periods: 2ms, 5 ms and 20 ms.

Among the artificial spike trains, both, sharpening obtained for the widest gmaxe range and the highest iS values are found for short ISIs (i.e. refractory period of 2 ms). For spike trains with short refractory periods (minimum 2 ms) the sharpening at SPN, for all ten simulated spike trains, is achieved for an interval of $g_{max,e}$ =[0.07 – 0.1] µS (Fig4b, red curve) more restricted than for the real ON-OFF DSRGCs for which we found sharpening for a larger interval $g_{max,e}$ =[0.05 – 0.1] µS (Fig. 2b). For these artificial spike trains, at $g_{max,e}$ =0.06 µS mean iS = 0.53

(std= 0.69, n=10), while at $g_{max,e}$ =0.06 μS the recorded ON-OFF DSRGCs show a much higher mean index of sharpening, iS=1.30. The best sharpening for all ten artificial spike trains has its mean iS value iS= 1.39 (std= 0.22, n=10). For the ten recorded spike trains the maximum value of sharpening is higher, iS=1.41(std=0.23, n=10).

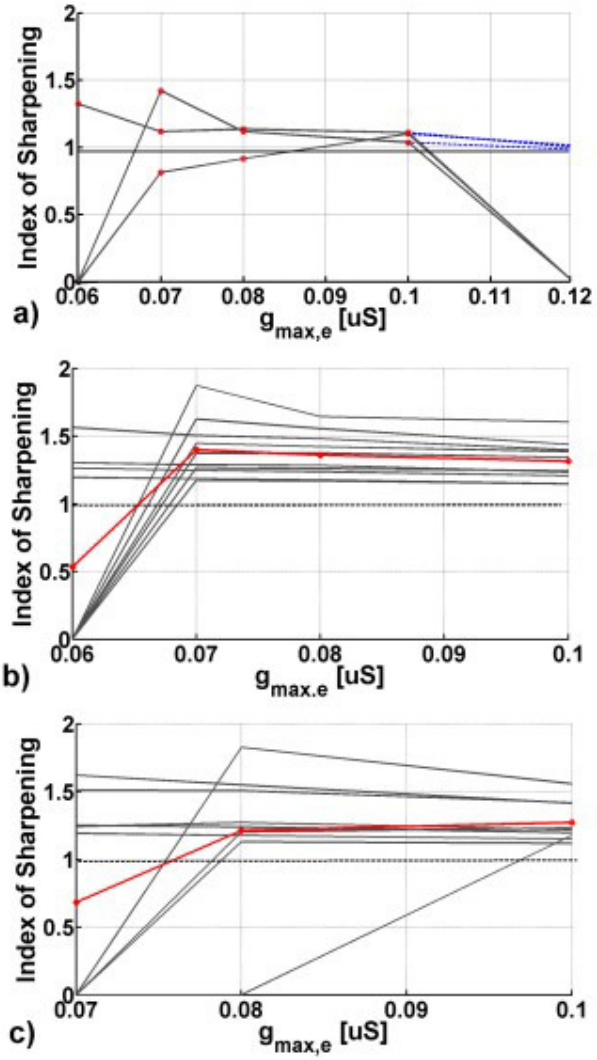

Fig. 4 Index of sharpening for ON DS and artificial spike trains

a) Index of sharpening for 3 ON DSRGCs . For ON-DSRGCs, sharpening is obtained only for conductances larger $g_{max,e} \geq 0.07$ μS. Red dots in the plots indicate $g_{max,e}$ values for which TFR is in the validation domain, while blue dashed lines indicate the iS value if TFR were ignored.

b) Index of sharpening for 10 artificial spike trains mimicking the 10 ON-OFF DSRGCs recorded and post-synaptic model counterparts. Refractory period is 2 ms. Mean iS (red curve) is indicating a sharpening for a more restricted $g_{max,e}$ interval than for recorded cells (Fig 2b) regardless the fact that they have similar firing rates and DSi. Best sharpening among artificial spike trains, is obtained for 2 ms refractory period spike trains and is less present as refractory period increase. At 20 ms iS>1 only at $g_{max,e}$ = 0.1 μS. For ON DSRGC we found iS>1 only for a single $g_{max,e}$ value = 0.1 μS.

c) Index of sharpening for 10 artificial spike trains mimicking the 10 ON-OFF DSRGCs recorded with a refractory period of 5 ms. For these artificial spike trains the sharpening at SPN is even more restricted.

Increasing the refractory period to 5 ms we found, the mean, sharpening for a more restricted interval of $g_{max,e}$ = [0.08 – 0.1] μS (Fig. 4c, red curve). Mean iS indicates the highest sharpening for these artificial spike trains at $g_{max,e}$ =0.08 μS, mean iS= 1.21 (std= 0.47, n=10). Thus for longer refractory periods, the sharpening achieved is also more restricted compared to recorded ON-OFF DSRGCs.

For the spike trains with 20 ms refractory period we found sharpening only for $g_{max,e}$ =0.1 μS(data not shown here). For the artificial spike trains mimicking ON DS cell we achieved sharpening only at $g_{max,e}$ =0.1 μS and only if the refractory period was set at 2 ms (data not shown here).

If firing rates of the presynaptic cell would be responsible for sharpening at postsynaptic neuron, subsequently one would expect similar iS (for similar $g_{max,e}$ values) to be obtained at the output of artificial spike trains with the same DSi as the recorded cells. Instead, we found a more restricted parameter range for which sharpening can be achieved for the artificial spike trains.

3.4. Burst-like spiking activity carries the directional-selective information

The results from the artificial spike trains indicate that sharpening of directional tuning does depend on the short inter spike intervals encountered in some direction selective cells. It does not depend on the neuron's firing rate that is different for the different recorded DSRGCs and artificial spike trains (compare Fig.2b and Fig.4). We therefore investigated the intrinsic spike train properties of DSRGCs. We selected a parameter often used in the analysis of LGN neurons: the percentage of bursting. Burst-like events were identified and quantified as described in Methods (Methods 2.3). We calculated the burst-rate in the response of ONOFF DS cells as well as ON DS and artificial Poisson-like spike trains.

We found that burst-like activity was more pronounced for the ON-OFF DSRCs than for the ONDS cells or for the artificial spike trains. As shown in Fig.5a burst rate at preferred direction for ON-OFF cells was highest, the mean for all ten cells was 2.29 +/- 0.9 (n=10) [bursts/sec], even ten times higher than for ONDS cells for which mean burst rate for all trials was only 0.07 +/- 0.06 (n=3) [bursts/sec]. For artificial spike trains we also found a lower burst rate at preferred direction even though the firing rate mimicked that of the ten recorded ONOFF DSRGCs. While for spike trains with 2ms refractory period we could find a sharpening more pronounced than for the spike trains with refractory period of 5ms and 20ms, we also found a burst rate at preferred direction higher for these spike trains with a mean of 0.54 +/- 0.15 [bursts/sec], (n=10). As in Fig.5a, once that refractory period increased the artificial spike trains diminished their burst-like activity, so that we found for 5ms refractory period a mean burst rate of 0.04 +/- 0.04 [bursts/sec], (n=10), and for 20ms refractory period 0.03 +/- 0.02 [bursts/sec], (n=10).

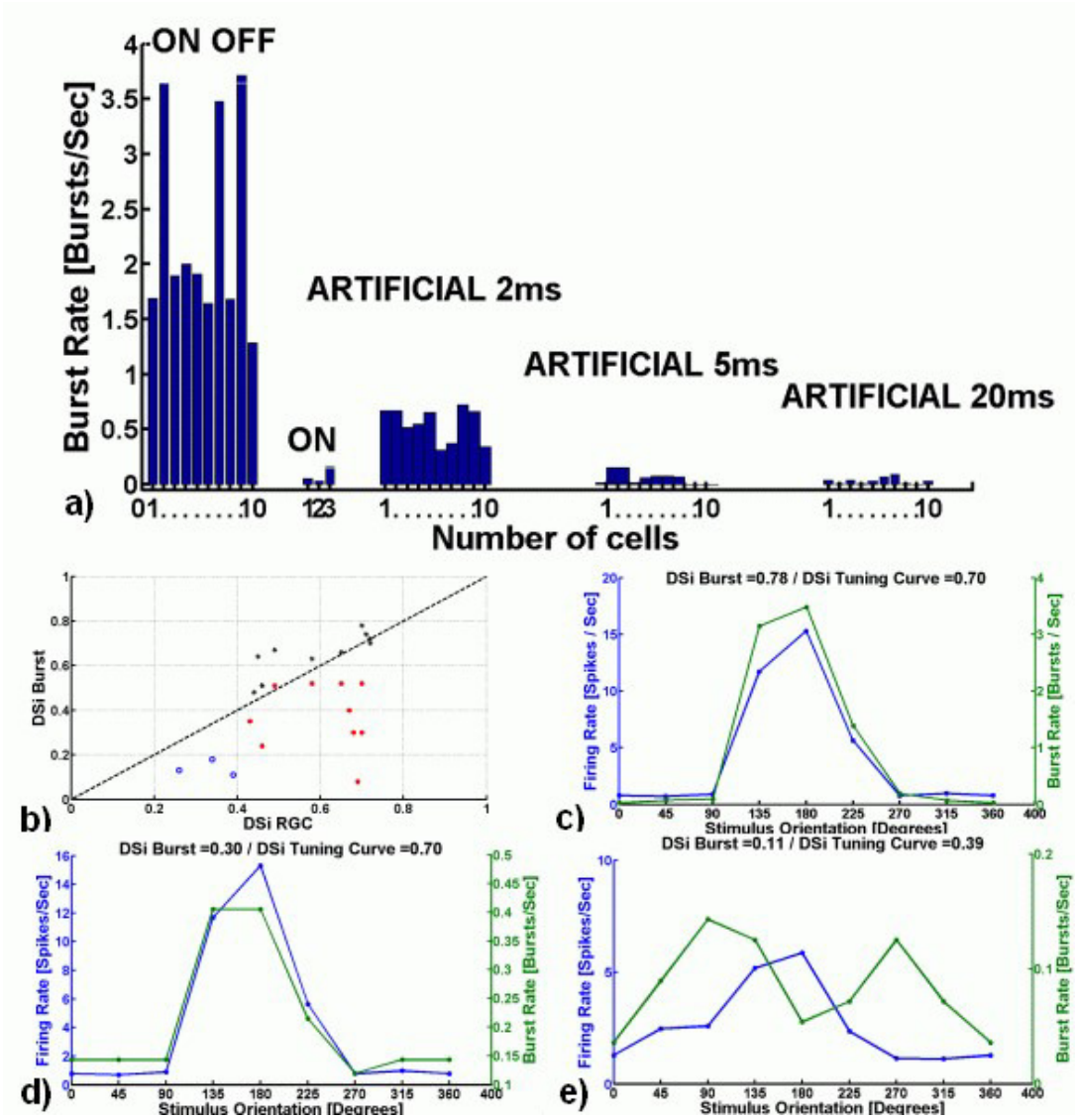

Fig. 5 Burst-like activity

a) Burst rates at preferred direction calculated for recorded cells and for artificial spike trains. The highest burstlike activity is obtained for ON-OFF DSRGCs. ON DS cells show almost no burst-like activity. Artificial spike trains also exhibit reduced burst-like activity. X axis indicate the number of cells for which the burst rate at preferred direction was quantified.

b) Index of selectivity for burst-like events (Y axis) and for firing rate (X axis) shows that only for ON-OFF DSRGCs (dark dots) DSi Burst is higher than DSi firing rate. For ON DS cells (blue dots) and for artificial spike trains (with 2 ms refractory period) DSi Burst is lower than DSi firing rate.

c) Tuning curves of firing rate (blue curve) and burst rate (green curve) for one ON-OFF DSRGC. Burst rate is more sharpened (DSi = 0.78) than firing rate (DSi = 0.70) and oriented at preferred direction.

d) Tuning curves of firing rate (blue curve) and burst rate (green curve) for one artificial spike train that mimics the ON-OFF DSRGC presented in Fig. a). In this case DSi^{burst} (DSi = 0.30) is considerable lower than DSi firing rate (DSi = 0.70) and does not singularly indicate the preferred direction.

e) Tuning curves of firing rate (blue curve) and burst rate (green curve) for one ON DS cell. Burst-like activity is clearly not pointing the preferred direction and it's DSi^{burst} = 0.11 is lower than DSi firing rate (= 0.39).

Beside this discrepancy there are two more factors that worth to be noted –one is that burst-like activity for ON-OFF DSRCs was tuned at preferred direction (Fig.5 c show the tuning curves for one ON-OFF DSRGC calculated from firing rate (blue) and burst rate (green) - the preferred direction indicated by maximal firing rate coincides with the preferred direction calculated from burst rate). That is, at preferred direction ON-OFF DSRGCs show burst-like activity more than at intermediate directions. In this way the probability of evoking an AP at SPN becomes higher at preferred direction while two (or more) closed (in time) EPSPs are more successful in rising membrane potential of SPN above the threshold. This phenomenon is known as paired spike enhancement and has been demonstrated at many synapses (Usrey *et al.* 1998, Carandini *et al.* 2007). The burst rate for ON DS cells and artificial spike trains was almost equal zero and pointing non-preferred directions (Fig.5d, e).

We used burst rate for each presentation direction to calculate the degree of directional selectivity. Once we calculated the burst rate at each direction of stimulus presentation we next used DSi^{burst} as described by Eq. (2), in a manner similar to that used for firing rate, and we calculate the direction selectivity index for burst-like spiking.

The other important factor is that tuning curves for burst rate were more sharpened than the tuning curves of firing rates for ON-OFF DSRGCs, so that the index of selectivity for burst-like activity (DSi^{burst}) was always higher than DSi firing rate (black dots Fig.5b). By contrary DSi^{burst} for ONDS cells (Fig.5b blue dots) and for artificial spike trains with 2ms refractory period (Fig.5b red dots) was lower than DSi calculated from firing rates.

In summary, for the ten ON-OFF DSRGCs we found a mean burst rate at preferred direction significantly higher than for ON DS cells or artificial spike trains. Burst-like activity is tuned at preferred direction and has a higher DSi than firing rate for ON-OFF DSRGCs as compared with ON DS or artificial spike trains which show the opposite results.

It is already well known that these two different RGC types possess different spike train signatures (Zeck et al 2007). Our analysis shows also that ON-OFF cell type exhibit burst-like activity at preferred direction while ON cell type has less or no burst-like activity.

That short ISIs in the presynaptic spike trains are recognized to be very important in transmitting information at different stages within the brain is already well known (Sincich *et al.* 2007, Rathbun *et al.* 2007). In our example burst-like activity seems to be the key in signaling better the direction of motion of visual stimulus at the output of retina.

We went further into more detailed analysis and calculated the number of postsynaptic APs due to presynaptic burst-like firing. We scanned the spike trains of both, presynaptic and postsynaptic cells, and counted the spikes at SPN due to burst-like activity in presynaptic spike train for each pair of pre- and post-synaptic cells. In this manner we could quantify the efficacy and influence of the presynaptic burst-like activity (B^e) as the number of spikes at SPN due to bursts at preferred direction divided by the total number of spikes at SPN, at preferred direction, for each pair of cells (Eq.3).

For the ten recorded ON-OFF DSRGCs we found that mean B^e has its maximum at the best sharpening observed. Remarkably, once that $g_{max,e}$ increases, mean TFR also increases, while both, mean B^e and iS decrease (Fig.6a, Fig.2b). This is explained by the fact that at low $g_{max,e}$ the number of postsynaptic spikes, at preferred direction, due to burst-like activity of the presynaptic cell is the highest compared with the total number of spikes at SPN, at preferred direction. At this point the best sharpening is observed. Once $g_{max,e}$ increases, the number of spikes at SPN increases, but the number of spikes at SPN due to a burst in presynaptic cell decreases and we notice a less pronounced sharpening. While for the best observed sharpening, B^e has a maximum, for less sharpening the number of spikes at nonpreferred direction increases

and the influence of the burst-like activity of the presynaptic cell is diminished. It is crucial to point out that these findings bring us to the following remark – burst-like spiking activity is carrying the information about direction selectivity. Thus, at best sharpening this component of the spike train that can inform about direction of stimulus movement at preferred direction is preserved (B^e has its maximum) while the components signaling the movement of stimulus at intermediate directions are lost.

The mean B^e for the ON-OFF DSRGCs was at its maximum 0.45 +/- 0.25 (n=10) and it decreased to 0.36 +/- 0.18 (n=10) at its minimum.

For the artificial spike trains with 2 ms refractory period mean B^e at its maximum was only 0.12 +/- 0.06 (n=6) and decreased at 0.06 +/- 0.03 (n=6) at its minimum (Fig.6b).

Once we calculated the number of spikes at SPN due to burst-like activity at presynaptic cell for each pair of cells, we then calculated (in the same manner as for firing rates) the indexes of selectivity of these SPN spikes, due to bursts ($DSi\ SPN^{burst}$). Fig.6c shows that for the ON-OFF DSRGCs, mean $DSi\ SPN^{burst}$ is always higher than DSi SPN and is decreasing as $g_{max,e}$ increases and sharpening decreases. This means that if the spike trains at SPN were only due to burst activity in the presynaptic cells we were having a higher degree of sharpening. Due to the fact that the TFR is increasing with $g_{max,e}$, the increasing number of APs at non-preferred directions is lowering the degree of sharpening. However, $DSi\ SPN^{burst}$ always remains higher than DSi SPN and indicates the burst events control the degree of sharpening.

For the artificial spike trains (Fig.6d) the effects are different. Firstly, we always observed that DSi at SPN is higher than $DSi\ SPN^{burst}$, so that the number of spikes due to bursts is not able to control the sharpening at SPN. Moreover, even if $DSi\ SPN^{burst}$ is increasing as $g_{max,e}$ increases (opposed as in ON-OFF DSRGCs case), the degree of sharpening is decreasing (DSi SPN decreases). This strengthens the fact that burst-like activity for artificial spike trains (substantially less present than for ON-OFF DSRGCs) does not control the sharpening at SPN.

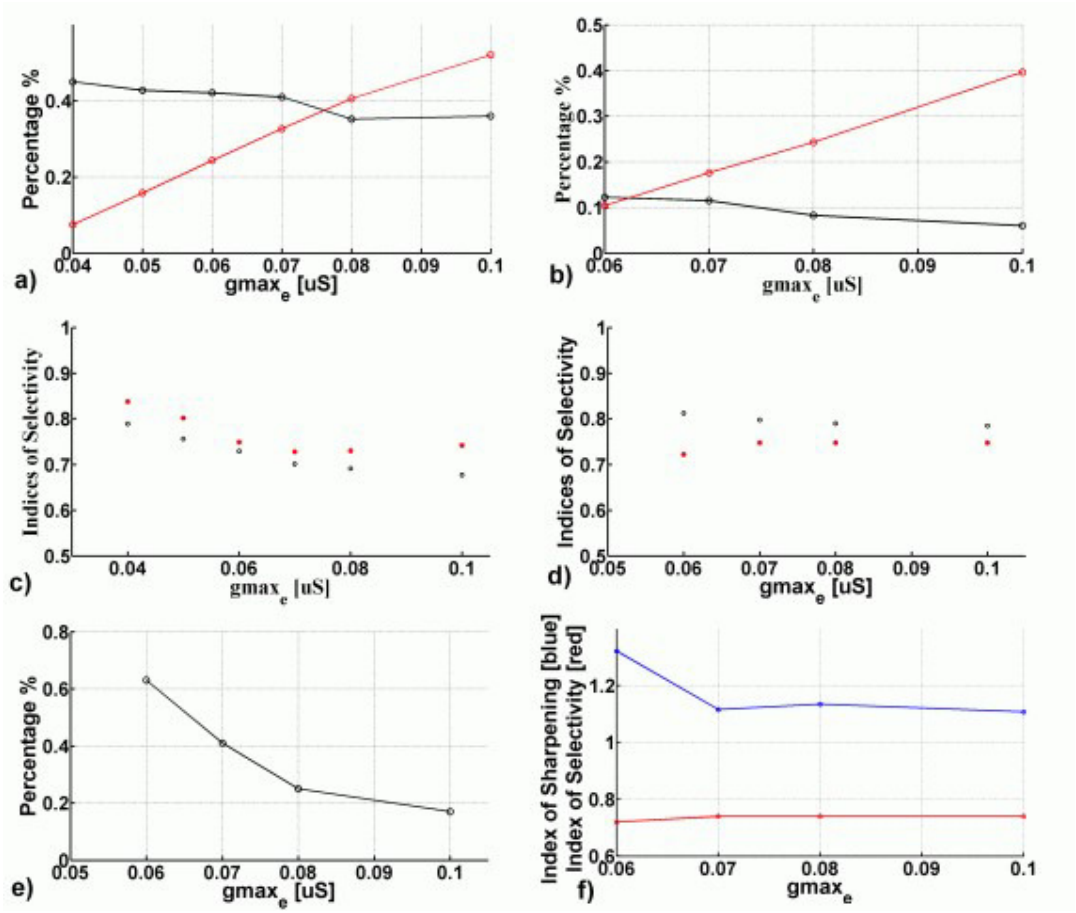

Fig. 6 Burst efficacy and index of sharpening

a) Black dots represent mean burst efficacy (B^e) as described by Eq.3, for 10 ON-OFF DSRGCs. Red dots show the TFR course as $g_{max,e}$ increases. B^e is decreasing as TFR increases due to a larger number of spikes at intermediate direction, as a consequence iS is decreasing too (see Fig. 2b).

b) Black plot is mean burst efficacy and red dot is mean transfer ratio. For the artificial spike trains that mimic the 10 recorded ON-OFF DSRCs B^e is lower than for the recorded cells and also decreases as TFR increases.

c) DSi at SPN due to burst-like activity measured for 10 ON-OFF DSRCs (red dots) is higher than DSi at SPN (black dots) and is controlling the sharpening at SPN. As $g_{max,e}$ increases DSi at SPN due to burst-like activity is decreasing and as a consequence iS is also decreasing.

d) For the artificial spike trains that mimic the recorded cells DSi at SPN due to burst-like activity (red dots) is permanently lower than DSi SPN (black dots) and is increasing as iS decreases, hence proving no control mechanism over the sharpening at SPN.

e) One single ON DS cell presented spikes at SPN due to burst-like activity at the presynaptic level. This cell has

B^e (black dots) with a drop as $g_{max,e}$ increases.

f) Index of sharpening (blue dots) and index of selectivity (red dots) for the same ON DS cell as above. Interestingly, as $g_{max,e\ increases}$ from 0.06 to 0.07, DSi increases while iS decreases. Moreover Fig. 6e) shows that as $g_{max,e}$ increases from 0.07 to 0.08, B^e decreases but contradictory iS increases (blue dots) showing that there is no direct mechanism based on burst-like activity to enhance sharpening (iS) for ON DS cell.

For two of the ONDS cells we did not find any spike at the SPN, at preferred direction, due to burst-like activity at the presynaptic level. For the third ONDS cell we found at SPN level a few spikes due to burst-like activity at the presynaptic level. In this case (Fig.6e, f) we found that while B^e decreases from $g_{max,e}$ =0.07 to 0.08, the index of sharpening is slightly increasing, for the same parameter values (Fig.6,f -blue dots). Additionally, DSi^{burst} increases for $g_{max,e}$ = 0.06 to 0.07 (Fig.6,f -red dots) while index of sharpening is decreasing for the same values of $g_{max,e}$ (Fig.6,f -blue dots) . Altogether with the fact that DSi^{burst} was always lower than DSi_{SPN} and the very low burst rate that we found, led us to the conclusion that burst-like activity is not at the origin of sharpening we found for ONDS cell, indeed for a more restricted parameter range than for the ON-OFF DSRGCs.

3.5. How is the enhancement performed at the postsynaptic cell?

So far we have found that burst-like activity carries the information about direction of stimulus movement. This intrinsic property is commonly found at ON-OFF DSRGCs and is predominant at preferred direction of stimulus movement. It has been already shown that PSP summation and spike threshold suffice to explain the transformation of the retinal input spike train to a new spike train output of LGN cell. In our simulation conditions, summation of the incoming retinal EPSPs combined with postsynaptic spike threshold act as a temporal filter to perform a selective reduction in gain for long ISI presynaptic discharge and to increase in gain for short ISI spike trains.

To see more in details how this filter works, we checked firstly the relation between spike threshold membrane potential ($V_{threshold}$) at the SPN and index of sharpening for a typical input of ON-OFF DSRGC and middle value of $g_{max,e}$ = 0.06 μS (Fig.7a). We varied $V_{threshold}$ from -55mV up to -25mV. As $V_{threshold}$ increased iS also increased, so that at -51 mV we found iS=1.1 and at $V_{threshold}$ = -39 mV iS increased at iS=1.58.

This is explained very simple. Once that $V_{threshold}$ increased, at $g_{max,e}$ constant, it is necessary to have more closed in time EPSPs to raise the membrane potential above the threshold value, that is, a pronounced burst-like activity (short ISI) in the DSRGC spike train. At the intermediary directions of stimulus movement, burst-like activity (short ISI) is lower than at the preferred directions for ON-OFF DSRGCs (Fig.5c) and thus the summation of EPSPs become less efficient as $V_{threshold}$ increases. The result is that for intermediary directions less APs at SPN will be evoked so that the information about these directions of stimulus movement will be lost. By contrary, at preferred directions, burst-like activity (short ISI) is more accentuated, and will be sufficient amount of closed EPSPs to sum and raise the membrane potential above the threshold to produce APs at SPN. Thus, this component of the input spike train, signaling the preferred direction, will be preserved. As expected, if $V_{threshold}$ continue to further increase, at some value, too little amount of APs at SPN will be evoked so that TFR will be below its limit and iS becomes zero (Fig.7a).

Furthermore, we checked the relations between cell's time constant (τ_m) and iS for a middle value of V_{thresh} = -45 mV and a middle value of $g_{max,e}$ = 0.06 μS (Fig. 7b). At τ_m = 6 ms, iS = 1.58, while at τ_m = 20 ms we found iS = 1.14. For a low τ_m value, if the ISi is large (slow input spike train) EPSPs do not sum together to force the membrane potential to reach the threshold. Thus, at preferred directions, where the ISI is shorter, the chance to have APs at SPN is greater and thus iS is higher. Once that τ_m increases, the ISI necessary for temporal summation to take place increases also, so that at intermediary directions the chances to have APs at SPN increases too, resulting in a decrease of iS (Fig. 7b).

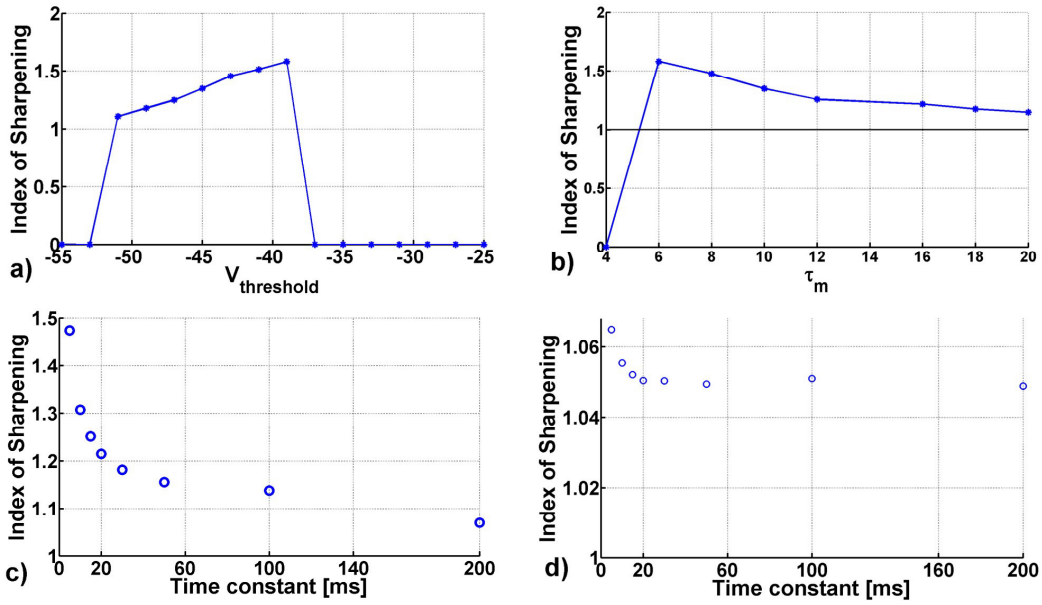

Fig. 7. Model enhancement mechanism

a) Relation between iS and $V_{threshold}$ for a typical input spike train of an ON-OFF DSRGC with DSi=0.49. As spiking threshold increases the sharpening obtained is larger due to the fact that only at preferred direction EPSPs summation can raise the membrane potential above the threshold. However, for large thresholds there are only a few APs evoked at the SPN, so that iS=0.

b) Cell's membrane time constant variation is depicted on X axis. Best sharpening is at low time constant values. Indeed for low τ_m values, the EPSPs are closed enough in time, in order to realize the temporal summation, only at preferred direction during the burst-like spiking activity.

c) Nonlinear amplifier with a specific time constant (X axis) applied to an incoming retinal spike train with a middle DSi = 0.49. Index of sharpening (Y axis) decreases as time constant increases.

d) Nonlinear amplifier with a specific time constant (X axis) applied to an incoming retinal spike train with a very high DSi = 0.72. The temporal filter gives a sharpening for τ_m = 5ms, almost as good as for τ_m = 200ms. The influence of the temporal filter is reduced comparing with low tuned presynaptic cell.

To have a better intuition over the temporal filter that acts upon the incoming retinal input we built a simpler mathematical model which depicts a nonlinear amplifier with a specific time constant and applied it over the inverse spike intervals of a typical input spike train

(Fig47c). Briefly, we calculated the ISI for a typical recorded spike train of one ON-OFF DSRGC (DSi=0.49). We established two thresholds, the low limit representing the refractory period and high limit representing the specific time constant (τ). Once that ISI is higher than the low limit and lower than the high limit, we hypothesized that PSPs summation was possible and we counted an AP at the SPN. We then calculated the tuning curve of the SPN and thus the index of sharpening. At low values of time constant $\tau = 5$ ms we found the best sharpening iS = 1.47. As τ increased the sharpening decreased, so that at $\tau = 200$ ms we found iS = 1.06. Therefore, if $\tau<5$ ms we found best sharpening and indicates the fact that most of the short ISI (ISI<5 ms) spiking activity is encountered at preferred direction strengthening the probability that closed EPSPs to sum and evoke APs at SPN. As τ increase sharpening becomes weaker indicating that large ISI spiking activity is often found at intermediate directions of stimulus movement, so that when cell's time constant becomes larger, temporal summation of EPSPs will evoke APs at intermediate directions too, decreasing iS.

We also have shown that the degree of sharpening depends on the tuning of the presynaptic cell so that for input spike trains with high DSi the index of sharpening obtained was lower than for input spike trains with low DSi (Fig. 2d). This simpler mathematical model which shows the ISI distribution explains why iS is low for high presynaptic DSi. Briefly, for a recorded spike train of one ON-OFF DSRGC with high DSi (DSi=0.72) we found a sharpening iS=1.06 at $\tau=5$ ms and iS=1.04 at $\tau=200$ ms (Fig.7d). Therefore, even that time constant varied with almost 200 ms the sharpening suffered only a slight change. The result indicates that for cells with very high DSi the distribution of short ISI is highly concentrated at preferred direction. The temporal filter which acts upon the input spike train and enhances the sharpening has a lower effect in this case, while long ISI spiking activity (component which is lost for cells with lower DSi in order to enhance the sharpening) is less present. Comparing Fig.7c and Fig.7d one can observe the difference in the influence of the temporal filter and spike threshold over the

index of sharpening. We found for low tuned ON-OFF DSRGC a decrease in iS of about 1.42 since for highly tuned presynaptic cell the decrease of iS was only 1.01, and thus iS remaining almost the same.

3.6. Polysynaptic directional selective input upon one model neuron

So far we considered monosynaptic connections of different pairs each consisting in one recorded DSRGC and one model neuron. It is assumed that several retinal cells can converge on the same postsynaptic target (Blitz and Regehr 2005; Sincich *et al.* 2007; Usrey *et al.* 1998). In the following we consider the hypothetical case of polysynaptic input with equal weights from several DSRGCs to a model postsynaptic neuron. In this hypothetical case of polysynaptic input we aligned the spike trains of the two convergent inputs according to the peak measured in their spike trains cross- correlogram. We asked what the effect is over the sharpening at SPN of simultaneous convergent synaptic inputs from two ON-OFF DSRGCs with the same preferred directions compared with the scenario of two ON-OFF DSRGCs having opposed preferred direction.

We recorded two ON-OFF DSRGCs in the same retinal portion responding preferentially to the same direction of stimulus movement (90 degrees preferred direction). In a second recording portion we recorded another pair of ON-OFF DSRGC with opposed preferred direction (180 and 0 degrees respectively). We calculated cross correlation histograms (CCH) for these pairs of neurons simultaneously recorded. We found a correlated activity with a time lag in CCH of 2 ms for which a maximum correlation between their spike trains was achieved. Further on we aligned the spike trains of formed pairs, extracting the peak observed in the CCH, in order to build simultaneous synaptic inputs to the same postsynaptic neuron.

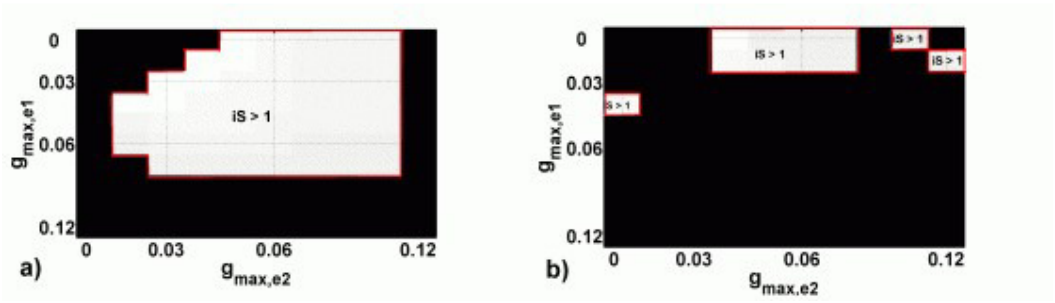

Fig.8 Polysynaptic connectivity

a) Index of sharpening at SPN for the case of two different ON-OFF DSRGCs which send simultaneous convergent inputs to the postsynaptic cell. Presynaptic cells have different indices of selectivity, DSi1=0.59 and DSi2=0.72. The two cells have the same preferred direction at 90 degrees. Index of sharpening at SPN is calculated as DSi SPN / DSi2 DSRGC.

b) Index of sharpening at SPN (iS = DSi SPN / DSi2 DSRGC) for the case of two different ON-OFF DSRGCs which send simultaneous convergent inputs to the postsynaptic cell. Presynaptic cells have different indices of selectivity, DSi1=0.46 and DSi2=0.58. The two cells have opposite preferred direction at 180 and 0 degrees, respectively. The sharpening in direction selectivity in this case is much more restricted as in the case with two cells of the same preferred direction. iS>1 comprises also the areas with one of the synaptic strength equal to zero which leads to the monosynaptic case.

Firstly, we found that the effect of hypothetical simultaneous polysynaptic input consisted in shifting the range of the values for $g_{max,e}$ at which sharpening in direction selectivity was achieved. This shift was toward lower $g_{max,e}$ values. As expected, if two simultaneous excitatory synaptic inputs converge on the same postsynaptic target, then the strength of the synaptic conductances must not be too high. At low values of $g_{max,e}$ (even less than 0.03 µS) already the maximum sharpening is achieved for polysynaptic mechanism. When $g_{max,e}$ is increased, the number of APs at SPN increased also and for relatively high values of $g_{max,e}$ (>0.07 µS) the transfer ratio is already exceeding the maximum limit of 0.7 for most of the polysynaptic mechanism SPN and thus iS becomes zero (Fig.8a).

Another important remark comparing Fig.8a and Fig.8b is that for the case of two simultaneous convergent inputs of ON-OFF DSRGCs with opposed directions the sharpening obtained at SPN is considerably reduced than iS for the scenario of two convergent inputs with the same preferred directions, and thus information regarding direction of stimulus motion will be at least not enhanced if not diminished at the postsynaptic level.

4. Discussion

The complexity of synaptic connectivity from retina to higher brain areas has been extensively studied (Kara and Reid 2003; Levick *et al.* 1969; Usrey *et al.* 1998).

Recently, important findings (Casti *et al.* 2008, Carandini *et al.* 2007, Sinchich *et al.* 2007) suggest that at retinogeniculate synapse the variability in response of LGN cell is mainly due to intrinsic properties of retinal input and moreover, no special mechanism beyond simple summation of PSPs combined with spike threshold is necessary to accurately describe the LGN cell discharge as response to an incoming retinal input. It is beyond the scope of our work to validate a new model to characterize retinogeniculate transmission; instead we took advantage of the successfully validated model of Casti (Casti *et al.* 2008) and their simple approach used to describe the information processing between two first stages of the primary visual system, and investigated how information regarding direction of stimulus movement is shaped at the output of retina.

Sincich *et al.* (2007) have demonstrated that every spike within a burst at LGN neurons is generated by an EPSP evoked by a retinal spike. During bursts of rapid firing activity there are higher chances to observe more postsynaptic APs. Our simulation results show the same. Burst-like activity at preferred direction was responsible for a higher number of APs at SPN than at the intermediary directions (and thus sharpening of directional tuning). We found for all tested ON-

OFF DSRGCs burst-like activity tuned at preferred direction, substantially higher than for ON DSRGCs. We therefore suggest that at preferred direction ON-OFF cells have a higher probability to successfully elicit an AP at postsynaptic target and thus to enhance the degree of direction selectivity. Recent evidences suggest also, that ISI preceding a retinal spike essentially influence the spike transmission at retinogeniculate synapse (Rathbun *et al.* 2007). In our simulations, when short ISI was present in the presynaptic spike trains, sharpening in directional tuning at the postsynaptic counterpart was enhanced. At least in our simulation conditions, the key factor for a better signaling the direction of stimulus movement, from retina to higher brain areas, seems to be played by burst-like activity which is more accentuated in one type of DSRGCs known as ON-OFF type (Zeck and Masland 2007). This explains in part why in our simulations, monosynaptic excitatory connectivity between ON-OFF DSRGC and its postsynaptic target becomes the simplest scheme to achieve sharpening in direction selectivity.

We found that apparently, the presynaptic degree of directional tuning does not provide evidence how the sharpening works - we constructed artificial spike trains mimicking recorded DSRGCs and thus having the same directional tuning, but at the postsynaptic level we did not obtained similar iS for the artificial spike trains with the same DSi as the recorded cells. Instead, we found a more restricted parameter range for which sharpening can be achieved for these artificial spike trains. We then found that burst-like activity is less present in the artificial spike trains than in the recorded ON-OFF DSRGCs discharge. Moreover, ONOFF DSRGCs show burst-like activity predominantly at preferred direction and less at intermediate directions of stimulus movement. The finding that each time the burst-like spiking activity at preferred direction was higher (as in the case of ON-OFF DSRGCs) we found the best sharpening in direction selectivity, lead us to the conclusion that this rapid firing activity at preferred direction of stimulus movement is the principal component of the spike train which carries the directional information. We varied most of the parameters involved in transformation of input spike train within the physiological plausible values. The output of all scenarios pointed toward the same conclusion that the sharpening in direction selectivity was at its best when the component of the

input spike train which carried the directional information - burst like spiking activity at preferred direction - was preserved and the components (isolated spikes) regarding stimulus direction at intermediary directions were lost in spike transmission.

As a conclusion of the above mentioned discussion upon the above mentioned results of our simulations we would like to strengthen the following remarks regarding burst-like activity:

1. Firstly, monosynaptic input was the simplest scheme, in our simulations, to achieve sharpening in direction selectivity at the output of DSRGCs.
2. We found sharpening for a larger parameters' values interval for ON-OFF DSRGCs than for ON DSRGCs.
3. Firing rate does not primordially explain the values obtained for the index of sharpening as we could notice from artificial spike trains mimicking DSRGCs with the same firing rate and DSi but showing different iS values.
4. To explain this discrepancy we focused on an intrinsic property of the retinal spike trains and thus we quantified the burst-like activity. We found that burst-like activity was larger for ON-OFF DSRGCs than for ON DSRGCs and artificial spike trains.
5. Burst-like activity was highly tuned at preferred direction for ON-OFF DSRGCs (DSi Burst > DSi Firing Rate) and thus increasing the chance to produce APs at the SPN at the preferred direction of stimulus motion.
6. Every time we found the best sharpening following parameters modification, we also had best burst-like activity effect upon the SPN.

Those bursts are found at many synapses within the central nervous system is already well known (Sincich *et al.* 2007, Swadlow and Gushev 2001). It is also assumed that bursts are very important in transmitting important information at higher level within visual system (Usrey *et al.* 1999, Swadlow *et al.* 2002). In our case, presumably, their role is to signal the information regarding the direction of visual stimulus.

Once we learned out what component of retinal spike train is carrying the information about direction of stimulus movement, we asked how the simulated postsynaptic neuron does the enhancement of direction selectivity. The main effect responsible for the enhancement of direction-selectivity is presumably the spike threshold for the integrate-and-fire model and the cell's time constant, which determines the effect of temporal summation of PSPs. For slow input spike trains PSPs do not sum and the membrane potential of postsynaptic cell remains below the threshold. Indeed we varied the spiking threshold ($V_{threshold}$) and we found that the sharpening in direction selectivity increased as the $V_{threshold}$ took higher values. At this high threshold values predominantly at preferred directions, EPSPs succeed to sum together in order to raise the membrane potential above and evoke APs at postsynaptic level. Postsynaptic cell's membrane time constant (τ_m) variation made even clearer the manner in which the enhancement of directional selectivity is performed. At low values of τ_m short ISI spiking activity is necessary so that EPSPs can sum and evoke APs at SPN level. Short ISI spiking activity is predominant at preferred direction enabling the temporal summation and thus increasing the sharpening. Once that τ_m increased the temporal summation was also possible for larger ISI too, commonly found for intermediary directions, so that we noticed a reduction in sharpening of direction selectivity.

That enhancement of directional tuning at SPN is realized by the nonlinearity of the spike threshold applied with the temporal filter upon DSRGC spike train (combined with burst-like spiking activity at preferred direction) was more simply demonstrated by using an intuitive mathematical model consisting in a nonlinear amplifier, with a specific time constant, applied to ISI distribution of the retinal input spike train. We again found that if the temporal summation of PSPs was allowed only for small time constant than chances to have APs at SPN were greater at preferred directions (were short ISIs were predominant) and thus iS was largest.

Contribution of membrane potential threshold upon editing neuronal spike trains from presynaptic stage to postsynaptic level, has been intensively studied either for different neuron types, i.e. at retinogeniculate synapse (Casti *et al.* 2008, Carandini *et al.* 2007, Sincich *et al.* 2007), at geniculocortical synapse (Carandini *et al.* 2000, Jagadeesh *et al.* 1997, Priebe and

Ferster 2005) or for different particularities of the visual stimulus presented to which recorded neurons are tuned, i.e. orientation selectivity (Volgushev et al 2000, Carandini *et al.* 2000), direction selectivity (Jagadeesh *et al.* 1997, Volgushev *et al.* 2000, Carandini et al 2000, Priebe and Ferster 2005). At both synapses, in order to account for the sharpening in direction selectivity, a nonlinear mechanism had to be taken into account (Priebe and Ferster 2008). For the direction selectivity, it is well known that cells in higher brain areas, i.e. primary visual cortex, are much more selective than cells in retina or LGN, so that V1 becomes an ideal stage to investigate sharpening in directional selectivity. In 1997 Jagadeesh et al, explained that enhancement of the direction selectivity of simple cells in V1 is generated at least in part by nonlinear mechanisms. Extracellular recordings from neuronal responses to moving stimulus could not be predicted accurately from linear combination of the responses of stationary stimuli presented at different spatial positions within the cell's receptive field. To differentiate between several possible early nonlinear mechanisms, such as shunting inhibition, or PSP – to –spike transformation, i.e. spike threshold, intracellular recordings and a linear model of direction selectivity was used to analyze the synaptic potentials evoked by stationary sinewave gratings. The direction selectivity of synaptic potentials was considerably smaller than that of the intracellularly recorded action potential indicating a non-linear mechanism such as threshold to enhance the direction selectivity of the cell's output over that of its synaptic input. Following Jagadeesh results, other scientific studies (Carandini *et al.* 2000, Priebe and Ferster 2005, Volgushev *et al.* 2000) remarked that spike threshold sharpens the direction selectivity in simple cortical cells evoking that spike threshold quantitatively accounts for the nonlinear component of direction selectivity amplifying the direction of selectivity of spike output relative to that of synaptic input. They have found that the spike threshold contributes substantially to the sharpening of directional tuning, creating a strong "iceberg effect" (Carandini *et al.* 2000).

Another related scientific result was that the degree of sharpening in individual cells was very different; sometimes a strong sharpening was created from poor directional tuning input

and thus the degree of sharpening was high, and sometimes highly tuned cells provide little or no sharpening at the postsynaptic target (Volgushev *et al.* 2000). The sharpening was not correlated with resting membrane potential, threshold or optimal PSP amplitude and moreover was not cell type specific. Indeed we found this variation in degree of sharpening within the same cell type, ON-OFF DSRGCs. In our simulations we also found that the degree of sharpening of directional tuning is inversely related to the presynaptic DSi, that is, highly tuned presynaptic cells provided only small iS while low tuned presynaptic cells provided largest iS.

The model we used showed that for highly tuned ON-OFF DSRGCs, short ISI spiking activity is very concentrated at the preferred direction (Fig.7d). For these cells we found less activity with large ISI even at non-preferred direction. Thus spike threshold mechanism altered very little to not at all the degree of directional tuning (iS was almost the same for τ=5ms as for τ = 20ms). For low tuned presynaptic cells, we found many more isolated spikes (with large ISI) at non-preferred direction. Consequently, the temporal summation and spike threshold eliminated more isolated spikes at non-preferred directions and sharpens the directional tuning. Thus, we were able to measure higher iS for these cells. A comparison of the spike threshold effect in these two cases can be seen from Fig. 7c (low tuned presynaptic cells) and Fig. 7d (highly tuned presynaptic cells).

Presumably for highly tuned cells, it is important rather to faithfully reproduce the information about the stimulus and thus the degree of sharpening is almost the same, while for low tuned cells it is strikingly important to better improve their directional tuning and thus to better transmit the information about the stimulus direction at the postsynaptic level (Volgushev *et al.* 2000).

When we varied most of the model parameters ($g_{max,e}$, $g_{max,i}$, τ_e) we noticed that their influence upon sharpening of direction selectivity, suggested two important parameters which characterize the temporal filter – $V_{threshold}$ and τ_m. Varying the other parameters the temporal

summation of PSPs, spike threshold and burst-like activity at preferred direction of stimulus movement, were acting together to dictate the best sharpening in the manner above described.

In discrepancy with the ON-OFF DSRGCs, for the other type of direction selective cells, the ON DSRGCs, we found less sharpening at their postsynaptic counterparts under the same simulation conditions. This finding could be apparently at least counterintuitive since DSi for this cell type is lower than DSi for ON-OFF DSRGCs. However, the explanation is relatively simple and straightforward. For ON DSRGCs we found much less burst-like activity than for ON-OFF DSRGCs. Thus, the mechanism described above acting upon the incoming spike train, does not provide the same enhancement of iS since summation of PSPs at the preferred direction is not followed by a relatively high short ISI spiking activity in the ON DSRGC's spike train. To account for an eventual sharpening at the output of ON DSRGC (which project to the AOS) presumably the polysynaptic connectivity arrangement (Soodak *et al.* 1988) is more likely to sharpen directional tuning at the postsynaptic target.

Finally, we hypothetically checked how polysynaptic mechanism influences the degree of sharpening at the postsynaptic target. Interestingly, our simulations results show that two ON-OFF DSRGCs sending simultaneous excitatory synaptic input onto the same postsynaptic target lead to a better signaling of stimulus movement direction if they have the same preferred direction compared with the case when they have opposite preferred direction.

5. Conclusions

Using a simple approach, consisting in recorded DSRGCs inputs combined with a variant of a leaky integrate-and-fire neuron model and not taking into account neither synaptic plasticity nor cortical feedback input, we learned out that neurons postsynaptic to directional selective retinal ganglion cells signal better the direction of stimulus movement. We suggest that

apparently, burst-like activity commonly found in the ON-OFF DSRGCs is carrying the information regarding direction of stimulus movement toward higher brain areas. This intrinsic property of presynaptic input together with temporal filter and the nonlinearity of spike threshold at postsynaptic target, act upon the retinal input. The result is that the information regarding direction of stimulus movement at preferred direction is preserved while the component of incoming spike train, which signals direction of stimulus movement at non-preferred directions, is lost in the process of input spike train editing and thus the sharpening in direction selectivity is enhanced. Spike threshold act as a filter allowing that an AP is produced once that the threshold value of the membrane potential is reached. Summation has the effect that EPSPs reach the threshold. In order that summation to be efficient it is needed more closed in time EPSPs, situation which take place mostly during burst-like activity. This burst-like activity, for ON-OFF DSRGCs is distributed at preferred direction. Thus, PSP-to-spike transformation has maximum efficacy at preferred direction, at the other intermediate directions we will notice a reduction of spikes and thus the sharpening increases.

References

Ackert, J.M., Wu, S.H., Lee, J.C., Abrams, J., Hu, E.H., Perlman, I., Bloomfield, S.A. (2006). Light-Induced Changes in Spike Synchronization between Coupled ON Direction Selective Ganglion Cells in the Mammalian Retina. The Journal of Neuroscience, 26(16), 4206–4215

Alitto, H.J., Usrey, W.M. (2005). Dynamic properties of thalamic neurons for vision. Progress in Brain Research, 149, 83–90.

Amthor, F.R., Takahashi, E.S., Oyster, C.W. (1989a). Morphologies of rabbit retinal ganglion cells with complex receptive fields. Journal of Comparative Neurology, 280(1), 97–121.

Bair, W. (1999). Spike timing in the mammalian visual system. Current Opinion in Neurobiology, 9, 447-453.

Barlow, H.B., Hill, R.M., Levick, W.R. (1964). Retinal ganglion cells responding selectively to direction and speed of image motion in the rabbit. Journal of Physiology, 173, 377–407.

Barlow, H.B., Hill, R.M., Levick, W.R. (1965). The mechanism of directionally selective units in rabbit's retina. J.Physiol.(Lond) 178, p.477.

Blitz, D.M., Regehr, W.G. (2005). Timing and specificity of feed-forward inhibition within the LGN. Neuron, 45(6), 917–928.

Buhl, E.H., Peichl, L. (1986). Morphology of rabbit retinal ganglion cells projecting to the medial terminal nucleus of the accessory optic system. Journal of Comparative Neurology, 253(2), 163–174.

Carandini, M., Horton, J.C., Sincich, L.C. (2007).Thalamic filtering of retinal spike trains by postsynaptic summation, Journal of Vision, 7(14), 1–11.

Carandini, M. and Ferster, D. (2000). Membrane potential and Firing rate in cat primary visual cortex. The Journal of Neuroscience, 20(1):470-484.

Casti, A., Hayot, F., Xiao, Y., Kaplan E. (2008). A simple model of retina-LGN transmission, Journal of Computational Neuroscience, DOI:10.1007/s10827-007-0053-7

Cleland, B.G. and Lewick, W.R. (1974). Brisk and sluggish concentrically organized ganglion cells in the cat's retina , Journal of Physiology, 240, 421-456.

Cleland, B.G., Lewick, W.R., Morstyn, R., Wagner, H.G. (1976). Lateral geniculate relay of slowly conducting retinal afferents to cat visual cortex, Journal of Physiology, 255, 299-320.

Damjanovic, I., Maximova, E., Maximov, V. (2009). Receptive field sizes of directionselective units in the fish tectum. Journal of Integrative Neuroscience, 8(1), 77-93.

Dann, J.F. and Buhl, E.H. (1987). Retinal ganglion cells projecting to the accessory optic system in the rat. Journal Comparative Neurology, 262(1), 141–158.

Devries, S.H. and Baylor, D.A. (1997). Mosaic arrangement of ganglion cell receptive fields in rabbit retina. J. Neurophysiol. 78(4), 2048–2060.

Euler, T., Detwiler, P.D., Denk, W. (2002). Directionally selective calcium signals in dendrites of starburst amacrine cells. Nature, 418(6900), 845-852.

Grasse, K.L., Cynader, M.S., and Douglas, R.M. (1984). Alterations in response properties in the lateral and dorsal terminal nuclei of the cat accessory optic system following visual cortex lesions. Experimental Brain Research, 55(1), 69–80.

He, S. and Masland, R.H. (1998). ON direction-selective ganglion cells in the rabbit retina: dendritic morphology and pattern of fasciculation. Visual Neuroscience, 15(2), 369–375.

Hoffmann, K. P. and Distler, C. (1989). Quantitative analysis of visual receptive fields of neurons in nucleus of the optic tract and dorsal terminal nucleus of the accessory optic tract in macaque monkey. Journal of Neurophysiology, 62(2), 416–428.

Huberman, A.D., Wei W., Elstrott, J.,. Stafford, B.K., Feller, M.B., and Barres, B.A.(2009). Genetic Identification of an On-Off Direction- Selective Retinal Ganglion Cell Subtype Reveals a Layer-Specific Subcortical Map of Posterior Motion. DOI: 10.1016/j.neuron.2009.04.014

Jack, J.J.B., Noble, D., Tsien, R.W. (1975). Electric current flow in excitable cells, Oxford: Oxford University Press

Jagadeesh, B., Wheat, H.S., Kontsevich, L.L., Tyler, C.R., Ferster, D. (1997). Direction selectivity of synaptic potentials in simple cells of the cat visual cortex. Journal of neurophysiology, 78:2772-2789.

Jensen, R.J., Devoe, R.D. (1983). Comparisons of directionally selective with other ganglion cells of turtle retina: Intracellular recording and staining. The Journal of Comparative Neurology, 17(3), 271-287.

Kara, P. And Reid, R.C., (2003). Efficacy of retinal spikes in driving cortical responses, The Journal of Neuroscience, 23(24), 8547– 8557

Kim, I.J., Zhang, Y.,Yamagata, M., Meister, M., and Sanes, J.R.(2008). Molecular identification of a retinal cell type that responds to upward motion. Nature 452, 478-482

Levick, W.R., Oyster. C.W., Takahashi E. (1969). Rabbit Lateral Geniculate Nucleus: Sharpener of Directional Information, Science, 165(3894), 712-714.

Levick, W.R. (1967). Receptive fields and trigger features of ganglion cells in the visual streak of the rabbits retina. Journal of Physiology, 188(3), 285–307.

Michael, C.R. (1966). Receptive Fields of Opponent Color Units in the Optic Nerve of the Ground Squirrel. Science, 152(3725),1095-1097.

Mustari, M.J. and Fuchs, A.F. (1989). Response properties of single units in the lateral terminal nucleus of the accessory optic system in the behaving primate, Journal of Neurophysiology, 61(6), 1207–1220.

Oyster C.W. (1968). The analysis of image motion by the rabbit retina. Journal of Physiology, 199, 613–635.

Priebe, N. and Ferster, D. (2005). Direction selectivity of excitation and inhibitionin simple cells of the cat primary visual cortex. Neuron, Vol. 45, 133–145.

Priebe, N. and Ferster, D. (2008). Inhibition, spike threshold and stimulus selectivity in primary visual cortex. Neuron, DOI 10.1016/j.neuron.2008.02.005.

Pu, M.L., and Amthor, F.R. (1990b). Dendritic morphologies of retinal ganglion cells projecting to the nucleus of the optic tract in the rabbit. Journal of Comparative Neurology, 302(3), 657–674.

Rall, W. (1967). Distinguishing theoretical synaptic potentials computed for different somadendritic distributions of synaptic inputs. Journal of Neurophysiology, 30, 1138-1168.

Rathbun, D.L, Alitto, H.J., Weyand, T.G., and Usrey, W.M. (2007). Interspike interval analysis of retinal ganglion cell receptive fields. Journal of Neurophysiology, 98, 911-919.

Soodak, R.E. and Simpson, J.I. (1988). The Accessory Optic System of Rabbit. I. Basic Visual Response Properties. Journal of Neurophysiology, 60, 2037-2054.

Shlens, J., Field, G.D., Gauthier, J.L., Grivich, M.I., Petrusca, D., Sher, A., Litke, A.M. and Chichilnisky, E.J. (2006). The Structure of Multi-Neuron Firing Patterns in Primate Retina. The Journal of Neuroscience, 26(32), 8254–8266.

Sincich, L.C., Adams, D.L., Economides, J.R., and Horton, J.C. (2007). Transmission of spike trains at retinogeniculate synapse. The Journal of Neuroscience, 27(10), 2683–2692.

Stanford, L.R. and Sherman, S.M. (1984). Structure/function relationships of retinal ganglion cells in the cat. Brain Research, 297(2), 381–386.

Swadlow, H.A, Gusev, A.G. (2001). The impact of "bursting" thalamic impulses at a neocortical synapse. Nat Neurosci 4:402-408.

Swadlow, H.A., Gusev, A.G., Bezdudnaya, T., (2002-01-01). Activation of a cortical column by a thalamocortical impulse (PDF). Journal of Neuroscience 22 (17): 7766–7773.

Taylor, W.R., and Vaney, D.I. (2002). Diverse Synaptic Mechanisms Generate Direction Selectivity in the Rabbit Retina, Journal of Neuroscience, 22(17), 7712–7720.

Usrey, W.M., Reppas, J.B., Reid, R.C. (1998). Paired-spike interactions and synaptic efficacy of retinal inputs to the thalamus. Nature, 395(6700), 384-387.

Usrey, W.M., Reppas, J.B., Reid, R.C. (1999). Specificity and strength of retinogeniculate connections. Journal of Neurophysiology, 82:3527-3540.

Usrey, W. M. (2002). Spike timing and visual processing in the retinogeniculocortical pathway, Philosophical Transactions of The Royal Society Lond. B Biological Sciences, 357, 1729–1737.

van der Togt, C., van der Want, J., and Schmidt, M. (1993). Segregation of direction selective neurons and synaptic organization of inhibitory intranuclear connections in the medial terminal nucleus of the rat: an electrophysiological and immunoelectron microscopical study. Journal of Comparative Neurology, 338(2), 175–192.

Vaney, D.I., Levick, W.R., and Thibos, L.N. (1981a). Rabbit retinal ganglion cells. Receptive field classification and axonal conduction properties. Experimental Brain Research, 44(1), 27–33.

Vaney, D.I., Peichl, L., Wassle, H., and Illing, R.B. (1981b). Almost all ganglion cells in the rabbit retina project to the superior colliculus. Brain Research, 212(2), 447–453.

Volgushev, M. Pernberg, J. and Eysel, U.T. (2000). Comparison of the selectivity of the postsynaptic potentials and spike responses in cat visual cortex. European Journal of Neuroscience, Vol.12, pp 257-263.

Weng, S., Sun, W., and He, S. (2005). Identification of ON–OFF direction-selective ganglion cells in the mouse retina. Journal of Physiology, 562(3), 915–923.

Wörgötter, F., and Koch, C. (1991). A detailed model of the primary visual pathway in the cat: Comparison of afferent excitatory and intracortical inhibitory connection schemes for orientation selectivity. Journal of Neuroscience, 11(7), 1959–1979.

Yonehara K, Ishikane H, Sakuta H, Shintani T, Nakamura-Yonehara K, *et al.* (2009). Identification of retinal ganglion cells and their projections involved in central transmission of information about upward and downward image motion. Plos One, 4(1), e4320

Zeck, G.M., Masland, R.H. (2007). Spike train signatures of retinal ganglion cell types. European Journal of Neuroscience, 26, 367-380.

Paper 3

Interspike interval based filtering of directional selective retinal ganglion cells spike trains

Aurel Vasile Martiniuc[1] and Alois Knoll[1] [1]Computer Science

Department VI, Technical University Munich, Garching, Germany.

Journal of Computational Intelligence and Neuroscience, June 2012.

doi:10.1155/2012/918030.

Summary of the paper

While the degree of motion direction is getting higher as advancing from one stage to the next within the hierarchical brain structures and I suggested that this sharpening can be explained by only direct one to one connectivity with excitatory feedforward input being sufficiently, I asked in this paper if already at presynaptic level the time spiking is shaping the neural response to stimuli so that the visual information is filtered and time coded before being sent toward postsynaptic target.

In this paper I analyzed data recorded using two types of visual stimulus, white noise and drifting bars, and shown that short ISI spikes are more often related to an optimal visual stimulus and carry more information than longer ISI spikes. It worths to be noted that correlation between stimulus and recorded neuronal response is best at short ISI spiking activity and decrease as ISI becomes larger. I then analyzed data generated by using grating bars stimulus and found that as ISI becomes shorter the signaling of visual stimuli motion becomes sharpened. These findings suggest that ISI-based temporal filtering integrates a mechanism for visual information processing at the output of retina toward higher stages within early visual system.

My contribution to this paper is as follows:

I defined the scientific project, I analyzed the recorded neural data, I wrote the paper, I edited the paper, I was the corresponding author and I did the major and minor revisions according to peer reviewing process by scientific comitee within the editorial board of the journal.

IV. Interspike interval based filtering of directional selective retinal ganglion cells spike trains

Abstract

The information regarding visual stimulus is encoded in spike trains at the output of retina by retinal ganglion cells (RGCs). Among these, one type known as ON-OFF directional selective cell (DSRGC) is signaling the direction of stimulus motion. DSRGCs' spike trains show accentuated periods of short interspike intervals (ISIs) framed by periods of isolated spikes. ISI-based filtering of the retinal spike trains has been shown to play a crucial role in transmitting information at postsynaptic target. Here we use two types of visual stimulus, white noise and drifting bars, and show that short ISI spikes are more often related to an optimal visual stimulus and carry more information than longer ISI spikes. Firstly, our results show that correlation between stimulus and recorded neuronal response is best at short ISI spiking activity and decrease as ISI becomes larger. We then used grating bars stimulus and found that as ISI becomes shorter the signaling of visual stimuli motion becomes sharpened. However, for the other type of DSRGC, known as ON-DSRGC short ISI distribution, burst-like activity and information rates revealed consistent differences when compared with ONOFF DSRGC. These findings suggest that ISI-based temporal filtering integrates a mechanism for visual information processing at the output of retina toward higher stages within early visual system.

Keywords: retina, interspike interval, direction selectivity, visual information

1. Introduction

The information regarding visual stimulus is encapsulated initially in spike trains at the output of retina by retinal ganglion cells. In some of mammals (though not general to mammals), here already the direction of stimulus motion is signaled by well-known directional selective retinal ganglion cells (DSRGCs). They respond vigorously to the movement of stimulus at the preferred direction and are silent when stimulus movement is toward the opposite null direction (Levick *et al.*, 1969). In rabbit retina, one type of DSRGCs, the ON-OFF DSRGCs, have been already very well characterized (Barlow & Hill, 1963; Barlow *et al.*, 1964; Euler, 2002; Vaney *et al.*, 1981a; Vaney *et al.*, 1981b; Amthor *et al.*, 1984; Amthor *et al.*, 1989a). They respond at the beginning and the end of an increasing or decreasing light stimulus and project to the dorsal lateral geniculate nucleus (LGN) and to the superior colliculus (Cleland *et al.*, 1976; Vaney *et al.*, 1981a).

Receptive fields (RFs) become progressively more sophisticated along the synaptic hierarchies from retina to cortex. However, for the LGN cells the center surround RFs are similar with those of retinal afferents (Hubel & Wiesel, 1962; Kuffler, 1953; Reid *et al.*, 2004). With this advantage in mind, together with the fact that the receptive field center of LGN cells receive their main input from only one retinal ganglion cell (RGC) (Cleland *et al.*, 1971; Sincich *et al.*, 2007; Usrey *et al.*, 1999), the retinogeniculate synapse represent a major interest for studying the role of interspike interval based mechanism for spike filtering and visual information processing (Casti *et al.*, 2007, Rathbun *et al.*, 2007; Carandini *et al.*, 2007; Sincich *et al.*, 2009; Rathbun *et al.*, 2010). Already at the next stage within early visual system, neurons in layer 4 of primary visual cortex receive many more convergent inputs from LGN counterparts (Reid and Usrey, 2004) and thus rely more on the interaction between different inputs than on the interspike intervals (ISIs) of individual inputs as part of the mechanism to reach the spike threshold (Usrey *et al.*, 2000).

Many studies have shown that LGN cells seem to affect in an active manner the information relayed to cortex editing the input retinal spike trains in totally new output spike trains. Thus, it is already known that retinal spike trains contain much more spikes as the output spike trains of their LGN cells counterparts (Sincich *et al.*, 2007; Usrey *et al.*, 1998; Weyand, 2007). Consequently, not every retinal spike will evoke an action potential (AP) at the postsynaptic target in the LGN. The length of the ISIs of the retinal spike train input represents an important factor in determining whether a retinal spike will evoke an AP at the LGN cell counterpart (Levine and Cleland 2001; Usrey *et al.*, 1998; Mastronade, 1987; Weyand, 2007; Sincich *et al.*, 2007).

Retinal spikes with preceding short ISIs have greater chances to induce APs at their postsynaptic target than "isolated" spikes. The efficacy to evoke APs at the postsynaptic target in LGN decreases considerably with increasing of retinal ISIs so that for retinal ISI larger than about 30 ms there is no detectable influence of ISI on the production of postsynaptic spikes (Usrey *et al.*, 1998; Sincich *et al.*, 2007). Furthermore, recent studies suggest that this temporal filter acting upon retinal spiking activity is correlated with visual stimulus, so that visual information regarding optimal stimulus features is preserved and transmitted further on at the postsynaptic target (Rathbun *et al.*, 2007, Uglesich *et al.*, 2009, Sincich *et al.*, 2009; Rathbun *et al.*, 2010).

To have a better intuition of how ISI-based temporal filter acts upon retinal spike trains, we analyzed extracellularly recorded activity of different types of RGCs in response to two different types of stimuli – white noise and drifting grating bars, in rabbit retina.

Firstly, the results show that using white noise stimulus and reverse correlation analysis, we were able notice that the strength of the correlation between stimulus and recorded neuronal response was at its maximum for shortest ISI. We also found that correlation between stimulus and neural response decrease with increasing ISI and thus visual information varies with ISI. This extremely important finding suggests that ISI based temporal filter of retinal spike trains may influence the spike transfer at retinogeniculate synapse and serve to filter visual information

from retina to LGN. These findings are in concordance with previously reported results from cats (Rathbun *et al.*, 2007).

We then went further and asked if ISI based temporal filter remains robust for a different type of stimulus. We used drifting grating bars moving in different equidistant directions as being the optimal stimulus for ON-OFF DSRGCs (Levick *et al.*, 1969; Taylor and Waney 2002). Our results from recorded activity of ON-OFF DSRGCs in response to drifting grating bars, presented at eight different directions, indicate that short ISIs were always tuned at preferred direction of stimulus movement and contribute to preserve the directional information. It is already known that optimal stimuli induce higher firing rates and thus presumably short ISI spiking activity as well. To check if the tuning of short ISI is just strictly firing rate dependence and no other firing mechanism is involved, we built Poisson-like artificial spike trains with similar tuning and firing rates as the recorded ON-OFF DSRGCs. The discrepancy that we have noticed between the recorded cells and artificial spike trains regarding the short ISI distribution and firing rates lead us to suggest that there is not just a strictly dependence on firing rate and that another mechanism is involved. We then scanned the spike trains of the recorded cells and artificial spike trains and found that burst-like activity was significantly higher for the recorded ON-OFF DSRGCs and presumably is the key for explaining the discrepancy of short ISI distribution between the recorded and artificial spike trains.

Interestingly, the other direction selective retinal ganglion cell type, the ON-DSRGC revealed reliable difference in short ISI distribution, burst like activity distribution and information rates when recorded in response to the same stimulus. This cell type is known to be less direction selective than ON-OFF DSRGC, have larger receptive fields, signal global motion and projects consistently to the accessory optic system (AOS) signaling the global retinal motion (Soodak and Simpson, 1988). The mechanism used here is consistently different when compared with the mechanism for information transmission used at retinogeniculate synapse, at least from the point of view of a large convergence of many ONDSRGCs on a single AOS counterpart cell (Ackert *et al.* 2006).

In the last set of investigations we checked whether the information regarding visual stimuli carried by individual spikes varies with ISI. We found that the amount of information per spike decreased as the ISI increased. This together with the above presented results suggest that ISI based filtering of retinal spike trains is part of the mechanism that helps in preserving information about the important features of visual stimuli as it travels from retina to cortex, increasing the information efficiency to improve signaling the optimal stimulus features as has been suggested also by recent studies in macaque and cat (Rathbun *et al.*, 2010; Uglesich *et al.*, 2009; Sincich *et al.*, 2009).

2. Materials and methods

2.1 White noise stimulus

Experiments were performed on whole-mount retinas in accordance with the animal use committee of the Massachusetts General Hospital. Procedures have been described previously (Yang & Masland, 1994; Koizumi *et al.*, 2004).

We analyzed the extracellularly recorded neuronal activity from ON-OFF retinal ganglion cells of the 4 adult isolated rabbit retinas stimulated with white noise and drifting grating bars. We used a sixty channel multi-electrode array, with a 30 µm spatial resolution, (Multichannelsystems, Reutlingen, Germany) for electrophysiological recordings. Data acquisition and off-line analysis has been previously described in (Zeck *et al.*, 2007). Briefly, the receptive field was mapped using white noise stimulus (temporal flat power spectrum in the 1–30 Hz range) which comprised a 16x16 array of squares (pixels) with the updating rate of the frames of 50 Hz. The luminance of each square was independently modulated by an m-sequence (Reid *et al.*, 1997). The size of each square was 75 µm and the size of the receptive field of each cell was calculated by reverse correlating stimulus and spike response, and considering checkers

whose intensity at the temporal maximum of the mean effective stimulus exceeded by a factor of 3 the SD of the squares in the background (DeVries & Baylor, 1997). The duration of stimulus was T= 30 s and the stimulus was repeated n = 30 times.

2.2 Spike triggered analysis

Spike triggered average (STA) was calculated after the spikes were sorted into different categories according to ISIs values $0 < ISI \leq 10$ ms; $10 < ISI \leq 20$ ms; $20 < ISI \leq 50$ ms; $50 < ISI \leq 100$ ms and in the last category STA was calculated for all spikes in the spike trains.

We calculated STA as classically defined (Paninski, 2003; Schwartz *et al.*, 2006) as the average over all the stimuli which shortly preceded a spike.

$$STA(\tau) = \frac{1}{\langle Nsp \rangle} \langle \sum_{i=1}^{Nsp} S(ti - \tau) \rangle$$

, where Nsp is the number of spikes, ti is the time of occurrence of spike i, s(t) is the stimulus at time t, and the angle brackets represent averaging over trials. We represent the spike train ρ(t) as a sum of infinitesimally narrow, idealized spikes in the form of Dirac δ functions:

$$\rho(t) = \sum_{i=1}^{Nsp} \delta(t - ti)$$

Thus, STA(τ) can be expressed as an integral of the stimulus times the neural response function :

$$STA(\tau) = \frac{1}{\langle Nsp \rangle} \int_0^T r(t) s(t - \tau) dt$$

, where T is the total duration of a trial and r(t) is the firing rate at time t. The correlation function of the firing rate r at time t and stimulus s at time (t+τ) is denoted by:

$$Corr(\tau)_{rs} = \frac{1}{T}\int_0^T r(t)s(t+\tau)dt\ .$$

Finally, STA(τ) as the correlation between stimulus and neural response was calculated by:

$$STA(\tau) = \frac{T}{\langle Nsp \rangle} Corr(-\tau)_{rs} = \frac{1}{\langle r \rangle} Corr(-\tau)_{rs}\ ,\ \text{MCorr} = \max\ (|\text{STA}\ (\tau)|) \tag{1}$$

Maximum value of STA (τ), given by MCorr, was indicating the maximum correlation between stimulus and neuronal response, for each of the ISI categories, and has the dimension of light intensity.

2.3 Grating bars stimulus

We then used a second stimulus consisting in drifting grating bars moving in eight different directions 45 degrees apart.

Thus, direction selectivity was tested using a square wave spatial grating moved in $N = 8$ equally separated directions $\varphi_i = i\cdot(2\pi/N)$, $i = 0,1,\ldots,N-1$.

For each direction the stimulus was presented for a duration T = 12 seconds followed by a stimulus free interval of the same length.

For each equally separated direction of movement we performed n = 7 repetitions of the stimulus.

The total stimulus length was 672 seconds, consisting in 12 seconds for each direction multiplied by 8 different directions and by 7 different trials. The spatial extent of the moving grating was 2500 μm on the retina and thus, multiple cells were stimulated and recorded simultaneously.

Individual tuning curves were obtained considering the firing rate of each cell for each of the eight equidistant directions. The firing rates for each cell and for each of the stimulus direction were averaged over the number of stimulus repetitions (seven repetitions of the stimulus presentation were done for each different direction of movement).

In this study we used data from 20 retinal ganglion cells. Three of the cells were ON direction selective (ON DSRGC), twelve of the cells were ON-OFF direction selective (ON-OFF DSRGC) and five of the cells were non-directional selective (NON-DSRGC).

2.4 Direction Selectivity Index

To quantify the directional tuning of a neuron, we used the direction selectivity index (*DSi*) as described by Taylor and Vaney (2002),

$$DSi = \frac{\left\| \sum_i \vec{v}_i \right\|}{\sum_i r_i}, \quad \vec{v}_i = r_i \begin{pmatrix} \cos\varphi_i \\ \sin\varphi_i \end{pmatrix}. \qquad (2)$$

$\vec{v}_i$ is a vector pointing in the direction of the stimulus with the length equal to the number of spikes recorded during presentation of the stimulus (r_i). The *DSi* explains the directional tuning based on the firing rates for different particular movement directions of the visual stimulus. The minimum value of 0 characterizes a non-directional neuron whereas the maximum value of 1 characterizes a neuron that responds for a single direction of movement. The higher the *DSi* the higher direction selectivity is.

2.5 ISI Directional Index

Once we quantified the directional tuning of the recorded ON-OFF RGCs we asked what influence the ISI distribution may have over the calculated DSi. In this sense we isolated ISIs of each recorded spike trains as response of each direction of stimulus movement again into the following categories: $0 < ISI \leq 10$ ms; $10 < ISI \leq 20$ ms; $20 < ISI \leq 50$ ms; $50 < ISI \leq 100$ ms and all spikes. To compare the direction selectivity for different ISIs values with the direction selectivity for entire recorded activity we defined the following index as ISI directional index (SI):

$$SI = \frac{DSi(ISI)}{DSi(DSRGC)}. \qquad (3)$$

DSi(DSRGC) represents the index of selectivity calculated for all recorded activity as indicated in the eq. 1., and DSi(ISI) represents the directional tuning calculated for the separated retinal spikes according with different ISI values, as mentioned above. This index is quantified similar with the DSi in Eq.1 having into account that for each direction of stimulus movement we took into account the total number of ISIs (of a certain value) instead of total number of spikes.

2.6 Bursting activity

It is already well known that optimal stimulus elicit neurons to raise their firing rates in response. To check if the short ISI activity is strictly firing rate dependence we scanned the recorded spike trains and evaluated the bursting activity. As already described burst

firing events were considered when at least two spikes occurred after an ISI larger than a threshold of 50 ms and are followed by an ISI shorter than 5 ms (Godwin *et al.*, 1996b; Guido *et al.*, 1995; Lu *et al.*, 1992). Burst rate r^{burst} was quantified by dividing the number of bursts per total duration of stimulus presentation for each trial for each cell.

2.7 Artificial spike trains

If the short ISI activity tuning at preferred direction would be strictly firing rate dependence one presumes that Poisson-like artificial spike trains with the same firing rate as the recorded spike trains would give similar ISI distribution. Thus we generated artificial spike trains with the firing probability distributed according to a Poisson process with a refractory period of 5 ms. As mentioned before these artificial spike trains hold the same averaged firing rates and as a consequence the same DSi as the recorded DSRGCs.

2.8 Entropy

To calculate the post stimulus time histograms (PSTH) we aligned the spike sequences with the onset of stimuli that repeated n times. For periodic stimulus (grating bars), we moved the response sequence back to time zero after each time period T, and count n as the total number of periods of data. We then divided the stimulus period T into N bins of size Δ and counted the number of spikes ki from all n sequences that fall in the bin i. The optimal bin size Δ results from minimizing: $(2k-\sigma)/\Delta^2$, where k is the mean of ki and σ is the variance of ki (Shimazaki and Shinomoto, 2007).

We then averaged the calculated PSTH for the n repetitions of the stimuli (n = 30 for white noise stimulus and n = 7 for grating drifting bars stimulus) and obtained the time-varying average firing rates <r(t)>.

In order to evaluate the information about the stimulus carried by single spikes we used the above calculated time varying average firing rates <r(t)> and computed the estimates of entropy (H) as follows (Strong *et al.*, 1998; Brenner *et al.*, 2000; Sincich *et al.*, 2009; Casti *et al.*, 2009; Rathbun *et al.*, 2010):

$$H = \frac{1}{T}\int dt \frac{r(t)}{< r(t) >} \log_2 \frac{r(t)}{< r(t) >} \qquad (4).$$

We calculated H for n = 20 cells for white noise stimulus and n = 12 cells for drifting grating bar stimulus and for each of the ISI categories mentioned at the beginning. Additionally for the second stimulus we calculated H for each of the eight equidistant directions of stimulus movement. Thus, we could estimate the entropy tuning for each cell, and evaluate the amount of information carried at each direction of stimulus movement similarly with Eq. 2:

$$DSiH = \frac{\left\| \sum_i \vec{v}_i H \right\|}{\sum_i H_i} \;, \vec{v}_i H = H_i \begin{pmatrix} \cos\varphi_i \\ \sin\varphi_i \end{pmatrix} \qquad (5)$$

, where H_i represents the entropy for each of the stimulus direction of movement.

To take into account the problem of the size limitation of data and to correct the resulting bias, the information rates were estimated by extrapolating correct entropy H_c from segments of the total data, in an increasing order for different bin sizes ($\nabla\tau$) and fit by (Strong *et al.*, 1998):

$$H(T, \nabla\tau) = H_c(\nabla\tau) + \frac{H1(T, \nabla\tau)}{size} + \frac{H2(T, \nabla\tau)}{size^2}$$

The linear dependence gave a good fit for all cells included in our analysis. This measure of information rates does not make any deduction about the number of relevant stimulus features and let us know about the amount of information (bits/spikes) contained in single spikes.

Statistics: To check the statistical significant differences among different recorded data (ON-OFF DSRGCs and ON DSRGCs) or generated data (Artificial spike trains) we used statistical t-test and calculated the corresponding p values. In general the data was summarized over cell types and different trials by using the mean and standard deviation.

3 Results

Maximum correlation between stimulus and neural response

In order to investigate the correlation between visual stimulus and ISI distribution within neural response at the output of retina, we firstly applied white noise visual stimulus and recorded responses from 20 retinal ganglion cells of rabbit retina. Among them, 5 cells were non-directional selective (NDSRGCs) and 15 of them were directional selective cells (DSRGCs). Scanning the spike trains of each retinal ganglion cell in response to the stimulus applied, we found that for all of the cells most of the spikes were preceded by short time intervals, that is, the activity with short ISI was predominant. Similar results were also previously reported (Usrey *et al.*, 1998).

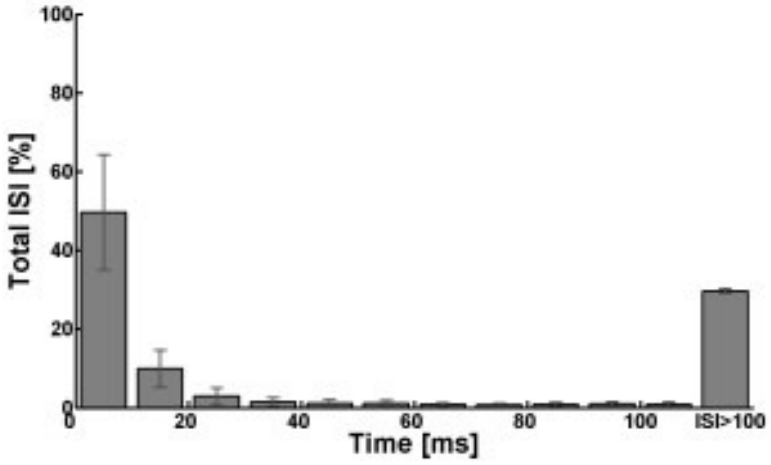

Fig. 1 Distribution of mean ISIs for all 20 cells. Y axis represents the percentage of all ISI for each ISI category distributed on X axis. Maximum of mean ISI distribution for all cells was at ISI between 0 and 10 ms.

Figure 1 shows the distribution of mean ISIs for all 20 cells. The majority of the ISIs was below 200 ms. Maximum of mean ISI distribution for all cells was at ISI between 0 and 10 ms. Thus, we found mean ISI = 49.60% +/- 14.63 (n=20) for ISI >0 and ISI≤ 10 ms, mean ISI = 9.89 +/- 4.73 % (n=20) for ISI between 10 and 20 ms and consistently decreased for larger ISIs.

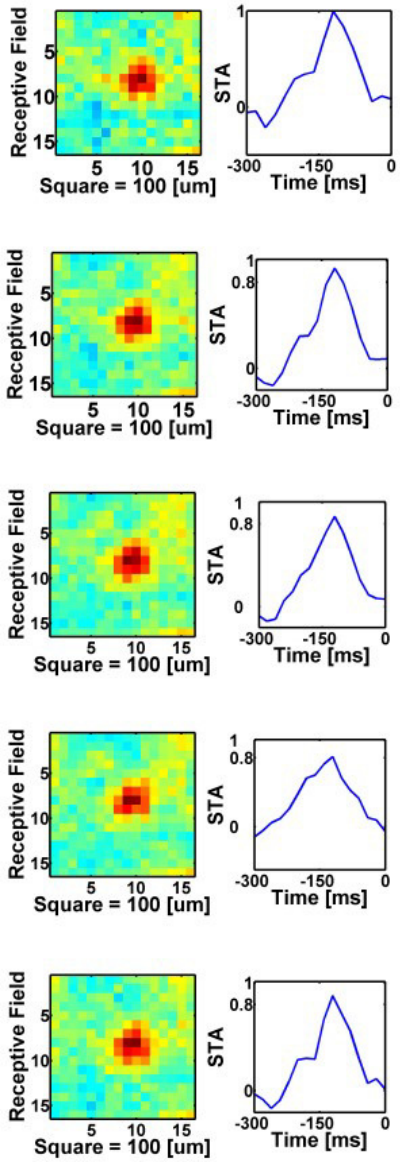

Fig. 2 The receptive field of a retinal ganglion cells for each of the mentioned ISIs categories, in the left side, and the maximum correlation found between stimulus intensity and recorded spiking activity, in the right side.

First row correspond to 0<ISI≤ 10 ms and presents the maximum correlation between stimulus and neural response. Second row is for 10<ISI≤ 20 ms, third row is for 20<ISI≤ 50 ms, fourth row is for 50<ISI ≤ 100 ms and last row is for all ISIs included. As ISI increases the maximum correlation between stimulus and neural response decreases.

Recent scientific results suggest that short ISIs in the retinal ganglion cell's spike trains are associated with cell's receptive field shape and stimulus intensity (Rathbun *et al.*, 2007). We used white noise and reverse correlation to map the receptive field of each cell for different values of ISI. To do so, we selected all the spikes in each cell's spike train with 0<ISI ≤ 10 ms, 10<ISI≤ 20 ms, 20<ISI≤ 50 ms, 50<ISI≤ 100 ms and applied reverse correlation analysis to check the correlation between the stimulus intensity and recorded neural response. Figure 2 shows the shape of the receptive field of a recorded DSRGC for each of the above mentioned ISIs categories, in the left side, and the maximum correlation found between stimulus intensity and recorded spiking activity, in the right side.

Firstly, we noticed that the spatial location of the ISI specific receptive field's center was not changed across the ISIs categories and thus remained fairly the same regardless the fact that ISIs varied. It is beyond our scope to study in details how the cells receptive field's size change as ISI varies. However, it worth to be noted that we also found slight changes in the size of receptive field of the recorded cells for different ISI categories and for each cell, as previously reported. Instead, our aim is to ask how ISI distribution is correlated with visual stimulus applied. Thus, we used reverse correlation and mapped the ISI specific receptive field and quantified the maximum correlation between stimulus and recorded spiking activity as described by MCorr, see 2.2 Methods, Eq.1 (Fig.2 – right column).

For all cells and cell types we found that maximum correlation between visual stimulus and recorded neural response was for ISIs shorter than 10 ms. As ISIs increase up to 20 ms (i.e. 10< ISI ≤ 20 ms) maximum correlation between stimulus and neural response

decreases down to about 85% of the value for 0<ISI≤ 10ms and continue to decrease for 20< ISIs ≤ 50 ms when it becomes slightly lower than maximum correlation found for all spikes in the recorded activity (all ISIs category). At this value maximum correlation is about 80% of the value for 0< ISI ≤ 10ms. For all spikes ISI category, maximum correlation is slightly higher, about 82% of value for 0< ISI≤ 10ms. For 50< ISI ≤100 ms the maximum correlation between stimulus and recorded neural activity decreases even more, toward 60% of shortest ISI category. Figure 3 shows the distribution of normalized MCorr for all ISIs categories and for all 20 cells recorded. Thus, for 0< ISI <10 ms normalized MCorr has the highest value obtained and continue to decrease as ISI increased: 10<ISI≤ 20 ms MCorr= 0.851 +/- 0.09 (n=20), 20<ISI≤ 50 ms MCorr = 0.793 +/- 0.09 (n=20), 50<ISI≤ 100 ms MCorr = 0.616 +/- 0.08 (n=20) and for all spikes MCorr = 0.845 +/- 0.09 (n=20).

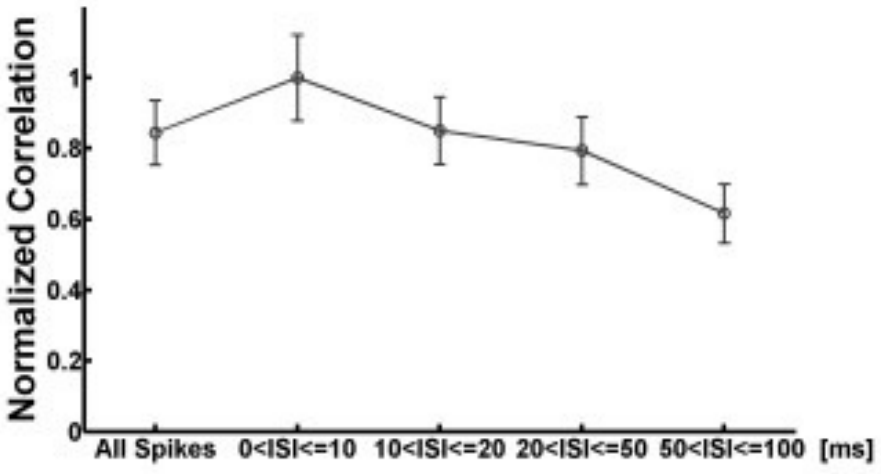

Fig.3 Relationship between normalized correlations (Y axis) calculated from the recorded neural response following the stimulus presentation, and different ISI categories (X axis).

It is already known that the efficacy to evoke an action potential (AP) at the postsynaptic target, is greatest for spikes preceded by short interspike intervals (ISI ≤ 10 ms). This efficacy decreases as ISI increases so that for ISI longer than 30 ms has almost no

significant influence (Carandini *et al.*, 2007; Sincich *et al.* 2007). This together with our results suggests that there is a positive association among maximum correlation between stimulus and ISI of the recorded spike trains and the efficacy of evoking an AP at the postsynaptic target. In this logic ISI based filtering of retinal spike trains varies with stimuli and help preserving particular visual information, which might be of a maximum significance, toward the next stage within early visual system. We next checked if this association is robust for different visual stimulus. To do so we applied drifting grating bars moving in 8 different directions, to the retinal ganglion cells sample. We chose this stimulus due to the fact that for direction selective retinal ganglion cells drifting grating bars moving in the preferred directions represents the optimal stimulus and thus evoke the maximum response. If this ISI based filtering holds true, the information regarding the preferred direction of stimulus movement should be preserved against the intermediate directions.

Optimal stimulus and ISI based filtering

In the next step we analyzed the recorded neural activity applying a different stimulus consisting in drifting grating bars (see 2.3 Methods). At each direction of stimulus motion we recorded the cells' responses consisting in different spike trains. Thus we calculated the directional tuning of each cell and quantified it as directional selectivity index (DSi) as described in Methods 2.2, Eq.2. Twelve of the cells were ON-OFF directional selective (ONOFF DSRGCs), three of the cells were ON direction selective (ON DSRGC) while the other five cells were non-directional selective (NDS). The mean index of selectivity for ON-FF DSRGCs was DSi = 0.64 +/-0.08 (n=12), for ON DSRGC the mean DSi= 0.34 +/- 0.06 (n=3) while for NDSRGCs we found that mean index of selectivity was DSi = 0.06 +/-0.01 (n=5), (Fig. 4a) in accordance with previously reported results (Zeck *et al.* 2007, Taylor & Vaney 2002).

The results, using white noise stimulus and reverse correlation, indicated that shortest ISI spiking activity was associated with maximum correlation between stimulus and recorded spiking activity in response to the stimulus presented. That is, when short ISIs are present one would expect that the stimulus applied influenced at maximum the receptive field of the cell and thus the probability that the cell transmit further on that particular information about the stimulus. Direction selective cells have the property that respond vigorously at the preferred direction of stimulus movement and are silent for the opposite null direction. Thus, the stimulus feature of maximum importance for the ON-OFF DSRGCs is the direction of stimulus motion.

We firstly scanned all the spike trains of each cell, quantified the ISI distribution and found that for ON-OFF DSRGCs the peak is obtained for $0<ISI<10$ ms and is significantly higher than for the peak obtained for the rest of the RGCs (ON-DS and NDS) which did not show a clear prominent peak in ISI distribution. The short ISI spiking activity for all ON-OFF DSRGCs shows a mean ISI of 65.2 % for $0<ISI\leq 10$ms, decreasing for $10<ISI\leq 20$ ms at 9.48 %, for $20<ISI\leq 50$ at 2.41 % and for $50<ISI\leq 100$ ms at only 1.65 %. By contrary, NDS presented a lower mean ISI value for $0<ISI\leq 10$ ms than for directional selective cells, about 41.1 % of total ISIs. As ISI increases we noticed higher mean ISI for NDS as follows: 17.18 % for $10<ISI\leq 20$ ms, 6.6% for $20<ISI\leq 50$ ms and 4.62 % for $50<ISI\leq 100$ ms (Fig.4b). ISI spiking activity is more concentrated on short values for directional selective cells than for NDS where ISI spread out toward higher values.

Further on we scanned again the recorded spike trains of all cells and selected in to separate categories, spiking activities containing $0<ISI\leq 10$ ms, $10<ISI\leq 20$ ms, $20<ISI\leq 50$ ms and $50<ISI\leq 100$ ms. For each of these selected spike trains we calculated the directional tuning and quantified it again with an index of selectivity similar as in Eq.2 (see 2.4 Methods).

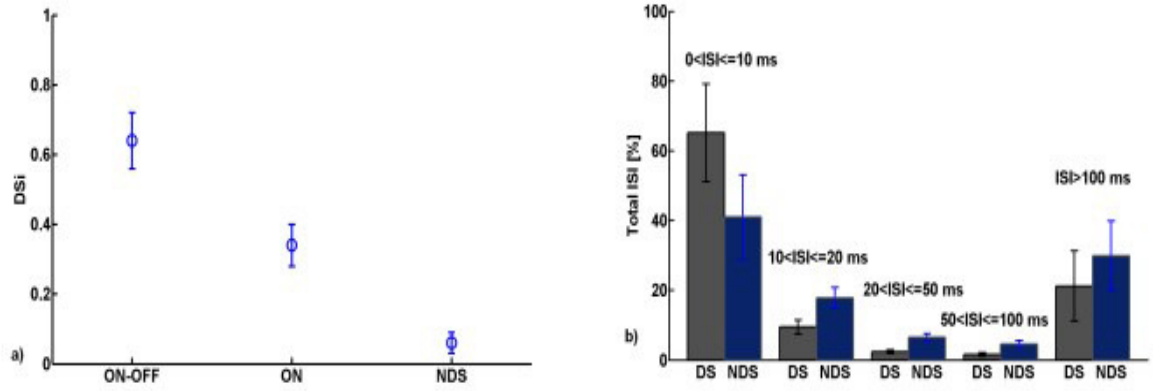

Fig.4 **a)** Index of Selectivity (DSi) for three different types of the recorded cells in response to moving grating bars. **b)** Total ISI distribution for directional selective neurons (DS) gray bars and non-directional selective neurons (NDS) blue bars.

Firstly, we noticed that for ON-OFF DSRGCs, the highest activity with short ISI was distributed at preferred direction and thus correlating the short ISI spiking activity with signaling the direction of stimulus motion.

We found the highest DSi for the spiking activity of the ON-OFF DSRGCs with $0 < ISI \leq 10$ ms. Moreover, once that ISI increased the DSi decreased. That is, the shorter the ISI is the better direction of stimulus movement is signaled by the ON-OFF DSRGCs.

Indeed Fig.5a shows how sharpening in direction selectivity is produced for spikes with short ISIs. Thus for the ON-OFF DSRGC exemplified in Fig.5a, for $0< ISI \leq 10$ ms, we found DSi = 0.70, and decrease as ISI value increase, such as for $10< ISI \leq 20$ ms, DSi = 0.62, for $20< ISI\leq 50$ ms DSi = 0.59, for $50<ISI\leq 100$ DSi = 0.56 and for all spikes DSi = 0.49.

The decreasing in index of selectivity as ISI increases was found for all twelve recorded ON-OFF DSRGCs (Fig.5b). Thus, at shortest ISI, $0<ISI\leq 10$ ms we found the

highest DSi = 0.67 +/- 0.08 (n=12), for 10<ISI≤ 20 ms, DSi= 0.57+/- 0.1 (n=12), for 20<ISI≤ 50 ms, DSi= 0.49 +/_ 0.08 and for 50<ISI≤ 100 ms, DSi= 0.38 +/- 0.07 (n=12).

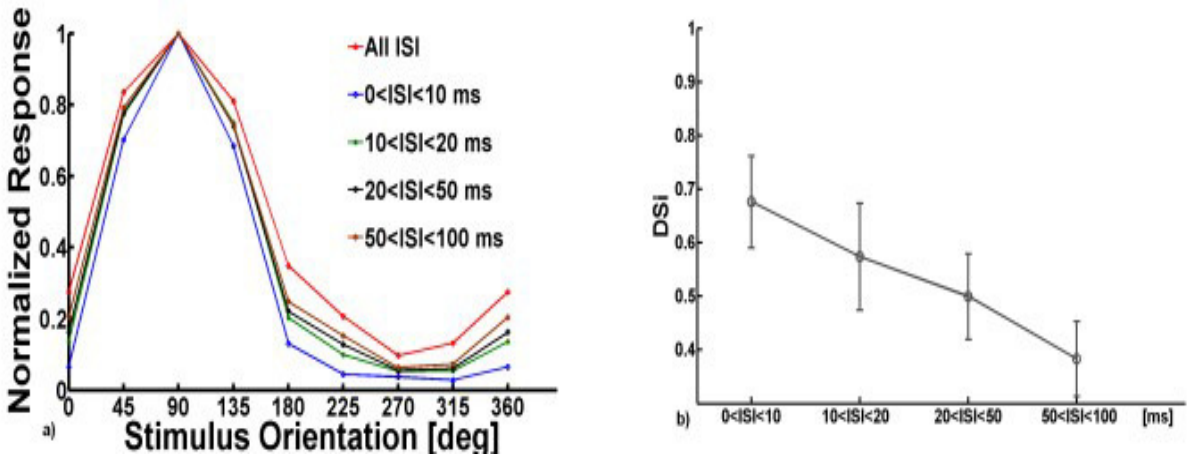

Fig.5 a) Example of sharpening in tuning curves for an recorded ON-OFF DSRGC for different ISI categories.

b) Distribution of DSi for all recorded ON-OFF DSRGCs for all ISI categories.

Furthermore, Fig.6 depicts the ISI distribution for all ON-OFF DSRGCs reflecting the finding that short ISI activity is focused at preferred directions of stimulus motion. We found that for 0<ISI≤ 10 ms, a percentage of 38% +/- 5.1 (n=12) from all ISIs of this category, was at preferred direction. At opposite direction of stimulus motion we found only 0.9% +/- 0.5 (n=12) of all ISIs in this category.

In the next ISI category, 10<ISI≤ 20 ms, from the total of ISIs which belong to this category we found at preferred direction 32.8% +/- 6.6% (n=12) since at opposite direction we noticed only a small percentage of 1.4% +/- 1.4 (n=12). However, one can observe a slight increasing in 10<ISI≤ 20 ms spiking activity at opposite direction.

Further on, for 20<ISI≤ 50 ms, at preferred direction we found 32.16% +/- 0.8 (n=12) and at opposed direction 2.3% +/- 2 (n=12). Finally, for the last ISI category, 50 <ISI≤ 100 ms at preferred directions we found 23.8% +/- 4.8 (n=12) and at opposed direction 3.7% +/- 2.2 (n=12) of total ISIs from this category.

Thus, we found that the percentage of short ISIs at preferred direction becomes lower as ISI category increases and the percentage of short ISIs at opposed direction increases as ISI category increases. In this way the decreasing of DSi noticed above (Fig.5b) as ISI increases might have an explanation in this distribution of short ISI activity at preferred direction. As ISI increases we found increasing short ISI activity at the intermediate and opposed directions too, and thus the selectivity becomes weaker (Fig. 6).

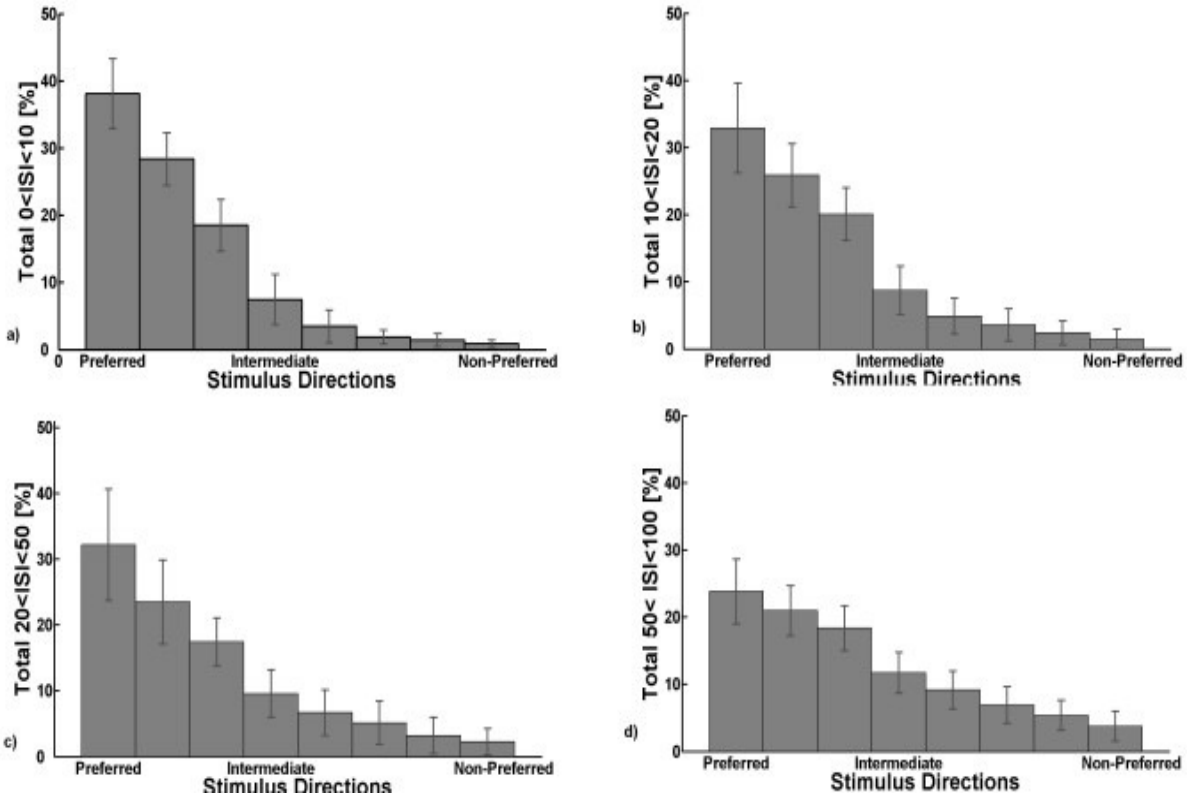

Fig.6 a-d) Total ISI distribution for all recorded ON-OFF DSRGCs, at preferred, intermediate and opposite directions of stimulus movement, for all ISI categories.

In the next set of investigations, to better exemplify the relation between ISI and directional tuning, we quantified the ISI Directional Index (SI, Eq.3. 2.5 Methods) as a measure of directional selectivity for each ISI category in comparison to the entire spike train. Figure 7 shows how this index varies with different ISI values. Briefly, for ON-OFF

DSRGCs the best sharpening is observed at ISI = 5 ms where SI = 1.47 +/- 0.09 (n=12) and decreases as ISI increases, down to 1 which means that signaling the direction of stimulus motion is as good as for all spikes in the spike train. SI = 1.30 +/- 0.08 (n=12) for ISI = 10 ms, SI=1.25 +/- 0.08 (n=12) for ISI =15 ms, SI = 1.21 +/- 0.09 (n=12) for ISI = 20 ms, SI = 1.18 +/-0.08 (n=12) SI = 1.13 +/- 0.08 (n=12) for ISI = 100 ms and SI= 1.07 +/- 0.08 (n=12) for ISI =200 ms.

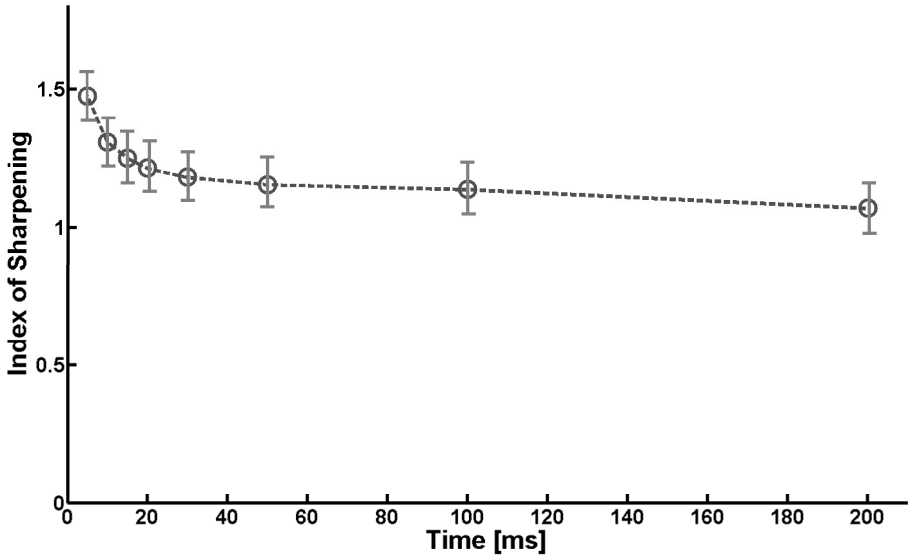

Fig.7 ISI Directional Index variation for all ON-OFF DSRGCs.

Firing Rate dependence

Up to now we have seen applying white noise and reverse correlation analysis that for different ISI values the correlation between stimulus and neural response varies and that maximum correlation between stimulus and neural response is obtained for shortest ISI category (0<ISI≤10 ms). We then noticed that for a different stimulus, drifting grating bars, short ISI spiking activity was focused at preferred direction (optimal stimulus for DSRGCs) and that index of directional selectivity was decreasing as ISI was increasing. Our results

together with the already known paired spike efficacy and the major influence of short ISI activity in signaling information about visual stimulus at different synapses along early visual system (Sincich *et al.*, 2007, Uglesich *et al.*, 2009, Rathbun *et al.*, 2010, Sincich *et al.*, 2009) bring us to the hypothesis that ISI temporal filtering might be part of a mechanism responsible for preserving information in the transmission process from retina to LGN.

Further on to check whether is just a strictly dependence of short ISI activity at optimal stimulus by the firing rate or presumably another mechanism is involved (i.e. burst firing) we constructed Poisson-like artificial spike trains with similar firing rate and tuning (same DSi) as the recorded ON-OFF DSRGCs (see 2.7 Methods).

Additionally we scanned the spike trains of all 12 ON-OFF DSRGCs and quantified the bursting activity as described in 2.6 Methods.

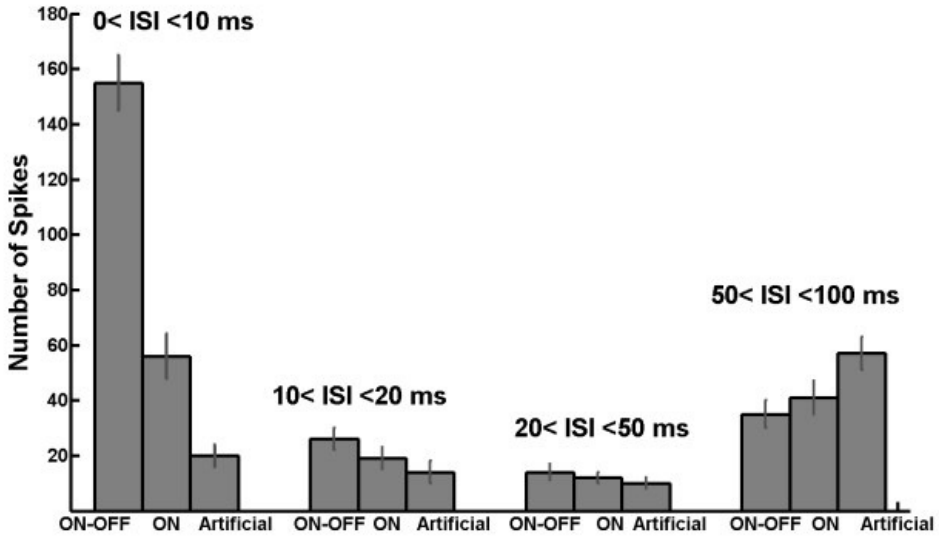

Fig.8 Distribution of spikes for all ISI categories, in number of spikes, for ON-OFF, ON and artificial spike trains.

Figure 8 shows the number of spikes for each of the ISI categories at preferred direction of stimulus movement. For ON-OFF DSRGCs we noticed at preferred direction

within 0<ISI≤ 10 ms category, a mean number of spikes = 155 +/- 10 (n=12). For artificial spike trains with similar firing rates and DSi we found a mean number of spikes = 20 +/- 4 (n=12). For the other DSRGC type, the ON-DS we found a mean of 56 +/- 8 (n=3). Further on, for the category 10<ISI≤ 20 ms the mean number of spikes for ON-OFF DSRGCs was 26+/-4 (n=12) since for artificial 14+/-4 (n=12) and for ON-DS 19 +/-4 (n=3).

As ISI increases (20<ISI≤ 50 ms) the mean number of spikes for ON-OFF decreases to 14 +/- 3 (n=12), for artificial spike trains 10 +/- 2 and for ON-DS to 12 +/- 2 (n=3). Finally for the last category, 50<ISI≤ 100 ms, for ON-OFF the mean number of spikes was 35 +/- 5 (n=12), for artificial spike trains 57 +/- 6 (n=12), and for ON-DS 41 +/-6 (n=3).

Since the artificial spike trains have the same firing rates and tunings as the recorded ON-OFF cells one would expect similar number of spikes for each ISI categories. By contrary we found a statistically significant difference ($p<0.02$) between the short ISI distribution of the ON-OFF recorded spike trains and the artificial spike trains. The difference that our findings show, consistently indicate that the increase in number of spikes for short ISI spiking activity cannot be predicted by stochastic Poisson process and that another mechanism should be involved within distribution short ISI spiking activity and thus it is not just a strictly firing rate dependence. Additionally, for artificial spike trains the short ISI spiking distribution did not show large differences between different ISI categories and was significantly larger just for ISI >50 ms. This could also explain the direction selectivity which has also an almost uniform distribution for different ISI categories except for the largest one (Figure 9). We found for 0<ISI≤ 10 ms a DSi = 0.76 +/-0.14 (n=12), for 10<ISI≤ 20 ms DSi = 0.76 +/- 0.13 (n=12), for 20<ISI≤ 50 ms DSi = 0.73 +/- 0.14 (n=12) and for 50<ISI≤ 100 ms DSi=0.53 +/- 0.14 (n=12).

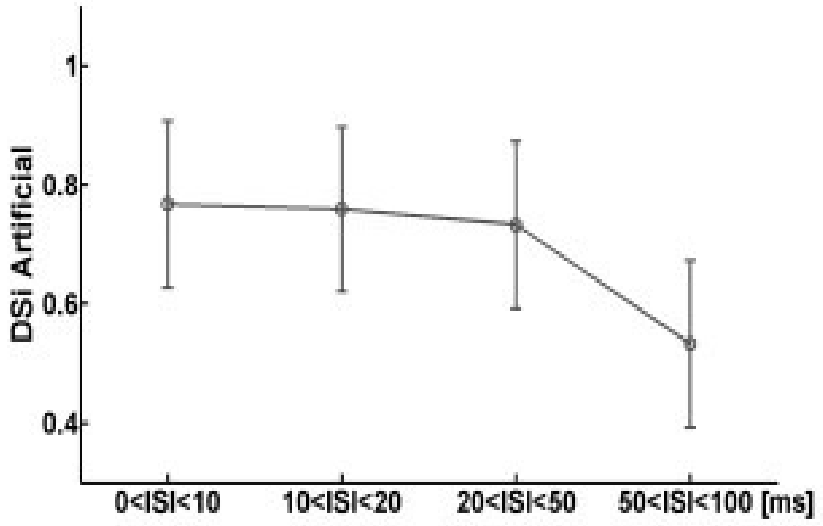

Fig.9 Variation of DSi for artificial spike trains versus different ISI categories.

The results from the artificial spike trains indicate the degree of directional tuning does depend on the short ISI activity at preferred direction encountered in ON-OFF direction selective cells. It does not depend on the neuron's firing rates that are different for the different recorded DSRGCs and artificial spike trains (compare Fig 5b and Fig. 9).

Since firing rate strictly cannot explain the neural response regarding the short ISI spiking activity and optimal stimulus, we suggest that an intrinsic spiking property of ONOFF DSRGCs, namely bursting activity is carrying part of the responsibility of short ISI spiking activity at preferred direction (optimal stimulus).

Next step we scanned the spike trains of the recorded ON-OFF DSRGCs and the artificial spike trains mimicking the 12 recorded ON-OFF cells and quantified the bursting activity in each spike train according to 2.6 Methods. Figure 10 shows the mean number of bursts per trial at preferred direction for each of the recorded cells and the simulated spike trains.

We found that burst-like activity shows statistically significant difference ($p<0.0001$) between ON-OFF DSRCs spike trains and the artificial spike trains. As shown in Fig. 8

burst activity at preferred direction for individual ON-OFF cells was significantly larger than for the artificial spike trains, the mean for all twelve cells was 17.45 +/- 5.4 (n=12) (Figure 10corresponding red dot). For artificial spike trains we found a lower burst rate at preferred direction (twenty times lower than for ON-OFF) even though the firing rate mimicked that of the ten recorded ON-OFF DSRGCs, burst rate artificial = 2.94+/- 1.5 (n=12) (Fig 10 corresponding red dot).

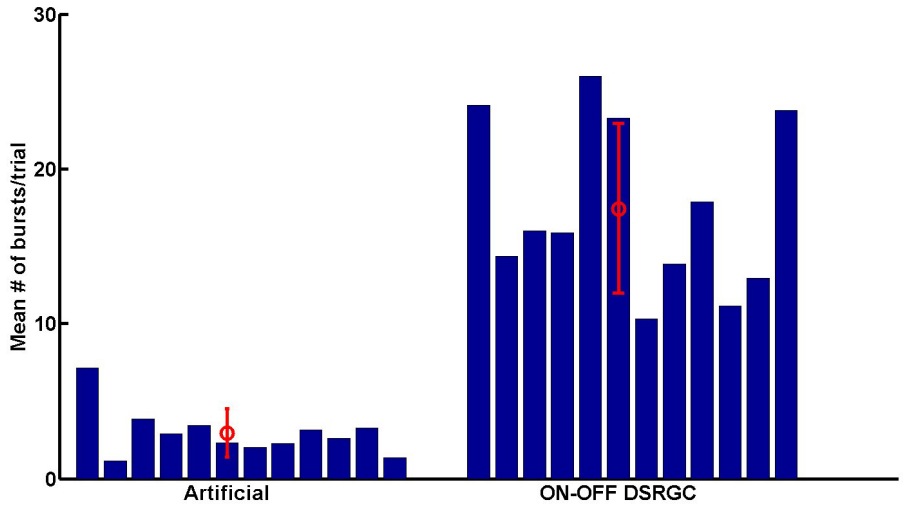

Fig.10 Burst activity (mean number of bursts/trial) for individual cells. ON-OFF DSRGCs at right and at left side artificial spike trains. Red dots are mean values for all ON-OFF DSRGCs and for all artificial spike trains, respectively.

Beside this discrepancy there is another factor that worth to be noted – that burst-like activity for ON-OFF DSRCs was tuned at preferred direction (data not shown) since the burst rate for artificial spike trains was almost equal zero and pointing non-preferred directions.

Information Rates

In the next set of investigations we checked how much information regarding visual stimuli different ISI categories carries on. Not only for white noise stimulus but also for drifting grating bars shortest ISI category, 0<ISI≤10 ms, carried the highest information rate. As ISI increased we found lower amount of information within the each increasing ISI categories.

We calculated the entropy for all 12 recorded ON-OFF DSRGCs and for each ISI category, firstly for the drifting grating bars stimulus (Figure 11a). We found that maximum entropy was achieved for shortest ISI category, 0<ISI≤ 10 ms, H= 2.03 +/- 0.49 [bits/spike] (n=12). As ISI increased the amount of information about visual stimulus decreased so that for 10<ISI<20 ms H=1.26 +/- 0.52 [bits/spike] (n=12), for 20<ISI≤ 50 ms H= 0.85 +/- 0.55 [bits/spike] (n=12) and finally for 50<ISI≤ 100 ms H=0.55 +/-0.45 [bits/spike] (n=12).

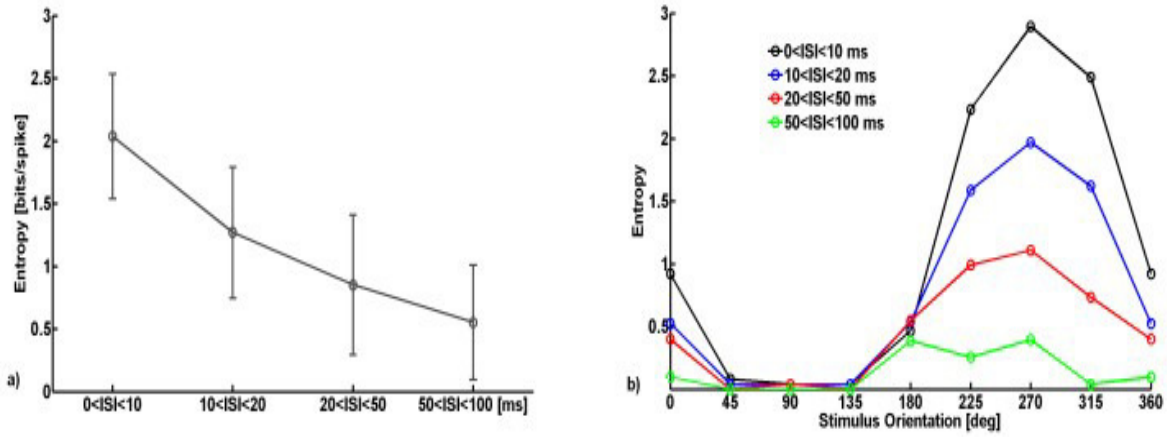

Fig.11 a) Variation of entropy in bits/spikes for all ON-OFF DSRGCs versus different ISI categories.

b) An example of entropy (bits/spike) tuning curve for one recorded ON-OFF DSRGC for all ISI categories.

Using Eq.5 (see 2.8 Methods), similarly to index of directional selectivity for firing rates, we calculated the tuning of entropy for all ISI categories. Figure 11b shows one

example of an ON-OFF DSRGC and indicate that as ISI decreases the information tuning becomes more sharpened.

For all 12 recorded ON-OFF DSRGCs we found that index of selectivity for entropy (DSiH) decreased as ISI increased (see Figure 12). For 0<ISI<10 ms DSiH= 0.54 +/- 0.17 (n=12), for 10<ISI≤ 20 ms DSiH=0.45 +/- 0.2 (n=12), for 20<ISI≤ 50 ms DSiH=0.40 +/- 0.2 (n=12) and for 50<ISI≤ 100 ms DSiH=0.35 +/- 0.2 (n=12).

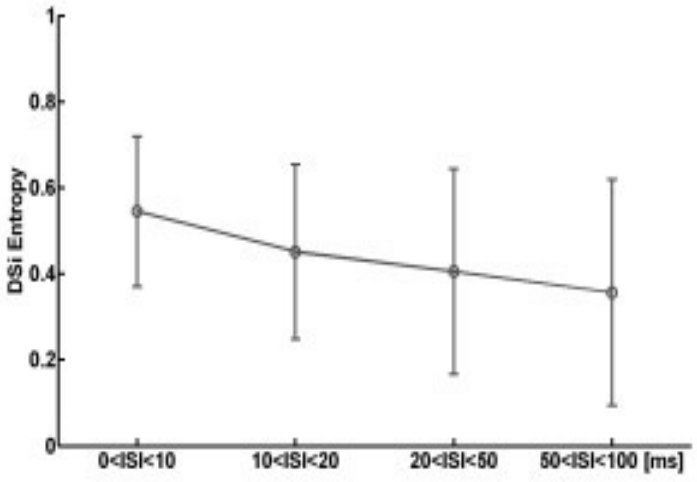

Fig.12 Variation of index of selectivity (DSi) of entropy for all recorded ON-OFF DSRGCs and for all ISI categories.

All together we found for all twelve ON-OFF DSRGCs that the amount of information regarding visual stimulus was highest for shortest ISI category and was tuned at preferred direction of stimulus movement.

Finally, for white noise stimulus we noticed the same trend in decreasing the information rates as ISI increased (Figure 13). Thus, for 0<ISI≤ 10 ms DSiH= 0.70 +/-0.2 (n=20), for 10<ISI<20 ms DSiH=0.41 +/- 0.2 (n=20), for 20<ISI≤ 50 ms DSiH = 0.32 +/- 0.2 (n=20) and for 50 <ISI≤ 100 ms DSiH= 0.15 +/- 0.1 (n=20).

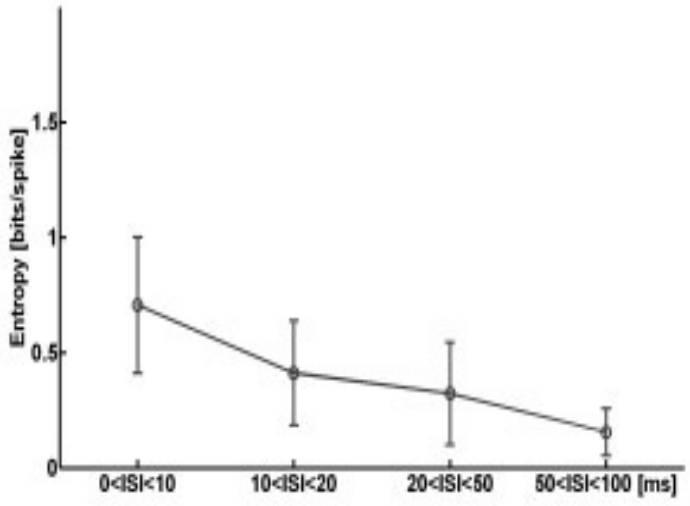

Fig.13 Variation of entropy (bits/spike) for all 20 RGCs recorded using white noise stimulus versus different ISI categories.

Consistent with our above mentioned results, these findings suggest that the ISI–based filtering of retinal spikes is part of the mechanism of information processing that recode the visual signal using a sparse coding (Olshausen and Field, 2004), to improve the overall coding efficiency from one stage to another within the visual system.

Comparison between ON-OFF DSRGCs and ON DSRGCs

As we have already seen in Fig.8 the two types of DSRGCs, the ON and ON-OFF, show statistically significant differences ($p<0.01$) concerning the ISI distribution within their recorded spike trains. ON DSRGCs responded to the stimulus presentation at preferred direction with only around one third of the number of spikes as compared with ON-OFF DSRGCs for the shortest ISI category. For the intermediate ISI categories (10<ISI<20 and 20<ISI<50 [ms]) ON and ON-OFF DSRGCs showed a similar number of spikes in each ISI category. Moreover for the largest ISI

category, we found for the ON DSRGC a slightly larger number of spikes than for ON-OFF DSRGC.

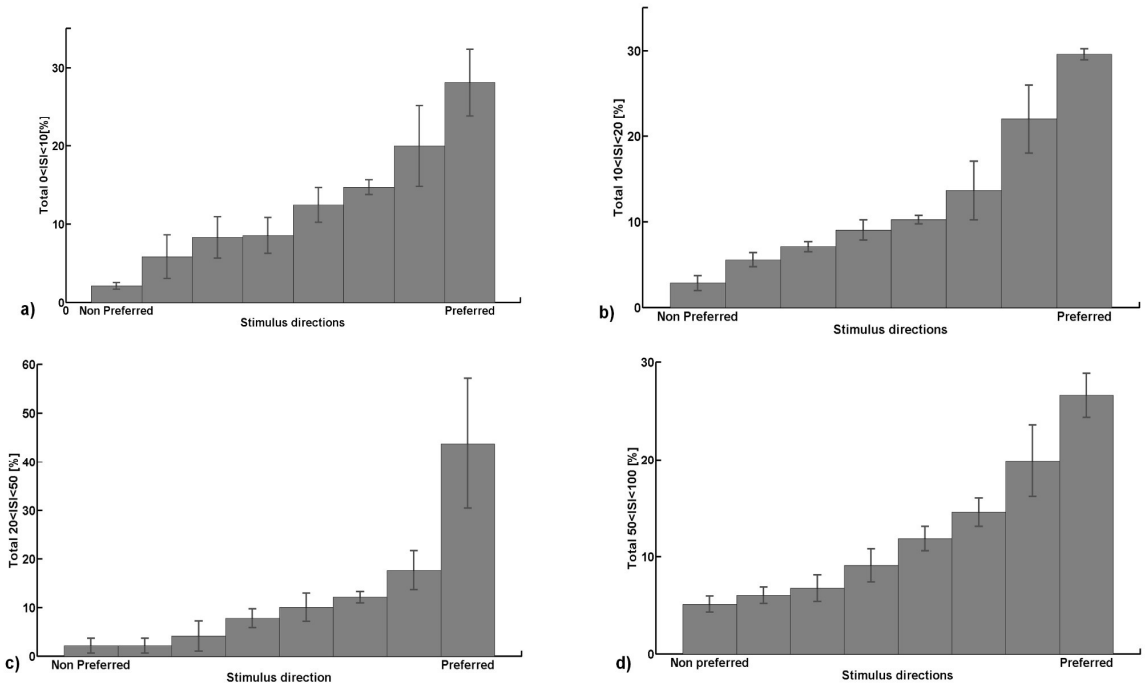

Fig.14a-d) Total ISI distribution for all recorded ON DSRGCs, at preferred, intermediate and opposite directions of stimulus movement, for all ISI categories.

Comparing Fig. 6 with Fig.14 we notice the differences of ISI distribution for each ISI category between ON-OFF and ON cell types. Thus, for ON cells we found at preferred direction (Fig. 14 a) for 0<ISI≤ 10 ms, a percentage of 28.12 % +/- 4.2 (n=3) from all ISIs of this category which represents 10% lower number of ISI than ON-OFF DSRGCs (Fig. 6a). At opposed direction we found a percentage of 2.1% +/- 0.4 (n=3) from all ISIs of this category, for ON DSRGCs which is larger than for ON-OFF DSRGCs. Thus, within shortest ISI category, ON DSRGCs have lower activity at preferred direction than ON-OFF DSRGCs and higher activity at opposed direction a discrepancy which may explain the weaker direction selectivity for ON DSRGCs than for ON-OFF DSRGCs. Interestingly for

20<ISI<50 ms category we found at preferred direction a percentage of 43.81% +/- 13 (n=3) of total ISIs (Fig. 14 c) which suggests that ON DSRGCs preferentially use this intermediate ISI category instead of shortest ISI category at preferred direction to signal the stimulus motion direction. By contrary for ON-OFF DSRGCs the shortest ISI category was found as having the highest percentage at preferred direction (Fig. 6 a). This difference is enhanced further on when calculating the index of selectivity for each of the ISI category (Fig.15). The highest direction selectivity was found for 20<ISI<50 ms category (DSi = 0.52 +/- 0.08 (n=3)) since for the rest of the ISI categories the directional selectivity remains almost constant around 0.3. For ONOFF DSRGCs a different situation was encountered (Fig. 5b). The highest direction selectivity was found for shortest ISI category and decreased as ISI category increased.

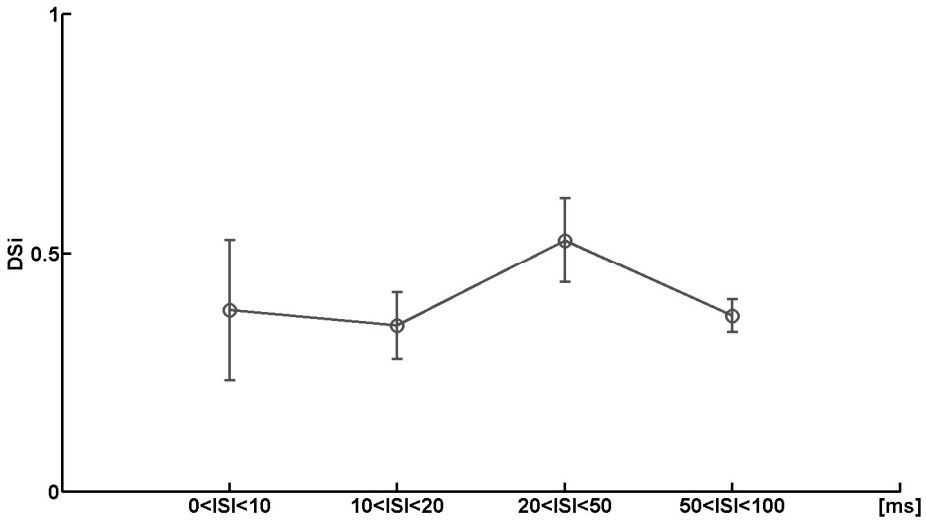

Fig.15 Distribution of DSi for all recorded ON DSRGCs for all ISI categories.

Further on, burst analysis revealed other statistically significant difference (p<0.0002) regarding the burst distribution between the two directional selective cell types. Fig. 16 shows the mean number of bursts per trial at preferred directions for each cell and

cell types. ON-OFF DSRGCs have shown consistently larger number of bursts at preferred direction than ON DSRGCs. Mean number of bursts per trial for ON-OFF was 17.45 +/- 5.4 (n=12) (Figure 16 -right side corresponding red dot) since for the ON DSRGCs the mean number of bursts per trial was 1 +/- 0.7 (n=3) (Figure 16 -left side corresponding red dot).

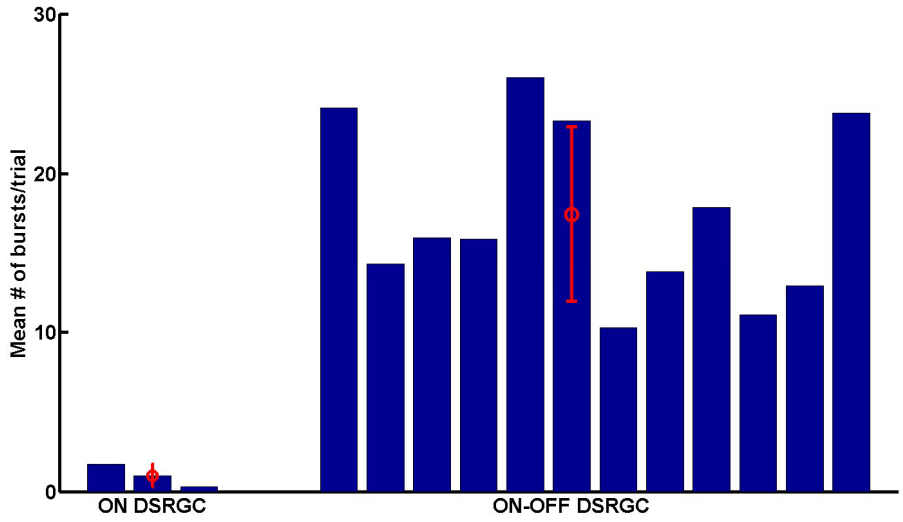

Fig.16 Burst activity (mean number of bursts/trial) for individual cells. Left ON DSRGCs, right side ON DSRGCs. Red dots indicate mean values for all ON-OFF DSRGCs and for all ON-OFF DSRGCs, respectively.

The differences between the two cell types regarding the burst activity consisted not only in the mean number of burst at preferred direction but also in mean number of spikes per burst. Fig. 17a) shows the colored coded distribution of mean number of spikes per burst for each cell. In the first four rows of squares are the ON-OFF cells and in the last row are the three ON cells. For each square the X axis depicts the stimulus directions and the Y axis represents the burst category as the number of spikes per burst. Thus, first row in each square represents the mean number of bursts with two spikes per burst for each of the eight different stimulus direction. Second row represents the mean number of burst with three spikes per burst for each direction and so on to the last row which represents the mean number of bursts with 10 spikes per burst for each direction.

Shortest burst category, consisting in 2 spikes per burst, was preferred by both cell types as spiking activity in response to stimulus presentation. However, for ON-OFF cells the mean number of bursts within this burst category (with 2 spikes per burst) was larger than for ON DSRRGCs. Interestingly, ON DSRGCs did not respond to the stimulus presentation with bursting activity consisting in more than 2 spikes per burst, unless occasionally. By contrary ON-OFF DSRGCs showed consistent burst-like activity with bursts having more than 2 spikes per burst. Thus, for each ON-OFF DSRGCs we found bursts consisting in 3 spikes per burst up to 6 spikes per burst concentrated at the preferred directions. Indeed, burst categories with 8, 9 or 10 spikes per burst were rarely used not only by ON DSRGCs but also by ONOFF DSRGCs (Fig 17 a - last rows of each square). The mean number of bursts for each burst category is shown in Fig. 17 b) as the mean for all 12 ON-OFF DSRGCs - left image, and the mean for all 3 ON DSRGCs - right side image. One can notice how ON-OFF DSRGCs used not only short bursts, with 2 spikes per burst, but also larger bursts with 2, 3, 4, 5 and 6 spikes per burst in order to signal the direction of stimulus motion. By contrary, ON DSRGCs responded mostly with shortest burst category consisting in 2 spikes per burst. Additionally for ON-OFF DSRGCs we found large bursts (bursts with more than 2 spikes) predominantly at preferred direction since at opposed and intermediate directions we found a lower number of bursts mostly consisting in 2 spikes per burst.

Figure 17 c, d) show how ON DSRGCs use predominantly shortest burst category, with 2 spikes per burst at preferred direction. The mean number of bursts consistently decreased for bursts with more than 2 spikes, mean number of bursts with 2 spikes represented a percentage of almost 62% of total bursts at preferred direction since for bursts with three and four spikes per bursts we found a very low percentage around 10% of total bursts at preferred direction. For larger bursts we found 0% for 5 and 6 spikes per burst and only around 3% for bursts with more than 6 spikes.

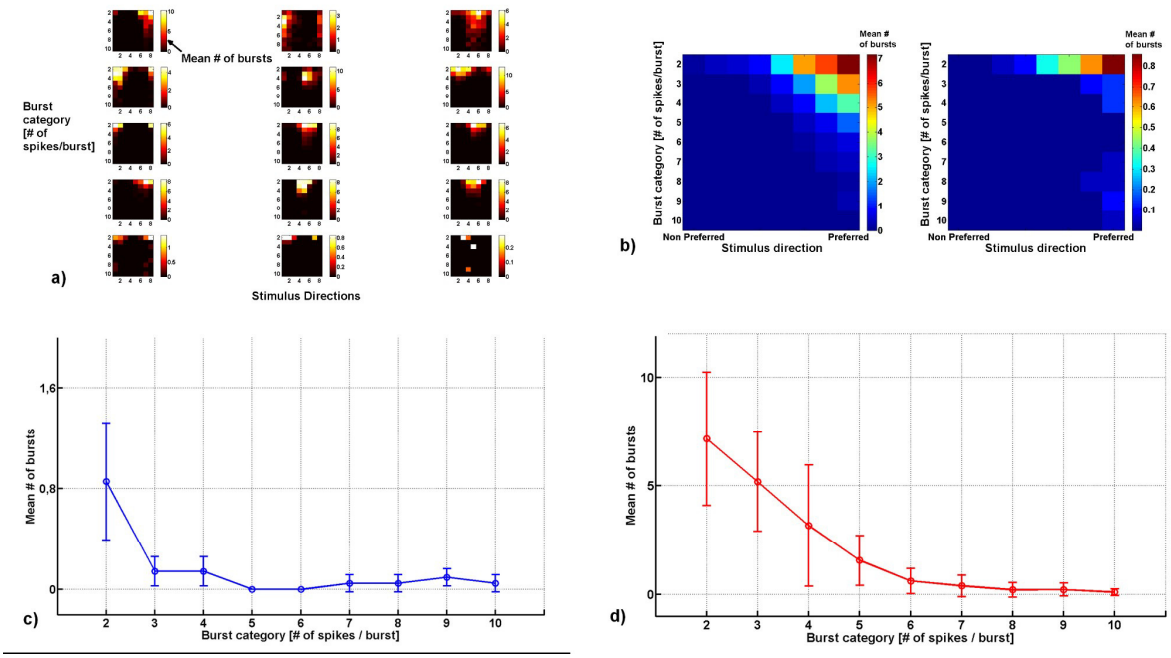

Fig.17 a) Color coded burst activity for each of the recorded cells. First four rows represent each of the 12 recorded ON-OFF DSRGCs since the last row stands for the three recorded ON DSRGCs. The color code represents the mean number of bursts per trial. For each square the Y axis depicts the burst category starting with first row as 2 spikes/burst following with increasing number of spikes per burst up to the last category consisting in bursts with 10 spikes per burst. X axis for each square represents the eight different stimulus directions of movement.

b) Left color map represents the mean burst activity for all 12 ON-OFF DSRGCs. Y axis represents the different burst categories in number of spikes/burst. X axis represents the stimulus directions. Right color map represents the same for all 3 ON DSRGCs.

c) Mean number of bursts for each of the burst category (in number of spikes/burst) at preferred direction for all ON DSRGCs.

d) Mean number of bursts for each of the burst category (in number of spikes/burst) at preferred direction for all ON-OFF DSRGCs.

For ON-OFF DSRGCs the largest percentage was 38%, also for the shortest burst category but did not decrease abruptly for larger burst where we found 27% for 3 spikes per burst and 18% percent for 4 spikes per burst and 8% for 5 spikes per burst. Larger bursts

were rarely accounted and summed remained below 10% of total bursts at preferred direction.

The differences between ON-OFF DSRGCs and ON DSRGCs were statistically significant ($p<0.02$) regarding the information about stimulus contained by each ISI category. Fig.11-a shows that for ON-OFF DSRGCs as ISI increased we found lower amount of information within the each increasing ISI categories. For ON DSRGCs Fig.18-b shows that for two of the ISI categories, namely 0<ISI<10 ms and 20<ISI<50 ms the entropy was almost the same: H=0.52 +/- 0.1 [bits/spike] (n=3) and H=0.51+/- 0.3 [bits/spike] (n=3), respectively.

This suggests not only that the entropy did not decrease as ISI increase (as it happened for ON-OFF DSRGCs) but also that the highest amount of information for ON DSRGCs was comparable with the lowest amount of information found for ON-OFF DSRGCs at largest ISI category, H=0.55 +/-0.4 [bits/spike] (n=12).

Additionally for ON DSRGCs, the index of selectivity for entropy DSiH (Fig. 18a) was highest for the largest ISI category50<ISI<100 ms (DSi H = 0.55 +/-0.07, n=3) and not for the shortest ISI category as it was noticed for ON-OFF DSRGCs.

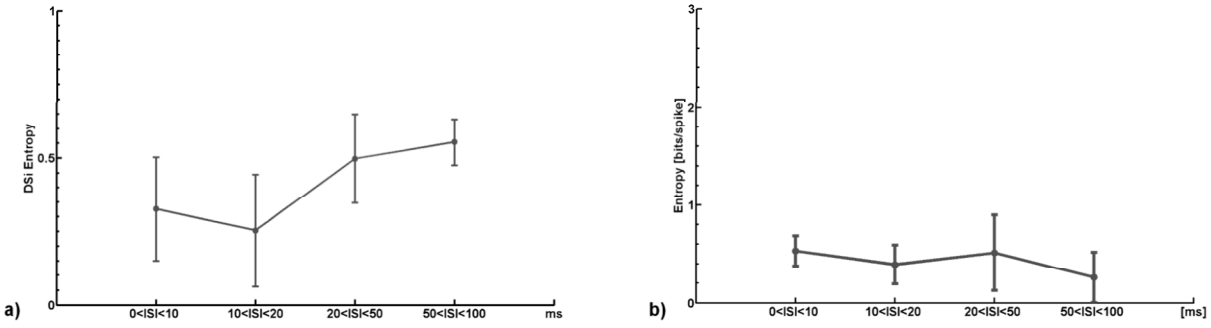

Fig.18 a) Variation of index of selectivity (DSi) of entropy for all recorded ON DSRGCs and for all ISI categories.

b) Variation of entropy (bits/spike) for all ON DS RGCs recorded using grating bar stimulus versus different ISI categories.

4. Discussion

Retinal ganglion cells represent the output of the retina toward higher brain areas, encoding in their spike trains the representation of the visual stimuli which act upon their receptive fields. It is already well known that their firing rate is an important parameter to consider how the relation between stimulus and RGC response has to be characterized. However many scientific evidence suggests that spike timing, within RGCs spike trains, is another parameter which influences how information is transmitted from retina to the lateral geniculate nucleus (LGN), which represents the next stage in early visual stimulus (Uglesich *et al.*, 2009; Sincich *et al.*, 2009; Rathbun *et al.*, 2010). Most of the neurons postsynaptic to a RGC, in the LGN, fire about half the number of incoming number of retinal counterparts' spikes, in the process of editing the input spike trains (Hubel & Wiesel, 1961; Kaplan *et al.*, 1987; Usrey *et al.*, 1998).

Moreover, it has been showed that the precise time between two spikes, within a RGC's spike train is crucial in defining the success of triggering an AP at the postsynaptic target in the LGN. Scientific studies demonstrated that within retinal spike trains, spikes following an ISI lower than 30 ms are more effective than spikes following longer ISIs in evoking an AP at their LGN counterparts (Sincich *et al.*, 2007; Usrey *et al.*, 1998). Within this time scale, the temporal summation of excitatory postsynaptic potentials (EPSPs) is mediated mostly by NMDA current so that almost all EPSPs add together to bring the membrane potential of the postsynaptic cell to the spike threshold, with a stronger efficacy at more depolarized membrane potentials (Blitz and Regehr, 2003).

By contrary, the retinal spikes with ISI larger than 30 ms induce a source of noise into the retinal filter that lowers their information capacity (Sincich *et al.*, 2009). In this sense, the constraint imposed by this temporal summation of closed in time EPSPs selects the stimuli to those that can evoke such EPSPs sequence and thus bring the LGN cell to the spike threshold. Thus, the transmission of visual stimulus toward the cortex is refined,

irrelevant stimulus features are excluded and consequently LGN cells preserve the important information firing less number of spikes.

This ISI based filtering presumably represents part of the robust mechanism to process visual information from retina to higher brain areas (Rathbun *et al.*, 2007) and let us know more information about visual stimulus with less number of spikes at postsynaptic counterpart within retinogeniculate synapse (Uglesich *et al.*, 2010; Sincich *et al.*, 2009).

Having these into account we simply asked how this ISI based temporal filter is related to signaling new stimulus or important features of the visual stimulus which acts upon the RGCs' receptive fields.

Across our retinal ganglion cells sample, firstly, we found that their spike trains were consistently arranged in periods with high firing rate and interposed periods with isolated spikes (Zeck *et al.*, 2007; Fairhall *et al.*, 2006). Most of the ISIs were shorter than 200 ms and the peaks in the ISI histograms were found for ISI shorter than 30 ms for both types of visual stimulus we used.

The most important result using white noise stimulus was that we found the maximum correlation between stimulus and RGCs neural activity for shortest ISI category (ISI $\leq$ 10 ms). As ISI increased the maximum correlation between stimulus and cells' response decreased so that for ISI > 30 ms the correlation dropped below the value found for all ISIs in the spike trains.

Short ISI spiking activity (ISI < 10 ms) apparently represents the cells response to the optimal feature of the visual stimulus presented and presumably the LGN cell counterpart is about to use this ISI based filtering in order to refine the visual information within its information processing toward higher brain areas (Sincich *et al.*, 2009).

Retinogeniculate synapse have the great advantage of the one to one connection between retinal cells and their LGN cells counterpart (a LGN cell has a single retinal main driver acting upon the center of the receptive field and only up to five retinal afferents which

affect the surroundings and have a weak influence) and thus the spike timing within the spike trains are of a major importance in information processing. At higher synapses, i.e. LGN to V1, the convergence of many more cells act together to bring the V1 cell to spike threshold (Cleland *et al.*, 1971; Sincich *et al.*, 2007; Usrey *et al.*, 1999).

To further investigate the influence of the ISI on signaling the optimal stimulus we used a second stimulus consisting in drifting grating bars moving in different equidistant directions. This type of stimulus is well known as being the optimal stimulus for ON-OFF DSRGCs with the same preferred direction as of stimulus direction of movement (Levick et al., 1969). We found that short ISI activity was higher for ON-OFF DSRGCs than for the other RGC types. Additionally, the short ISI activity was tuned at preferred direction of stimulus movement for all recorded ON-OFF DSRGCs.

Another interesting finding was that the direction selectivity index for all ON-OFF DSRGCs was the best for shortest ISI category and decreases as ISI increases. This result is strengthening the idea that directional information is better signaled for shortest ISI. An explanation for this DSi distribution was given by the ISI distribution for each of the ISI categories. For the $0<ISI\leq10$ ms most of the short ISI were focused at preferred direction and thus improving the DSi. As ISI increased the distribution of short ISI activity was less focused at preferred direction and thus the difference between preferred, intermediate and nonpreferred direction diminished resulting in lower DSi.

That ISI based filtering influence the signaling of directional information is supported also by the finding that ISI Directional Index (a measure of directional selectivity of each ISI category in respect with all spikes recorded in a spike train) consistently decreased as ISI increased.

Short ISI distribution cannot be predicted by simply increasing firing rate in a stochastic manner as shown by discrepancy between recorded ON-OFF directional selective cells and the Poisson-like artificial spike trains which mimic the recorded cells. Previous

scientific results have also shown that short ISI spiking activity is not strictly dependent on firing rates and that firing events of retinal ganglion cells have a higher precision than firing statistics expected by a purely Poisson spike generator (Kara *et al.*, 2000; Rathbun *et al.*, 2010). To explain this discrepancy we scanned the spike trains and found burst-like firing activity more abundant and tuned at preferred direction for ON-OFF DSRGCs and almost inexistent for ON DSRGCs and artificial spike trains. We suggest that for ON-OFF DSRGCs burst-like firing activity plays a key role in explaining how these neurons encode the visual world in discrete firing events (Berry *et al.*, 1997). The impact of burst-like activity was previously demonstrated also at thalamocortical synapse (Swadlow and Gusev, 2001). Burst-like firing together with temporal summation and spike threshold act as mechanism to sharpen not only direction selectivity but also the selectivity for other stimulus features (i.e. orientation selectivity in V1) at different stages within the early visual system (Usrey *et al.*, 1999; Swadlow *et al.*, 2002; at retinogeniculate synapse - Casti *et al.* 2008; Carandini *et al.* 2007; Sincich *et al.* 2007; at geniculocortical synapse - Carandini and Ferster 2000; Jagadeesh *et al.* 1997; Priebe and Ferster 2005; orientation selectivity - Volgushev *et al.* 2000; Carandini and Ferster 2000; direction selectivity - Jagadeesh *et al.* 1997; Volgushev *et al.*, 2000; Carandini and Ferster 2000; Priebe and Ferster 2005).

Interestingly, for the other direction selective RGC type, the ON direction selective cell, we found less short ISI spiking activity at preferred direction. For this cell type we also found a lower index of selectivity too. Additionally, ON DSRGCs show the highest spiking activity for larger ISI category and also lower information rates than the ON-OFF DSRGCs. The differences between the ON-DSRGCs and the ON-OFF DSRGCs could be explained by the fact that for ON-DSRGCs we found much less burst-like activity than for ON-OFF DSRGCs. In this case the burst-like activity as part of the mechanism described above would give a weaker influence upon improving signaling the directional information at postsynaptic target. To account for an eventual improvement in directional information

transmission at the output of ON DSRGC (which project to the Accessory Optic System) presumably the polysynaptic convergent connectivity arrangement must be taken into account (Soodak and Simpson, 1988; Ackert *et al.* 2006; Oyster 1968).

Finally, our last results show that the amount of information regarding the visual stimulus was highest at shortest ISI category and decreased as ISI increased. Moreover the entropy was tuned at preferred direction of stimulus motion having an index of selectivity which decreased as ISI increased. These findings clearly show that most of the information regarding visual stimulus are carried by shortest ISI and are robustly correlated with the preferred stimulus feature.

Our results are in the same trend with other results from recent studies which have shown that the amount of information carried by the LGN cell spike train could be even similar to that of its retinal counterpart but with about half number of spikes for the relay spike train (Uglesich *et al.*, 2009; Sincich *et al.*, 2009). These findings suggest that at the output of LGN cell the retinal information is represented in a sparse form and thus with an increasing efficiency. Another recent scientific evidence supports this idea and shows that the average information conveyed by a single spike increases across the retinogeniculate synapse by selectively transmitting retinal spikes with the most information (Rathbun *et al.*, 2010).

It is already well known that sparse coding used by neurons increasingly from one stage to another is of a fundamental importance concerning coding efficiency, energy efficiency, speed of information processing and increasing the storage capacity of memory (Olshausen and Field 2004).

As opposed to the retinogeniculate synapse which holds the major advantage of one to one connection between retinal ganglion cell and its LGN cell counterpart and thus makes easier to study the role of ISI –based filtering in process of information transmission, at higher stages, i.e. V1, the large polysynaptic connectivity mechanism set hurdles in

evaluating the ISI influence on the visual information processing. However, some scientific results (Reich *et al.*, 2000) supports the idea that ISI- based filtering plays a role in information transmission in visual cortex and that they are also consistent with other types of decoding schemes that do not make use of ISIs (averaging the firing rates across many neurons that convey similar information).

5 Conclusions

Using two different types of stimuli and extracellularly recording activity of different types of retinal ganglion cells, we learned out how ISI based filtering of RGCs spike trains helps preserving the information regarding the optimal stimulus features. Maximum correlation between stimulus and neural response is at shortest ISI spiking activity (Rahbun *et al.*, 2007).

Short ISIs carry the most information, are focused at optimal (preferred) stimulus features (in our case direction of stimulus motion) and are not strictly related to firing rate. Short ISI spiking activity is part of a mechanism which perform the so called “iceberg effect” at postsynaptic target (Carandini et Ferster 2000).

Thus, at presynaptic level already, ISI based filtering is a part of a mechanism that sharpens the information from one stage to another along the early visual system. This mechanism is prominent for ON-OFF DSRGCs which form one to one connection with their postsynaptic target. However it is less evident for ON-DSRGCs which form massive convergence of synaptic inputs upon their postsynaptic target in AOS.

References

Ackert, J.M., Wu, S.H., Lee, J.C., Abrams, J., Hu, E.H., Perlman, I., 2006. Light-induced changes in spike synchronization between coupled ON direction selective ganglion cells in the mammalian retina. The Journal of Neuroscience, 26(16), 4206-4215.

Amthor, F.R., Oyster, C.W., Takahashi, E.S., 1984. Morphology of on–off direction-selective ganglion cells in the rabbit retina. Brain Research, 298(1), 187–190.

Amthor, F.R., Oyster, C.W., Takahashi, E.S., 1989a. Morphologies of rabbit retinal ganglion cells with complex receptive fields. J. Comparative Neurology 280(1), 97–121.

Barlow, H.B. & Hill, R.M., 1963. Selective sensitivity to direction of movement in ganglion cells of the rabbit retina. Science 139, 412–414.

Barlow, H.B., Hill, R.M. & Levick, W.R., 1964. Retinal ganglion cells responding selectively to direction and speed of image motion in the rabbit. Journal of Physiology 173, 377–407.

Berry, M.J., Warland, D.K., Meister, M., 1997. The structure and precision of retinal spike trains. Proc Natl Acad Sci U S A 94:5411–5416.

Blitz, D.M., Regehr, W.G., 2003. Retinogeniculate synaptic properties controlling spike number and timing in relay neurons. J Neurophysiol 90:2438 –2450.

Brenner, N., Strong, S.P., Koberle, R., Bialek, W., de Ruyter van Steveninck, R.R., 2000.

Synergy in a neural code. Neural Comput 12:1531–1552.

Carandini, M. and Ferster, D., 2000. Membrane potential and Firing rate in cat primary visual cortex. The Journal of Neuroscience, 20(1):470-484.

Carandini, M., Horton, J.C. & Sincich, L.C., 2007. Thalamic filtering of retinal spike trains by postsynaptic summation. Journal of Vision 7(14), 1–11.

Casti, A., Hayot, F., Xiao, Y. & Kaplan, E., 2008. A simple model of retina-LGN transmission, Journal of Computational Neuroscience, doi:10.1007/s10827-007-0053-7.

Cleland, B.G., Levick, W.R., Morstyn, R., Wagner, H.G., 1976. Lateral geniculate relay of slowly conducting retinal afferents to cat visual cortex. Journal of Physiology 255, 299-320.

Cleland, B.G., Dubin, M.W., Levick, W.R., 1971. Simultaneous recording of input and output of lateral geniculate neurones. Nat New Biol 231:191–192.

De Vries, S.H. & Baylor, D.A., 1997. Mosaic Arrangement of Ganglion Cell Receptive Fields in Rabbit Retina. Journal of Neurophysiology 78:2048-2060, 1997.

Euler, T., Detwiller, P.D. & Denk, W., 2002. Directionally selective calcium signals in dendrites of starburst amacrine cells. Nature 418(6900), 845-852.

Fairhall, A.L., Burlingame, C.,A., Narasimhan, R, Harris, R.A., Puchalla, J.L., Berry, M.J., 2006. Selectivity for multiple stimulus features in retinal ganglion cells. J Neurophysiol 96:2724 –2738.

Ferster, D. and Miller, K.D., 2000. Neural mechanisms of orientation selectivity in the visual cortex Annual Reviews of Neuroscience, Vol. 23, pp. 441-471

Godwin, D. W., Vaughan, J. W., & Sherman, S. M., 1996. Metabotropic glutamate receptors switch visual response mode of lateral geniculate nucleus cells from burst to tonic. Journal of Neurophysiology, 76, 1800–1816.

Guido,W., Lu, S.M., Vaughan, J.W., Godwin, D.W., & Sherman, S.M., 1995. Receiver operating characteristic (ROC) analysis of neurons in the cat's lateral geniculate nucleus during tonic and burst response mode. Visual Neuroscience, 12, 723–741.

Hubel D.H. & Wiesel T.N., 1961. Integrative action in the cat's lateral geniculate body. Journal of Physiology 155: 385–398.

Hubel, D.H., & Wiesel, T.N., 1962. Receptive fields, binocular interaction and functional architecture in the cat's visual cortex. Journal of Physiology 160:106–154.

Jagadeesh, B., Wheat, H.S., Kontsevich, L.L., Tyler, C.R., Ferster, D., 1997. Direction selectivity of synaptic potentials in simple cells of the cat visual cortex. Journal of neurophysiology, 78:2772-2789.

Kara, P., Reinagel, P., Reid, R.C., 2000. Low response variability in simultaneously recorded retinal, thalamic, and cortical neurons. Neuron 27:635– 646.

Kaplan, E, Purpura, K. & Shapley, R.M., 1987. Contrast affects the transmission of visual information through the mammalian lateral geniculate nucleus. Journal of Physiology 391: 267–288.

Koizumi, A., Jakobs, T.C. & Masland, R.H., 2004. Inward rectifying currents stabilize the membrane potential in dendrites of mouse amacrine cells: patchclamp recordings and singlecell RT-PCR. Mol. Vis., 10, 328–340.

Kuffler, S. (1953). Discharge patterns and functional organization of mammalian retina.

Journal of Neurophysiology 16:37–68.

Levick, W. R., Oyster, C. W. & Takahashi, E., 1969. Rabbit Lateral Geniculate Nucleus:

Sharpener of Directional Information. Science 165(3894), 712-714.

Levine, M.W., Cleland, B.G., 2001. An analysis of the effect of retinal ganglion cell impulses upon the firing probability of neurons in the dorsal lateral geniculate nucleus of the cat. Brain Res 902:244 –254.

Mastronade, D.N., 1987. Two classes of single-input X-cells in cat lateral geniculate nucleus. II. Retinal inputs and the generation of receptive-field properties. J Neurophysiol 57:381– 413.

Olhause, B.A., Field, D.J., 2004. Sparse coding of sensory inputs. Curr Opin Neurobiol 14:481– 487.

Oyster, C. W., 1968. The analysis of image motion by the rabbit retina. The Journal of Physiology, 199, 613–635.

Paninski, L, 2003. Convergence properties of three spike-triggered analysis techniques. Network 14:437– 464.

Priebe, N. and Ferster, D., 2005. Direction selectivity of excitation and inhibitionin simple cells of the cat primary visual cortex. Neuron, Vol. 45, 133–145.

Rathbun, D. L, Allito, H.J., Weyand, T.G., & Usrey, W.M., 2007. Interspike interval analysis of retinal ganglion cell receptive fields. Journal of Neurophysiology 98, 911-919.

Rathbun, D. L, Warland, D.K., & Usrey, W.M., 2010. Spike timing and information transmission at retinogeniculate synapse.The Journal of Neuroscience 30(41):13558-13566.

Reid, R.C., Victor, J.,D., & Shapley, R.,M., 1997. The use of m-sequences in the analysis of visual neurons: linear receptive field properties. Vis. Neurosci., 14, 1015–1027.

Reid, R.,C., & Usrey, W.,M., 2004. Functional connectivity in the pathway from retina to visual cortex. In: The Visual Neurosciences, ed. CHALUPA, L.M. & WERNER, J.S., pp. 673–679. Cambridge, MA: MIT Press.

Schwartz, O., Pillow, J.W., Rust, N.C., Simoncelli, E.P., 2006. Spike-triggered neural characterization. J Vis 6:484 –507.

Shimazaki, H., Shinomoto, S., 2007. A method for selecting the bin size of a time histogram. Neural Computation 19 (6): 1503–152. doi:10.1162/neco.2007.19.6.1503

Sincich, L.C., Adams, D.L., Economides, J.R. & Horton, J.C., 2007. Transmission of spike trains at retinogeniculate synapse. The Journal of Neuroscience 27(10), 2683–2692.

Sincich, L.C., Horton, J.C. & Sharpee, T.O., 2009. Preserving Information in Neural Transmission. The Journal of Neuroscience 29(19):6207– 6216, 6207.

Soodak, R.E., Simpson, J.I., 1988. The accessory optic system of rabbit. I. Basic visual response properties. Journal of Neurophysiology, 60, 2037–2054.

Strong, S.P., Koberle, R., de Ruyter, van Steveninck, R.R., Bialek, W., 1998. Entropy and information in neural spike trains. Phys Rev Lett 80:197–200.

Swadlow, H.A., Gusev, A.G., 2001. The impact of "bursting" thalamic impulses at a neocortical synapse. Nat Neurosci 4:402-408.

Swadlow, H.A., Gusev, A.G., & Bezdudnaya, T., 2002. Activation of a cortical column by a thalamocortical impulse (pdf). The Journal of Neuroscience, 22(17), 7766–7773.

Taylor, W.R. & Vaney, D.I., 2002. Diverse Synaptic Mechanisms Generate Direction Selectivity in the Rabbit Retina, Journal of Neuroscience 22(17), 7712–7720.

Uglesich, R., Casti, A., Hayot, F. & Kaplan, E., 2009. Stimulus size dependence of information transfer from retina to thalamus. Frontiers in Systems Neuroscience doi:10.3389/neuro.06.010.2009.

Usrey, W.M., Reppas, J.B. & Reid, R.C., 1998. Paired-spike interactions and synaptic efficacy of retinal inputs to the thalamus. Nature 395(6700), 384-387.

Usrey, W.M., Reppas, J.B. & Reid, R.C., 1999. Specificity and strength of retinogeniculate connections. J Neurophysiol 82:3527–3540.

Usrey, W.M., Alonso, J.M., Reid, R.C., 2000. Synaptic interactions between thalamic inputs to simple cells in cat visual cortex. J Neurosci 20:5461–5467.

Vaney, D.I., Levick, W.R., & Thibos, L.N., 1981a. Rabbit retinal ganglion cells. Receptive field classification and axonal conduction properties. Experimental Brain Research 44(1), 27–33.

Vaney, D.I., Peichl, L., Wassle, H. & Illing, R.B., 1981b. Almost all ganglion cells in the rabbit retina project to the superior colliculus. Brain Research 212(2), 447–453.

Volgushev, M. Pernberg, J. and Eysel, U.T., 2000. Comparision of the selectivity of the postsynaptic potentials and spike responses in cat visual cortex. European Journal of Neuroscience, Vol.12, pp 257-263.

Weyand T.G., 2007. Retinogeniculate Transmission in Wakefulness. Journal of Neurophysiology 98: 769–785.

Yang, G. & Masland, R.H., 1994. Receptive fields and dendritic structure of directionally selective retinal ganglion cells. J. Neurosci., 14, 5267–5280.

Zeck, G.M., & Masland, R.H., 2007. Spike train signatures of retinal ganglion cell types. European Journal of Neuroscience 26, 367-380.

V. Discussions, Conclusions and Future Perspectives

Within my thesis I have studied the manner in which the information is processed at both single cell level and neural network level, involving not only stimulus induced activity but also spontaneous activity.

To study the information processing in spontaneous activity I investigated the neural activity in dissociated cultures of cortical and hippocampal neurons from rats. To do so I used the multielectrode array technology (MEA, Multichannel Systems, Reutlingen, Germany), a powerful tool which allow multisite recordings within the culture and thus investigations of spiking activity not only at single cell level but also at neural network level. The MEA set-up was arranged in a new technology outside the classical culture incubator and retains the main advantages of the possibility to perform uninterrupted (electro-) physiological and morphological data collection in long-term experiments, together with the reduction of handling artifacts (*e.g.*, temperature fluctuations, evaporation of medium, mechanical impact, and drift in pH during culture transfer from the incubator to the experimental setup). Analyzing the spiking activity with this novel laboratory set-up we could learn about the following aspects concerning the neural activity.

Neurons from dissociated brain tissue are capable of self-organizing their interconnectivity in cell culture. They become active even in the absence of any external sensory stimuli remarkably developing a wide range of spatiotemporal patterns of activity with dynamic shape and/or organization over time and spatial location, starting from the well-known synchronized network bursting activity (neural avalanches) to different types of self-organization such as depicted here, consisting in PS activity which robustly shapes the spontaneous activity at different developmental stages.

Little it is known about PS activity and its role within cultured neurons. Interestingly, we found that predominantly robust PS activity rather than bursts droves neural activity in the investigated cultures. PS not only developed stable spatiotemporal patterns, but also participated in shaping the interconnectivity map. Previous reports on its role *in vivo* and *in vitro* suggest that PS activity may act as a temporal filter and be part of a mechanism involved in information processing at different developmental stages, both at individual sites and at network level. Mainly, here we found that:

- PS activity does exist under a spontaneous activity paradigm in cultures of dissociated neurons of different types,
- PS forms spatiotemporal patterns of activity that become robust at later stages of development,
- PS persistently participates in formation of functional connectivity at different sites within the culture,
- PS participates in information processing within the culture and is actively involved in bi-directional information transfer between the neurons.

This trend is preserved at network level where the entire network activity remarkably shows an auto-correlated (oscillatory-like) neural activity following (with a short time delay) each second spike in a PS at different stages of development. Moreover, this PS correlated activity at network level is strongly involved in carrying information when PS activity was considered as an internal surrogate stimulus.

All these findings together suggest that PS activity may act as a stimulus for cultured neurons in lack of any external electrical or chemical stimulation and encourage that new scientific hypotheses are waiting to be tested regarding the ability of PS activity to control the neural response in cultures of dissociated neurons.

To study the manner in which the information processing is performed in stimuli induced activity I investigated the recorded neural response of directional selective retinal ganglion cells in rabbit retina.

In a mechanistic approach, a model was proposed to explain the sharpening of direction selectivity at the output of retina. The model, consisting in recorded DSRGCs inputs combined with a variant of a leaky integrate-and-fire neuron model and not taking into account neither synaptic plasticity nor cortical feedback input, explained how neurons postsynaptic to directional selective retinal ganglion cells signal better the direction of stimulus movement. Spike threshold act as a filter that allows an AP to be generated once the threshold value of the membrane potential is reached. Another important key of this mechanistic approach is the summation of the incoming EPSPs which has the effect that postsynaptic membrane potential reaches the threshold. Summation becomes efficient when two or more EPSPs are separated by a short time interval. This situation takes place mostly during burst-like activity and particularly within PS activity. This burst-like activity and PS activity for ON-OFF DSRGCs is distributed at preferred direction. Thus, PSP-to-spike transformation has maximum efficacy at preferred direction, while at the other intermediate directions we will notice a reduction of spikes and thus the sharpening increases. These results are also similar to those obtained at retinogeniculate synapse, *in vivo* for cat and monkey (Casti *et al.*, 2008,; Carandini *et al.*, 2007) or for rabbit, in the seminal work of Levick *et al.*, 1969.

Further on, remarkably, the interspike interval filtering of recorded spike trains has been shown to play an important role in order to preserve the information concerning the optimal feature of the visual stimulus in the transmission process from retina to LGN.

Shortest ISI spiking activity retained the maximum correlation between stimulus and neural response. Additionally it was clearly demonstrated that short ISIs carry the most information, are focused at optimal (preferred) stimulus features (in our case direction of stimulus motion) and are not strictly related to firing rate. Thus, at presynaptic level already, ISI based filtering is a part of a mechanism that sharpens the information from one stage to another along the hierarchical stages of the early visual system. This mechanism is prominent for ON-OFF DSRGCs which form one to one connection with their postsynaptic target. However this is less evident for ON-DSRGCs, which form massive convergence of synaptic inputs upon their postsynaptic target in the Accessory Optic System (AOS). These results are in concordance with other scientific works that investigate the manner in which information is processed from one stage to another within the nervous system (Rathbun *et al.*, 2007; Rathbun *et al.*, 2010; Uglesich *et al.*, 2009; Sincich *et al.*, 2009).

We have seen how the mechanism for sharpening in direction selectivity can be explained at the retinogeniculate synapse by means of PSP to spike transformation with great effect for burst-like activity. Moreover ISI of DSRGCs spike trains filter robustly the information about visual stimuli, with maximum correlation between receptive field and neural response at shortest ISI. However, at finer tuning, presumably the PS activity is playing the crucial role in explanation for all above mentioned results. For the same recorded RGCs within the same experimental method, as exemplified in Fig.1 for five ON-OFF DSRGCs with different preferred directions(and described in Chapter III, Methods 2.1 and 2.2), we scanned the recorded spike trains to quantify the PS activity (Chapter II, Methods 2.4) under the stimulus conditions this time. Remarkably, we found that PS activity was robustly involved in neural response of retinal ganglion cells of all types (ON-OFF DSRGCs, ON-DSRGCs and NONDSRGCs).

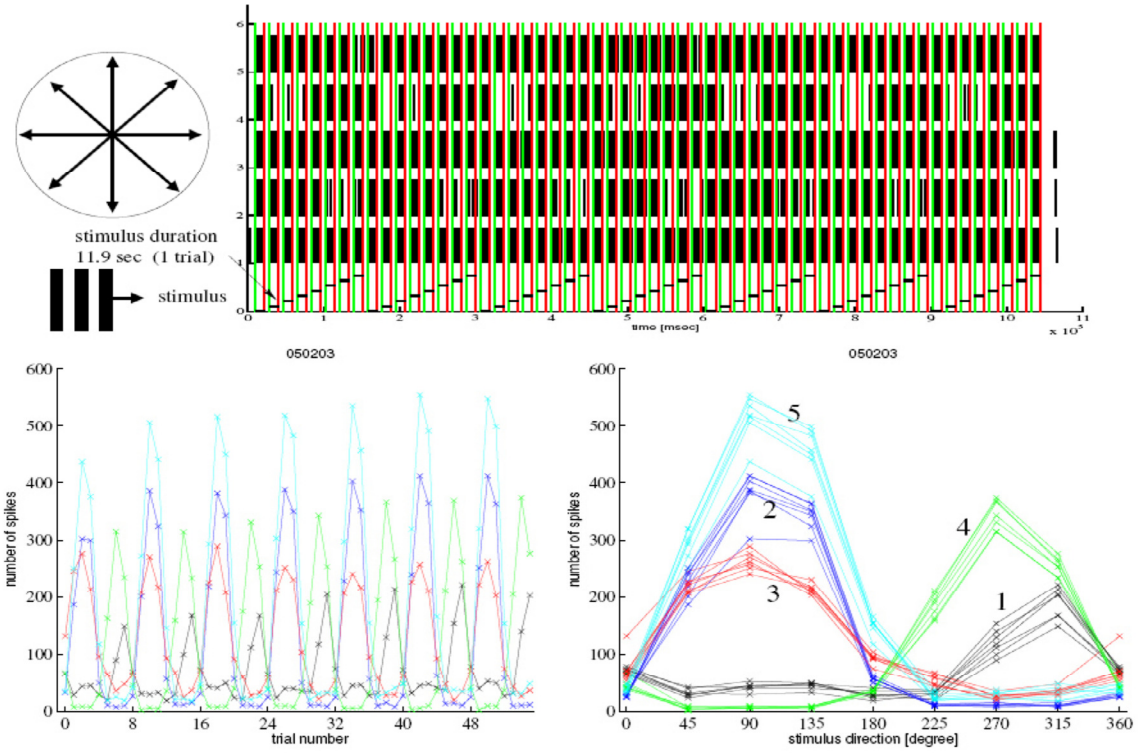

Fig. 1 Neural response extracellularly recorded of five ON-OFF DSRGCs. Stimulus presented consisted in drifting grating bars moved in 7 different directions 45 degrees apart. Direction selective neuron responses were recorded and tuning curves for all trials were built. Three of the cells have preferred direction at 90 degrees and two of them at 270 degrees and 315 degrees, respectively. Left lower side shows the neural response recorded for each trial and right side shows the tuning curves indicating the preferred directions.

Indeed PS activity plays a crucial role in the neural response of the stimulated ONOFF DSRGCs holding the largest index of selectivity (DSi, Chapter III, Methods 2.2) as exemplified in Fig. 2a for 25 recorded RGCs. Among them 16 cells were directional selective and for them PS presented the highest values indicating a primordial role in shaping the tuning curves in response to direction of stimulus movement. Moreover, Fig. 2b depicts the percentage of the information about stimulus direction transmitted from RGC to modeled postsynaptic LGN neuron (Chapter II, Methods 2.4). For ON-OFF DSRCs PS

activity alone carry most of the information regarding the stimulus direction, the lowest information percentage found was above 50% while for some ON-OFF DSRGCs the information transferred by PS related activity toward LGN modeled neuron was above 90%. Remarkably, for NON-DS and ON-DSRGCs the information percentage transferred toward LGN cell was under 20% for all cases. Interestingly, despite the DSi for ON DSRGCs was larger for PS activity than for the entire spike train the information transferred by PS, it was considerably lower than for ON-OFF DSRGCs.

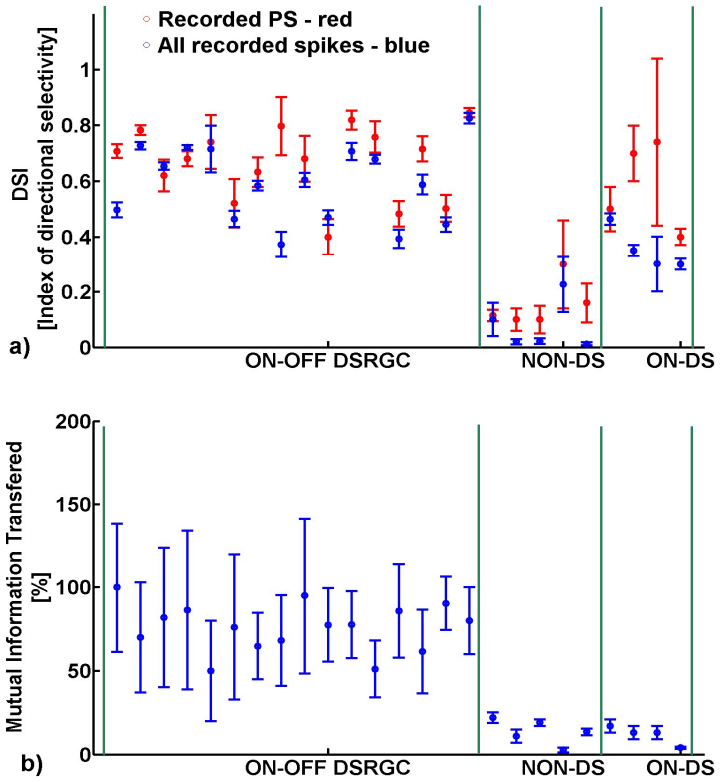

Fig. 2 a) DSi (Y axis) value for 25 RGCs, 16 cells are ON-OFF DSRGC – limited by left side green bars, 5 cells are NON-DS – limited by middle green bars and 4 cells are ON-DS –limited by right side green bars. b) Mutual Information transferred by PS activity to LGN modeled postsynaptic counterpart for the cells mentioned in a)

This finding is sustained by a morphological explanation: ON-OFF DSRGCs perform one-to-one connectivity with their LGN counterpart and thus PS from one single

cell becomes crucial, while in ON-DSRGCs multiple cells send convergent inputs toward their counterparts in accessory optic system (AOS) and thus, presumably, the information is going to be enriched as a consequence of heterosynaptic mechanisms. The latter mechanism holds true at higher brain areas (i.e. geniculo-cortical synapse) and suggests that presumably PS mechanism changes its shape from mono to polysynaptic contributions (these results are published in Proceedings of 9th MEA Meeting, 2014, p. 181-182).

In a different approach, a descriptive model to characterize a physiological property called the receptive field, which is fundamental in deciphering how particular neurons encode the incoming visual stimulus, was built to accurately predict the direction of stimulus motion based on recorded directional selective retinal ganglion cells response (these results are accepted at CNS 2014 conference and will be published in BMC Neuroscience Suppl., *in press*). Briefly, to build the model, space-time inseparability of the receptive fields of ONOFF DSRGCs together with additional static non-linearities was the principal key. The main steps I used are: build white noise stimulus, record from ON-OFF DSRGCs stimulated with white noise stimulus, calculate the STA in response to white noise stimulus and extract the kernel, find the optimal kernel by adjusting the estimated firing rate to the recorded firing rate, record data with new stimulus, consisting drifting grating bars, construct the linear model, add static non-linearities (i.e. spike threshold and saturation), compare predicted with recorded data (Fig. 3).

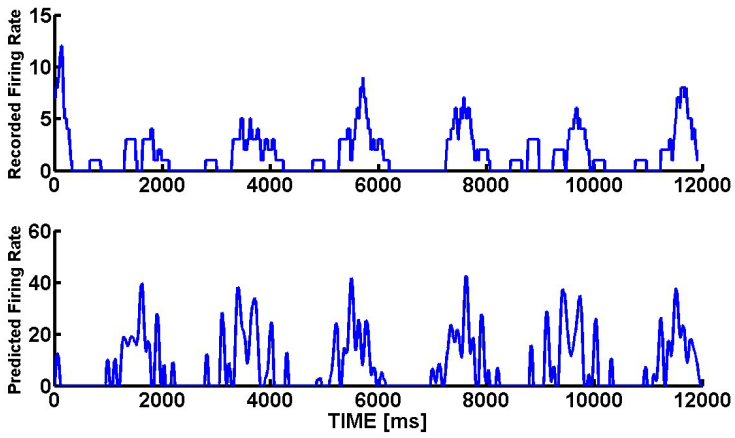

Fig. 3. Recorded and predicted firing rates. The lower plot is the rate predicted by integrating the product of stimulus intensity and a linear filter followed by a function applied over the linear filter. The upper plot shows the recorded data.

The kernel needed to describe direction selectivity of ON-OFF DSRGC visual response property was first extracted using white noise stimulus. We then used grating bars stimulus and constructed a complete model to predict the direction selectivity of the recorded cells.

The optimal kernel produces an estimate of the firing rate that is a linear filter of the stimulus. In order to deal with some of the deficiencies of the linear prediction we added a nonlinear function ($F(L)$) of the linearly filtered stimulus (Dayan and Abbott, 2001). F is a function of the linear filter value instantaneously evaluated at the time of the rate estimation. Once that F is bounded from above and below, the estimated firing rate will never be negative or unrealistically large. Static nonlinearities are used to introduce both firing thresholds and saturation into estimates of neural responses. The model of spike trains evoked by our stimulus has been constructed by using firing rate estimate of equation below, to drive a Poisson process of spike generation (Fig. 4).

$$L(t) = \int_0^{\infty} d\tau D_{xyt}(\tau) I_{xyt}(t-\tau);\ rest(t) = r_0 + F(L(t))$$

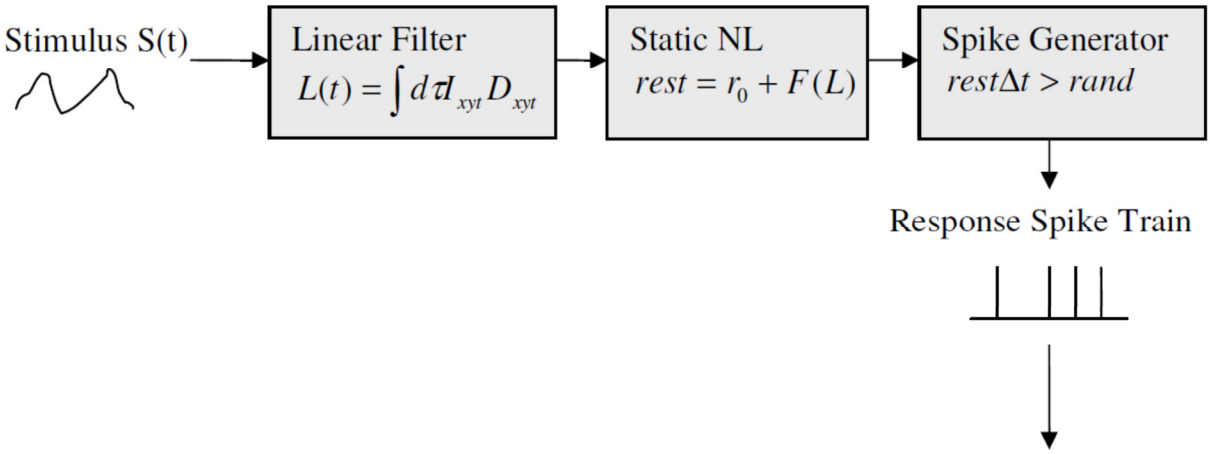

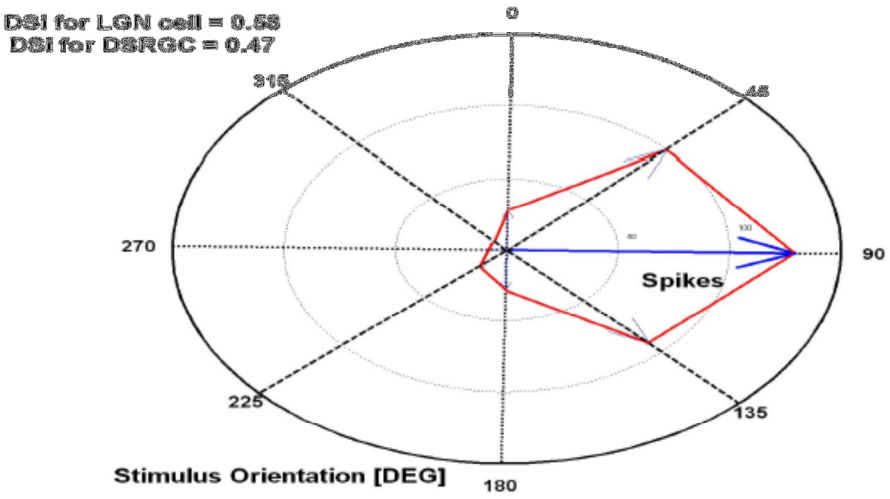

Fig. 4. Linear – Non-linear model to simulate spiking responses to stimuli. The integral of the stimulus I_{xyt} times the optimal kernel D_{xyt} is first computed as being the linear filter. The estimated firing rate is the background firing rate plus a nonlinear function of the output of the linear filter calculation.

Finally, the estimated firing rate is used to drive a Poisson process to generate the predicted spike trains. Ultimately, the DSi for the predicted activity is indicating the predicted degree of direction selectivity.

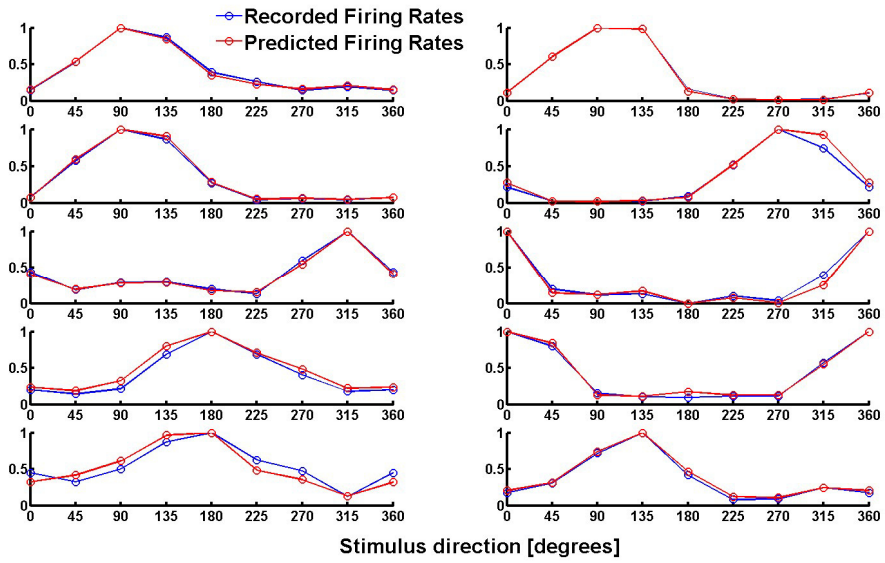

Fig. 5. Predicted (red curve) and recorded (blue curve) tuning curves for 10 ON-OFF DSRGCs.

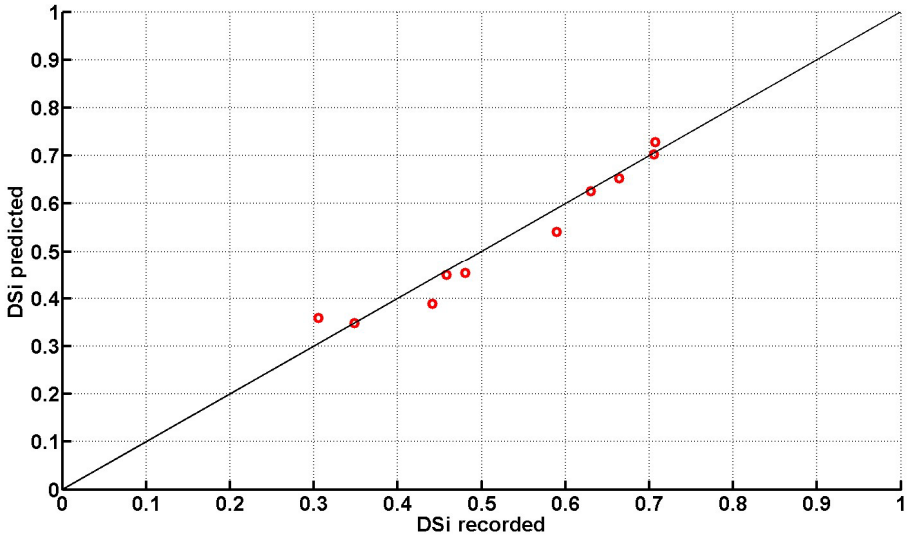

Fig. 6 DSi predicted vs. DSi recorded shows a clustering along the diagonal line which represents that the predicted and the recorded DSis are equals.

The fact that the model was able to predict each time accurately the direction of stimulus motion but it slightly underestimated the degree of the direction selectivity (Fig. 5 and Fig. 6) indicates that for such complex tasks as direction of stimulus motion and for the response of complex cells (i.e. ON-OFF DSRGCs in rabbit) higher order non-linearities

should be taken into account in order to improve the prediction. These results are in concordance with other scientific works for different neurons or neuronal populations and for different stimuli (Pillow *et al.*, 2005; Schwartz *et al.*, 2006).

In general, the results presented here show how complex and intriguing is the manner in which neurons perform information processing within the nervous system. Spontaneous activity investigations let us know how neuronal activity develop patterns and show an activity which starts with an almost unpredictable manner of information processing and develops toward a more stabilized one, based on robust neural connectivity. Using parameters as described here (i.e. Pair Spiking activity, ISI distribution, Burst distribution, Conditional Firing Probability, Information Rate, Transfer Entropy) one can extend these results to better characterize the information processing under spontaneous conditions and to propose models – for example, to predict neural activity during different stages of network development. On the other hand within the stimulus induced paradigm we have learned how different coding strategies (i.e. firing rates, burst-like spiking activity, short ISI spiking activity and Pair Spiking activity) are arranged in more complex mechanisms, so that the retinal information is represented in a sparse form and thus with an increasing efficiency.

VI. References

[1] Ackert, J.M., Wu, S.H., Lee, J.C., Abrams, J., Hu, E.H., Perlman, I., Bloomfield, S.A. (2006). Light-Induced Changes in Spike Synchronization between Coupled ON Direction Selective Ganglion Cells in the Mammalian Retina. The Journal of Neuroscience, 26(16), 4206–4215.

[2] Akerberg, O.A. and M.J. Chacron, (2011). In vivo conditions influence the coding of stimulus features by bursts of action potentials. J Comput Neurosci, 31(2): p. 369-83.

[3] Alitto, H.J., Usrey, W.M. (2005). Dynamic properties of thalamic neurons for vision. Progress in Brain Research, 149, 83–90.

[4] Amthor, F.R., Oyster, C.W., Takahashi, E.S., 1984. Morphology of on–off directionselective ganglion cells in the rabbit retina. Brain Research, 298(1), 187–190.

[5] Amthor, F.R., Takahashi, E.S., Oyster, C.W. (1989a). Morphologies of rabbit retinal ganglion cells with complex receptive fields. Journal of Comparative Neurology, 280(1), 97–121.

[6] Bair, W. (1999). Spike timing in the mammalian visual system. Current Opinion in Neurobiology, 9, 447-453.

[7] Banker, G. and K. Goslin, (1998). Culturing Nerve Cells. Cambridge: The MIT Press. 666. 2 ed.

[8] Barlow, H.B. & Hill, R.M., 1963. Selective sensitivity to direction of movement in ganglion cells of the rabbit retina. Science 139, 412–414.

[9] Barlow, H.B., Hill, R.M., Levick, W.R. (1964). Retinal ganglion cells responding selectively to direction and speed of image motion in the rabbit. Journal of Physiology, 173, 377–407.

[10] Barlow, H.B., Hill, R.M., Levick, W.R. (1965). The mechanism of directionally selective units in rabbit's retina. J.Physiol.(Lond) 178, p.477.

[11] Battaglia, D., Witt, A., Wolf, F., Geisel, T. (2012). Dynamic Effective Connectivity of Inter-Areal Brain Circuits. PLoS Comput Biol 8(3): e1002438. doi:10.1371/ journal.pcbi.1002438.

[12] Berry, M.J., Warland, D.K., Meister, M., 1997. The structure and precision of retinal spike trains. Proc Natl Acad Sci U S A 94:5411–5416.

[13] Bienenstock, E.L., Cooper,L.N., and Munro, P.W. (1982).Theory for the development of neuronselectivity: orientation specificity and binocular interaction in visualcortex. J. Neurosci. 2, 32–48.

[14] Blau, A., Neumann, T., Ziegler, C., and Benfenati, F. (2009). Replica-molded poly (dimethylsiloxane) culture vessel lids attenuate osmotic drift in long-term cell culturing. J. Biosci., 34(1): p. 59-69.

[15] Blankenship A. G., Feller M. B. (2010). Mechanisms underlying spontaneous patterned activity in developing neural circuits. Nat. Rev. Neurosci. 11, 18–29.10.103.

[16] Blitz, D.M., Regehr, W.G., (2003). Retinogeniculate synaptic properties controlling spike number and timing in relay neurons. J Neurophysiol 90:2438 –2450.

[17] Blitz, D.M., Regehr, W.G. (2005). Timing and specificity of feed-forward inhibition within the LGN. Neuron, 45(6), 917–928.

[18] Brader, J., Senn, W., and Fusi, S. (2007).Learning real-world stimuli in a neural network with spike-driven synaptic dynamics. Neural Comput. 19, 2881–2912.

[19] Brenner, N., Strong, S.P., Koberle, R., Bialek, W., de Ruyter van Steveninck, R.R., 2000. Synergy in a neural code. Neural Comput 12:1531–1552.

[20] Brewer, G.J., Boehler, M.D., Ide, A.N., Wheeler, B.C. (2009). Chronic electrical stimulation of cultured hippocampal networks increases spontaneous spike rates, J Neurosci Methods, 184, 104-109.

[21] Buhl, E.H., Peichl, L. (1986). Morphology of rabbit retinal ganglion cells projecting to the medial terminal nucleus of the accessory optic system. Journal of Comparative Neurology, 253(2), 163–174.

[22] Buehlmann, A. and Deco, G. (2010). Optimal information transfer in the cortex through synchronization. PLoS Comput Biol 6: e1000934.

[23] Carandini, M., Horton, J.C., Sincich, L.C. (2007). Thalamic filtering of retinal spike trains by postsynaptic summation, Journal of Vision, 7(14), 1–11.

[24] Carandini, M. and Ferster, D. (2000). Membrane potential and Firing rate in cat primary visual cortex. The Journal of Neuroscience, 20(1):470-484.

[25] Casti, A., Hayot, F., Xiao, Y., Kaplan E. (2008). A simple model of retina-LGN transmission, Journal of Computational Neuroscience, DOI:10.1007/s10827-007-0053-7.

[26] Chiappalone M, Vato A, Berdondini L, Koudelka-Hep M, Martinoia S. (2007). Network dynamics and synchronous activity in cultured cortical neurons. International Journal of Neural Systems 17: 87–103.

[27] Chiu C.Y., Weliky M. (2001). Spontaneous activity in developing ferret visual cortex in vivo. J Neurosci, 21(22):8906-8914.

[28] Cleland, B.G. and Lewick, W.R. (1974). Brisk and sluggish concentrically organized ganglion cells in the cat's retina, Journal of Physiology, 240, 421-456.

[29] Cleland, B.G., Lewick, W.R., Morstyn, R., Wagner, H.G. (1976). Lateral geniculate relay of slowly conducting retinal afferents to cat visual cortex, Journal of Physiology, 255, 299-320.

[30] Cleland, B.G., Dubin, M.W., Levick, W.R., 1971. Simultaneous recording of input and output of lateral geniculate neurones. Nat New Biol 231:191–192.

[31] Damjanovic, I., Maximova, E., Maximov, V. (2009). Receptive field sizes of direction-selective units in the fish tectum. Journal of Integrative Neuroscience, 8(1), 77-93.

[32] Dann, J.F. and Buhl, E.H. (1987). Retinal ganglion cells projecting to the accessory optic system in the rat. Journal Comparative Neurology, 262(1), 141–158.

[33] Dayan, P., and Abbott, L. F. (2001). Theoretical neuroscience: Computational and mathematical modeling of neural systems. Cambridge, MA: MIT Press.

[34] DeMarse, T.B., Wagenaar, D.A., Blau, A.W., Potter, S.M. (2001). The neurally controlled animat: Biological brains acting with simulated bodies. Autonomous Robots 11, 305–310.

[35] Devries, S.H. and Baylor, D.A. (1997). Mosaic arrangement of ganglion cell receptive fields in rabbit retina. J. Neurophysiol. 78(4), 2048–2060.

[36] Euler, T., Detwiler, P.D., Denk, W. (2002). Directionally selective calcium signals in dendrites of starburst amacrine cells. Nature, 418(6900), 845-852.

[37] Fairhall, A.L., Burlingame, C.,A., Narasimhan, R, Harris, R.A., Puchalla, J.L., Berry, M.J., 2006. Selectivity for multiple stimulus features in retinal ganglion cells. J Neurophysiol 96:2724 –2738.

[38] Feller, M. B. (1999). Spontaneous correlated activity in developing neural circuits. Neuron, vol. **22**, pp. 653–656.

[39] Ferster, D. and Miller, K.D., 2000. Neural mechanisms of orientation selectivity in the visual cortex Annual Reviews of Neuroscience, Vol. 23, pp. 441-471.

[40] Garofalo M, Nieus T, Massobrio P, Martinoia S. (2009). Evaluation of the performance of information theory-based methods and cross-correlation to estimate the functional connectivity in cortical networks. PLoS One 4: e6482.

[41] Godwin, D.W., Vaughan, J.W., & Sherman, S.M., 1996. Metabotropic glutamate receptors switch visual response mode of lateral geniculate nucleus cells from burst to tonic. Journal of Neurophysiology, 76, 1800–1816.

[42] Gourevitch, B., Eggermont, J.J. (2007). Evaluating information transfer between auditory cortical neurons. J Neurophysiol 97: 2533–2543.

[43] Graupner, M., and Brunel, N. (2012). Calcium-based plasticity model explains sensitivity of synaptic changes to spike pattern, rate, and dendritic location. Proc. Natl. Acad. Sci. USA 109, 3991–3996.

[44] Grasse, K.L., Cynader, M.S., and Douglas, R.M. (1984). Alterations in response properties in the lateral and dorsal terminal nuclei of the cat accessory optic system following visual cortex lesions. Experimental Brain Research, 55(1), 69–80.

[45] Graham, D.J., and Field, D.J. Statistical regularities of art images and natural scenes: spectra, sparseness and nonlinearities. (2007).Spatial Vision,21, 149-164.

[46] Guido,W., Lu, S.M., Vaughan, J.W., Godwin, D.W., & Sherman, S.M., 1995. Receiver operating characteristic (ROC) analysis of neurons in the cat's lateral geniculate nucleus during tonic and burst response mode. Visual Neuroscience, 12, 723–741.

[47] He, S. and Masland, R.H. (1998). ON direction-selective ganglion cells in the rabbit retina: dendritic morphology and pattern of fasciculation. Visual Neuroscience, 15(2), 369–375.

[48] Hoffmann, K. P., and Distler, C. (1989). Quantitative analysis of visual receptive fields of neurons in nucleus of the optic tract and dorsal terminal nucleus of the accessory optic tract in macaque monkey. Journal of Neurophysiology, 62(2), 416–428.

[49] Huberman, A.D., Wei W., Elstrott, J.,. Stafford, B.K., Feller, M.B., and Barres, B.A. (2009). Genetic Identification of an On-Off Direction- Selective Retinal Ganglion Cell Subtype Reveals a Layer-Specific Subcortical Map of Posterior Motion. DOI: 10.1016/j.neuron.2009.04.014.

[50] Hubel D.H. & Wiesel T.N., 1961. Integrative action in the cat's lateral geniculate body. Journal of Physiology 155: 385–398.

[51] Hubel, D.H., & Wiesel, T.N., 1962. Receptive fields, binocular interaction and functional architecture in the cat's visual cortex. Journal of Physiology 160:106–154.

[52] Jack, J.J.B., Noble, D., Tsien, R.W. (1975). Electric current flow in excitable cells, Oxford: Oxford University Press

[53] Jagadeesh, B., Wheat, H.S., Kontsevich, L.L., Tyler, C.R., Ferster, D. (1997). Direction selectivity of synaptic potentials in simple cells of the cat visual cortex. Journal of neurophysiology, 78:2772-2789.

[54] Jensen, R.J., Devoe, R.D. (1983). Comparisons of directionally selective with other ganglion cells of turtle retina: Intracellular recording and staining. The Journal of Comparative Neurology, 17(3), 271-287.

[55] Kara, P., Reinagel, P., Reid, R.C., 2000. Low response variability in simultaneously recorded retinal, thalamic, and cortical neurons. Neuron 27:635– 646.

[56] Kara, P. And Reid, R.C., (2003). Efficacy of retinal spikes in driving cortical responses, The Journal of Neuroscience, 23(24), 8547– 8557.

[57] Kaplan, E, Purpura, K. & Shapley, R.M., 1987. Contrast affects the transmission of visual information through the mammalian lateral geniculate nucleus. Journal of Physiology 391: 267–288.

[58] Kim, I.J., Zhang, Y.,Yamagata, M., Meister, M., and Sanes, J.R.(2008). Molecular identification of a retinal cell type that responds to upward motion. Nature 452, 478-482.

[59] Krahe, R. and F. Gabbiani, Burst firing in sensory systems. (2004).Nat Rev Neurosci, 5(1): p. 13-23.

[60] Koizumi, A., Jakobs, T.C. & Masland, R.H., 2004. Inward rectifying currents stabilize the membrane potential in dendrites of mouse amacrine cells: patchclamp recordings and single-cell RT-PCR. Mol. Vis., 10, 328–340.

[61] Kuffler, S. (1953). Discharge patterns and functional organization of mammalian retina. Journal of Neurophysiology 16:37–68.

[62] le Feber J, Rutten WLC, Stegenga J, Wolters PS, Ramakers GJA, *et al.* (2007). Conditional firing probabilities in cultured neuronal networks: a stable underlying structure in widely varying spontaneous activity patterns. Journal of Neural Engineering 4: 54–67.

[63] Levick, W.R., Oyster. C.W., Takahashi E. (1969). Rabbit Lateral Geniculate Nucleus: Sharpener of Directional Information, Science, 165(3894), 712-714.

[64] Levick, W.R. (1967). Receptive fields and trigger features of ganglion cells in the visual streak of the rabbits retina. Journal of Physiology, 188(3), 285–307.

[65] Levine, M.W., Cleland, B.G., 2001. An analysis of the effect of retinal ganglion cell impulses upon the firing probability of neurons in the dorsal lateral geniculate nucleus of the cat. Brain Res 902:244 –254.

[66] Lindner, M., Vicente, R., Priesemann, V., Wibral, M. (2011). TRENTOOL: a Matlab open source toolbox to analyse information flow in time series data with transfer entropy. BMC Neurosci., 12., p. 119.

[67] Lungarella, M. and Sporns, O. (2006). Mapping information flow in sensorimotor networks. PLoS Comput Biol 2: e144.

[68] Maccione, A., Garofalo, M ., Nieus, T., Tedesco, M., Berdondini, L., and Martinoia, S. (2012). Multiscale functional connectivity estimation on low density neuronal cultures recorded by high density CMOS Micro Electrode Arrays. Journal of Neuroscience Methods, Vol 207, Issue 2 doi:10.1016/j.jneumeth.2012.04.002.

[69] Martiniuc, A.V. and Knoll, A. (2012). Interspike Interval Based Filtering of Directional Selective Retinal Ganglion Cells Spike Trains. Computational Intelligence and Neuroscience. doi:10.1155/2012/918030.

[70] Martiniuc A.V., Zeck G., Stürzl W., Knoll A. (2011). Sharpening of directional selectivity from neural output of rabbit retina. J. Comput. Neurosci. 30(2):409-26.

[71] Mastronade, D.N., 1987. Two classes of single-input X-cells in cat lateral geniculate nucleus. II. Retinal inputs and the generation of receptive-field properties. J Neurophysiol 57:381– 413.

[72] Mazzoni A, Broccard FD, Garcia-Perez E, Bonifazi P, Ruaro ME, Torre V. (2007). On the dynamics of the spontaneous activity in neuronal networks. PLoS ONE 2: e439.

[73] Michael, C.R. (1966). Receptive Fields of Opponent Color Units in the Optic Nerve of the Ground Squirrel. Science, 152(3725),1095-1097.

[74] McCabe A. K., Chisholm S. L., Picken-Bahrey H. L., Moody W. J. (2006). The selfregulating nature of spontaneous synchronized activity in developing mouse cortical neurones. J. Physiol. **577**, 155–167.10.1113/jphysiol.2006.117523

[75] Mustari, M.J. and Fuchs, A.F. (1989). Response properties of single units in the lateral terminal nucleus of the accessory optic system in the behaving primate, Journal of Neurophysiology, 61(6), 1207–1220.

[76] Nadasdy Z. Spike sequences and their consequences. (2000). J. Physiol. 94: 505-524.

[77] Nomura, M., Ito, D., Tamate, H Gohara, K. and Aoyagi, T. (2009). Estimation of Functional Connectivity that Causes Burst-like Population Activities. Forma, Vol. 24 (No. 1), pp. 11-16.

[78] Novellino A., D'Angelo P., Cozzi L., Chiappalone M., Sanguineti V., Martinoia S. (2007). Connecting neurons to a mobile robot: an in vitro bidirectional neural interface. Comput. Intell Neurosci. 12725.

[79] Olhausen, B.A., Field, D.J., 2004. Sparse coding of sensory inputs. Curr Opin Neurobiol 14:481– 487.

[80] Oyster C.W. (1968). The analysis of image motion by the rabbit retina. Journal of Physiology, 199, 613–635.

[81] Paninski, L, 2003. Convergence properties of three spike-triggered analysis techniques. Network 14:437– 464.

[82] Pasquale, V., Martinoia, S. and Chiappalone, M. (2010). A self-adapting approach for the detection of bursts and network bursts in neuronal cultures. Journal of Computational Neuroscience, vol. 29, (no. 1-2), pp. 213--229, 1573-6873.

[83] Pasquale V, Massobrio P, Bologna LL, Chiappalone M, Martinoia S. (2008). Selforganization and neuronal avalanches in networks of dissociated cortical neurons. Neuroscience 153: 1354–1369.

[84] Pillow, J.W., Paninski, L., Uzzell, V.J., Simoncelli, E.P., & Chichilnisky, E.J. (2005). Prediction and decoding of retinal ganglion cell responses with a probabilistic spiking model. The Journal of Neuroscience, 25, 11003–11013.

[85] Pimashkin A., Kastalskiy I., Simonov A., Koryagina E., Mukhina I., Kazantsev V. (2011). Spiking signatures of spontaneous activity bursts in hippocampal cultures. Front. Comput. Neurosci. 5:46.10.3389/fncom.2011.00046.

[86] Priebe, N. and Ferster, D. (2005). Direction selectivity of excitation and inhibition in simple cells of the cat primary visual cortex. Neuron, Vol. 45, 133–145.

[87] Priebe, N. and Ferster, D. (2008). Inhibition, spike threshold and stimulus selectivity in primary visual cortex. Neuron, DOI 10.1016/j.neuron.2008.02.005.

[88] Pu, M.L., and Amthor, F.R. (1990b). Dendritic morphologies of retinal ganglion cells projecting to the nucleus of the optic tract in the rabbit. Journal of Comparative Neurology, 302(3), 657–674.

[89] Rall, W. (1967). Distinguishing theoretical synaptic potentials computed for different soma-dendritic distributions of synaptic inputs. Journal of Neurophysiology, 30, 11381168.

[90] Rathbun, D.L, Alitto, H.J., Weyand, T.G., and Usrey, W.M. (2007). Interspike interval analysis of retinal ganglion cell receptive fields. Journal of Neurophysiology, 98, 911919.

[91] Rathbun, D.L, Warland, D.K., & Usrey, W.M., 2010. Spike timing and information transmission at retinogeniculate synapse.The Journal of Neuroscience 30(41):1355813566.

[92] Reid, R.C., Victor, J.D., & Shapley, R.M., 1997. The use of m-sequences in the analysis of visual neurons: linear receptive field properties. Vis. Neurosci., 14, 1015–1027.

[93] Reid, R.C., & Usrey, W.M., 2004. Functional connectivity in the pathway from retina to visual cortex. In: The Visual Neurosciences, ed. CHALUPA, L.M. & WERNER, J.S., pp. 673–679. Cambridge, MA: MIT Press.

[94] Rolston, J.D., Wagenaar, D.A. & Potter, S.M. (2007). Precisely timed spatiotemporal patterns of neural activity in dissociated cortical cultures. Neuroscience, 148, 294–303.

[95] Rolston J., Gross R., Potter S. (2010). Closed-loop, open-source electrophysiology. Front. Neurosci. 4:31.10.3389/fnins.2010.00031.

[96] Ruaro, M.E., Bonifazi, P. and Torre, V. (2005). Toward the neurocomputer : Image Processing amd pattern recognition with neuronal cultures. IEEE Trans. Biomed. Engineering 52(3):371-383.

[97] Schreiber, T. (2000). Measuring information transfer. Phys Rev Lett 85: 461–464.

[98] Schwartz, O., Pillow, J.W., Rust, N.C., Simoncelli, E.P., (2006). Spike-triggered neural characterization. J Vis 6:484 –507.

[99] Shimazaki, H., Shinomoto, S. (2007). A method for selecting the bin size of a time histogram. Neural Computation 19 (6): 1503–152. doi:10.1162/neco.2007.19.6.1503

[100] Soodak, R.E. and Simpson, J.I. (1988). The Accessory Optic System of Rabbit. I. Basic Visual Response Properties. Journal of Neurophysiology, 60, 2037-2054.

[101] Shahaf, G. and Marom, S. (2001). Learning in Networks of Cortical Neurons. The Journal of Neuroscience, 21 (22):8782–8788.

[102] Shlens, J., Field, G.D., Gauthier, J.L., Grivich, M.I., Petrusca, D., Sher, A., Litke, A.M. and Chichilnisky, E.J. (2006). The Structure of Multi-Neuron Firing Patterns in Primate Retina. The Journal of Neuroscience, 26(32), 8254–8266.

[103] Sincich, L.C., Adams, D.L., Economides, J.R., and Horton, J.C. (2007). Transmission of spike trains at retinogeniculate synapse. The Journal of Neuroscience, 27(10), 2683– 2692.

[104] Sincich, L.C., Horton, J.C. & Sharpee, T.O., (2009). Preserving Information in Neural Transmission. The Journal of Neuroscience 29(19):6207– 6216, 6207.

[105] Soodak, R.E., Simpson, J.I., 1988. The accessory optic system of rabbit. I. Basic visual response properties. Journal of Neurophysiology, 60, 2037–2054.

[106] Stanford, L.R. and Sherman, S.M. (1984). Structure/function relationships of retinal ganglion cells in the cat. Brain Research, 297(2), 381–386.

[107] Strong, S.P., Koberle, R., de Ruyter, van Steveninck, R.R., Bialek, W., (1998). Entropy and information in neural spike trains. Phys Rev Lett 80:197–200

[108] Sun J.J., Kilb W., Luhmann H.J. (2010). Self-organization of repetitive spike patterns in developing neuronal networks *in vitro*. Eur. J. Neurosci. **32**.

[109] Swadlow, H.A, Gusev, A.G. (2001). The impact of "bursting" thalamic impulses at a neocortical synapse. Nat Neurosci 4:402-408.

[110] Swadlow, H.A., Gusev, A.G., Bezdudnaya, T., (2002). Activation of a cortical column by a thalamocortical impulse (PDF). Journal of Neuroscience 22 (17): 7766–7773.

[111] Taylor, W.R., and Vaney, D.I. (2002). Diverse Synaptic Mechanisms Generate Direction Selectivity in the Rabbit Retina, Journal of Neuroscience, 22(17), 7712–7720.

[112] Uglesich, R., Casti, A., Hayot, F. & Kaplan, E. (2009). Stimulus size dependence of information transfer from retina to thalamus. Frontiers in Systems Neuroscience. doi:10.3389/neuro.06.010.2009.

[113] Usrey, W.M., Reppas, J.B., Reid, R.C. (1998). Paired-spike interactions and synaptic efficacy of retinal inputs to the thalamus. Nature, 395(6700), 384-387.

[114] Usrey, W.M., Reppas, J.B., Reid, R.C. (1999). Specificity and strength of retinogeniculate connections. Journal of Neurophysiology, 82:3527-3540.

[115] Usrey, W.M., Alonso, J.M., Reid, R.C., (2000). Synaptic interactions between thalamic inputs to simple cells in cat visual cortex. J Neurosci 20:5461–5467.

[116] Usrey, W.M. (2002). Spike timing and visual processing in the retinogeniculocortical pathway, Philosophical Transactions of The Royal Society Lond. B Biological Sciences, 357, 1729–1737.

[117] van der Togt, C., van der Want, J., and Schmidt, M. (1993). Segregation of direction selective neurons and synaptic organization of inhibitory intranuclear connections in the medial terminal nucleus of the rat: an electrophysiological and immunoelectron microscopical study. Journal of Comparative Neurology, 338(2), 175–192.

[118] Vaney, D.I., Levick, W.R., and Thibos, L.N. (1981a). Rabbit retinal ganglion cells. Receptive field classification and axonal conduction properties. Experimental Brain Research, 44(1), 27–33.

[119] Vaney, D.I., Peichl, L., Wassle, H., and Illing, R.B. (1981b). Almost all ganglion cells in the rabbit retina project to the superior colliculus. Brain Research, 212(2), 447–453.

[120] van Pelt, J., Corner, M.A., Wolters, P.S., Rutten, W.L. & Ramakers, G.J. (2004). Longterm stability and developmental changes in spontaneous network burst firing

patterns in dissociated rat cerebral cortex cell cultures on multielectrode arrays. Neurosci. Lett., 361, 86–89.

[121] van Pelt, J., Vajda, I., Wolters, P.S., Corner, M.A. & Ramakers, G.J.A. (2005) Dynamics and plasticity in developing neuronal networks in vitro. Prog.Brain Res., **147**, 173–188.

[122] Vicente R, Wibral M, Lindner M, Pipa G. (2011). Transfer entropy — a model-free measure of effective connectivity for the neurosciences. J Comput Neurosci 30: 45–67. doi : 10.1007/s 10827 – 010 – 0262-3.

[123] Volgushev, M. Pernberg, J. and Eysel, U.T. (2000). Comparison of the selectivity of the postsynaptic potentials and spike responses in cat visual cortex. European Journal of Neuroscience, Vol.12, pp 257-263.

[124] Wagenaar, D.A., Madhavan, R., Pine, J. & Potter, S.M. (2005). Controlling bursting in cortical cultures with closed-loop multi-electrode stimulation. J Neurosci, **25,** 680-8.

[125] Wagenaar, D.A., Pine, J. & Potter, S.M. (2006). Searching for plasticity in dissociated cortical cultures on multi electrode arrays. J. Neg. Res. Biomed, **5**.

[126] Wagenaar DA, Nadasdy Z, Potter SM. (2006). Persistent dynamic attractors in activity patterns of cultured neuronal networks. Physical Review E73, 051907.

[127] Weng, S., Sun, W., and He, S. (2005). Identification of ON–OFF direction-selective ganglion cells in the mouse retina. Journal of Physiology, 562(3), 915–923.

[128] Weliky M, Katz LC. (1999). Correlational structure of spontaneous neuronal activity in the developing lateral geniculate nucleus in vivo. Science, 285(5427):599-604.

[129] Wibral, M., Pampu, N., Priesemann, V., Siebenhuehner, F., Seiwert, H., Lindner, M., Lizier, J. T. and Vicente, R. (2013). Measuring information-transfer delays. PloS one, 8(2)

[130] Wiener, N. The theory of prediction. (1956). In: Beckenbach, E. (Ed.), Modern Mathematics for Engineers. McGraw-Hill, New York.

[131] Weyand T.G., 2007. Retinogeniculate Transmission in Wakefulness. Journal of Neurophysiology 98: 769–785.

[132] Wörgötter, F., and Koch, C. (1991). A detailed model of the primary visual pathway in the cat: Comparison of afferent excitatory and intracortical inhibitory connection schemes for orientation selectivity. Journal of Neuroscience, 11(7), 1959–1979.

[133] Yang, G. & Masland, R.H., 1994. Receptive fields and dendritic structure of directionally selective retinal ganglion cells. J. Neurosci., 14, 5267–5280.

[134] Yonehara K, Ishikane H, Sakuta H, Shintani T, Nakamura-Yonehara K, *et al.* (2009). Identification of retinal ganglion cells and their projections involved in central transmission of information about upward and downward image motion. Plos One, 4(1), e4320

[135] Zeck, G.M., Masland, R.H. (2007). Spike train signatures of retinal ganglion cell types. European Journal of Neuroscience, 26, 367-380.

[136] Zullo L, Chiappalone M, Martinoia S, and Benfenati F. (2012). A “spike-based” grammar underlies directional modification in network connectivity: effect on bursting activity and implications for bio-hybrids systems. PLoS ONE, 7(11): e49299.

ACKNOWLEDGMENTS

First of all, I want to thank my advisor Prof. Dr. Alois Knoll for his encouragement, guidance, inspiration and patience. In the same time I would like to thank him for all his enthusiasm and energy and scientific knowledge that he shared with me during such a nice but in the same time complex project as NeuroversIT, which he lead it during 2007-2009 period of my thesis. It was of a much help to be involved within such a valuable international collaboration inside neuroscience scientific community.

Many thanks go to Dr. Gerhard Schrott for his mentoring support and strong optimism.

I have very appreciated scientific discussions with all my colleagues within the department and I especially and highly appreciated the optimism and sense of humor of Amy.

I have also to thank to Dr. Stuerzl for nice and helpful scientific discussions during my first year of PhD.

I have as well appreciative words to Dr. Zeck for providing part of the data I was using and for valuable scientific discussions.

Of a major help for this scientific work was my scientific collaboration with Dr. Axel Blau, to whom I would like to address special thanks!

Perhaps I don't have enough space here to say how much I appreciate my wife's efforts, understanding, encouraging, optimism, sometimes curiosity and ... much patience.

To my brother and my mother I have to say special thanks in principal for the reason that they trusted me.

I will not end before saying thanks to two brave persons decisive for my scientific work: Prof. Dr. Luc Cinotti, who initiated me in neuroscience long time ago and changed my life, and Dr. Victor Bocos-Bintintan, who shared with me his gifts both in science and in general in life.

And finally to my father ..... he would have been proud of me.